Technische Universität München
TUM School of Medicine and Health

Role of Ring Finger Protein 43 (Rnf43) in Common Bile Duct Cancer

Joanna Madej

Vollständiger Abdruck der von der TUM School of Medicine and Health der Technischen Universität München zur Erlangung eines

Doctor of Philosophy (Ph.D.)

genehmigten Dissertation.

Vorsitz: Prof. Dr. Angelika Harbauer

Betreuer: Prof. Dr. Dieter Saur

Prüfende der Dissertation:

1. Prof. Dr. Klaus-Peter Janssen
2. Prof. Dr. Maximilian Reichert

Die Dissertation wurde am 05.01.2024 bei der TUM School of Medicine and Health der Technischen Universität München eingereicht und durch die TUM School of Medicine and Health am 19.03.2024 angenommen.

Index

Figure Index

Table Index

Abbreviations

%	Percentage
×g	Times gravity
°C	Degree Celsius
2D	Two dimensions
3D	Three dimensions
µg	Microgram
µL	Microliter
µM	Micromolar
AKT	Serine-threonine kinase
APC	Adenomatous polyposis coli
AUC	Area under the dose response curve
bp	Base pairs
BSA	Bovine serum albumin
CBD	Common Bile Duct
CCA	Cholangiocellular carcinoma
CDKN2A	Cyclin-dependent kinase inhibitor 2A
Ck	Cytokeratin
CK7	Keratin 7
CTG	Cell Titer Glo
d	Day
DAB	3,3'-Diaminobenzidine
ddH_2O	Bidistilled water
dH_2O	Distilled water
DMEM	Dulbecco's modified Eagle's medium
DMSO	Dimethyl sulfoxide

DNA	Deoxyribonucleic acid
dNTP	Deoxynucleotide triphosphate
DPBS	Dulbecco's phosphate-buffered saline
DTT	1,4-Dithiothreitol
EDTA	Ethylenediaminetetraacetic acid
EGF	Epidermal growth factor
et al.	Et alii
EtOH	Ethanol
f	Flox
FCS	Fetal calf serum
FFPE	Formalin-fixed paraffin-embedded
fs	Frame-shift
Fzd	Frizzled receptor
g	Gram
GATA3	GATA binding protein 3
GEMM	Genetically engineered mouse model
GI50	Concentration for 50% growth inhibition
GSK3β	Glycogen synthase kinase 3 beta
h	Hour
H&E	Hematoxylin and eosin
H2O2	Hydrogen peroxide
HBV	Hepatitis B virus
HCV	Hepatitis C virus
IHC	Immunohistochemistry
kb	Kilo-base pair
KEGG	Kyoto Encyclopedia of Genes and Genomes
KO	Knockout

KRAS	Kirsten rat sarcoma virus
L	Liter
Lgr	Leucin-rich repeat containing G-protein-coupled
LOF	Loss of function
LRP5/6	LDL-receptor-related protein receptors 5/6
LSL	*Lox-STOP-Lox*
M	Molar
MetOH	Methanol
mg	Milligram
min	Minute
mL	Milliliter
mM	Millimolar
MMF	Midazolam, medetomidine, fentanyl
mTOR	Mammalian target of rapamycin
MYC	MYC proto-oncogene
n/a	Not applicable
nm	Nanometer
nM	Nanomolar
p	p-value
αp110	Phosphatidylinositol-4,5-bisphosphate 3-kinase, catalytic subunit alpha
PanIN	Pancreatic intraepithelial neoplasia
PBS	Phosphate-buffered saline
PCR	Polymerase chain reaction
PDAC	Pancreatic ductal adenocarcinoma
Pdx1	Pancreatic and duodenal homeobox 1
PFA	Paraformaldehyde

PI3K	Phosphoinositide 3-kinase
PIK3CA	Phosphatidylinositol-4,5-bisphosphate 3-kinase catalytic subunit alpha
PTEN	Phosphatase and tensin homolog deleted on chromosome 10
qPCR	Quantitative PCR
R26	Rosa26
RNA	Ribonucleic acid
RNA-seq	RNA sequencing
RNF	RING finger protein
rpm	Revolutions per minute
RT	Room temperature
scRNA-seq	Single cell RNA sequencing
SD	Standard deviation
sec	Second
SEM	Standard error of mean
TAE	Tris-acetate-EDTA
TCF/LEF	T cell factor/lymphoid enhancer factor family
TCF4	T cell factor 4
TEMED	N,N,N',N'-tetramethylethylenediamine
UV	Ultraviolet
V	Volt/Voltage
W	Watt
Wg	Winglwess
Wnt	wingless-type MMTV integration site
WT	Wild-type
Zn2+	Zinc
ZNRF3	E3 ubiquitin ligase Zinc and Ring finger 3

1. Summary

Common Bile Duct cancer is a relatively rare human malignancy that develops outside of the liver and forms cancerous lesions inside the bile duct. The 5-year survival rate of CBD is 17%, when diagnosed at an early stage, however when the cancer has spread to distant parts of the body, the 5-year relative survival rate drops to 2%.

Due to a challenging and complex diagnosis as well as absence of specific biomarkers, the majority of patients diagnosed with CBD cancer are classified as unresectable and receive radio- or chemotherapy. However, the underlying mechanisms driving CBD onset and progression remain poorly understood. Therefore, genome-wide *in vivo piggyBac transposon mutagenesis screening* was performed on genetically engineered mouse models harboring *Pik3ca*$^{H1047R/wt}$ mutation under control of *Pdx1-Cre* promoter to uncover novel sets of genes and pathways possibly involved in CBD carcinogenesis.

PiggyBac transposon mutagenesis enabled to identify *Ring finger protein 43* as one of the top hits of the forward genetic in vivo screen, indicating its importance in CBD development. Analysis of CIS (common insertion sites) pattern indicated a tumor suppressive role of *Rnf43* in CBD development. In order to elucidate the consequences of *Rnf43* loss of function, mice with both hetero- and homozygous knockout (KO) of *Rnf43* were subsequently crossed not only with *Pik3ca*-mutant mice but also with mice harboring an activating mutation in *Kras*.

This strategy provided valuable *in vivo* evidence confirming the tumor suppressive role of *Rnf43* in CBD, due to significantly shortened survival of mice harboring *Rnf43* KO in comparison to *Rnf43* wild-type mice. Furthermore, organoid cultures were established for conducting *in vitro* assays such as large-scale drug screens as well as functional assays for Wnt reporter activity. Additionally, transcriptomic analysis was performed to identify differential gene expression in *Rnf43*-proficient and -deficient organoid lines in.

In conclusion, the generated data supports the tumor suppressive role of *Rnf43* in CBD due to a shortened survival in *Rnf43* KO mice. In addition, further experiments might unravel possible vulnerabilities upon *Rnf43* loss of function, however further validation of the hits of the drug screen is needed to assess the efficacy and potential of various drugs. Identifying and targeting specific molecular pathways relevant to CBD carcinogenesis could potentially lead to the development of targeted therapies.

2. Zusammenfassung

Das extrahepatische Gallengangskarzinom ist eine relative seltene maligne Erkrankung die in den Gallengängen außerhalb der Leber entsteht und zu kanzerösen Läsionen der Gallengänge führt. Bei frühzeitiger Erkennung liegt die 5-Jahres-Überlebensrate bei 17%, sie fällt jedoch auf 2%, wenn sich der Tumor bereits auf weitere distale Organe des Körpers ausgebreitet hat.

Aufgrund der schwierigen und komplexen Diagnose und dem Mangel an spezifischen Biomarkern wird die Mehrheit der Patienten mit extrahepatischen Gallengangskarzinom als unresektabel eingestuft und bekommt Radio- oder Chemotherapie. Die genauen Mechanismen der Tumorentstehung und Tumorprogression des Gallengangskarzinom sind bisher nur unzureichend untersucht. Von daher wurden genomweite piggyBac Transposon Screens in genetisch veränderten Mäusen mit Mutation in *Pik3ca*$^{H1047R/wt}$ unter der Kontrolle des Pdx1-Cre Promoters durchgeführt um Gene und Signalwege zu identifizieren, die für die Tumorentstehung im extrahepatischen Gallengang eine ursächliche Rolle spielen.

Das *Ring finger protein 43 (Rnf43)* wurde dabei in den Transposon Screens als eines der wichtigsten Gene für die Karzinogenese des extrahepatischen Gallengangskarzinom identifiziert. Die Analyse der Transposon Insertions-Muster, der sogenannten CIS (common insertion sites), bestätigte nicht nur die Relevanz von *Rnf43* für die Onkogenese des Gallengangskarzinoms, sondern auch dessen tumorsuppressive Funktion. Um die Effekte der Auschaltung von *Rnf43* genauer zu untersuchen, wurden Mäuse mit hetero- als auch homozygoten Knockout (KO) von *Rnf43* sowohl in Mauslininen mit *Pik3ca*-Mutation als auch solche mit *Kras*-Mutation gekreuzt.

Dies bestätigte die tumorsuppressive Funktion von *Rnf43* im Hauptgallengang *in vivo,* da Mäuse mit Knockout von *Rnf43* ein deutlich verkürztes Überleben im Vergleich zu Mäusen mit Wildtyp *Rnf43* aufwiesen.

Darüber hinaus wurden Organoid Kulturen für die Durchführung von *in vitro* Assays wie Wirkstoff-Screens oder funktionaler Assays wie zum Beispiel für Wnt Reporteraktivität etabliert. Zusätzlich wurden Transkriptomanalysen durchgeführt um differentiell exprimierte Gene in Rnf43-profizienten und –defizienten Organoid-Linien zu identifizieren.

Zusammenfassend zeigen die Daten eine tumorsuppressive Funktion von *Rnf43* im Gallengangskarzinom, was durch das verkürzte Überleben der *Rnf43*-Knockout Mäuse belegt wird. In weiterführenden Experimenten könnten darüber hinaus potentiell therapeutische Vulnerabilitäten von *Rnf43*-deletierten Tumoren identifiziert werden, wofür allerdings eine tiefergehende Evaluation der Daten des Wirkstoff-Screens erforderlich ist um Potential und Wirksamkeit der verschiedenen Wirkstoffe besser einschätzen zu können. Die Identifikation spezifischer molekularer Signalwege, die relevant für die Tumorgenese des Gallengangkarzinoms sind, könnte somit zur Entwicklung von zielgerichteten Krebstherapien beitragen.

3. Introduction

The high mortality rate of patients diagnosed with cholangiocarcinoma (CCA) is directly linked with not only late diagnosis, but also lack of proper diagnostic tools and asymptomatic course of this disease. The urgency to provide better healthcare and treatment plans is still existing (Banales et al., 2020; Qureshi et al., 2014).

The complexity of CCA is associated with diverse risk factors, such as impact of tumor microenvironment, cancer stem cells, as well as epigenetic and genetic factors, which make the aim of treating this aggressive cancer subtype even more challenging (Rizvi & Gores, 2017).

Increasing awareness and implementing screening programs for early detection can help in the fight against CCA. However, it is furthermore crucial to unravel the complexity and heterogeneity of this cancer subtype, as better understanding of the underlying mechanisms of CCA development and progression will allow to identify new candidates and consequently develop more effective therapeutic strategies for all CCA patients (Rizvi & Gores, 2013, 2017).

3.1 Biliary tract

The biliary tract is a system of ducts responsible for transporting bile. Bile is produced in the liver, stored, and concentrated in the gallbladder to be in the end transported to the small intestine, where it takes part in lipid digestion. This digestive fluid is composed of bile salts, bilirubin, and cholesterol. The lining of the bile ducts is made up of specialized epithelial cells – so called cholangiocytes – which take an active part in the production of bile (Boyer, 2013; Esteller, 2008).

The complex system of biliary tree connects several organs. This system is composed of the right and left hepatic ducts (RHD and LHD, respectively) that drain the lobes of the liver and come together to form the common hepatic duct. The hepatic duct joins the cystic duct, which is directly connected to the gallbladder, to form the common bile duct (CBD) together (Castaing, 2008; Mortele et al., 2006).

Part of the CBD joins the main pancreatic duct forming the ampulla of Vater, which is located at the major duodenal papilla. The entry to the duodenum is known as the sphincter of Oddi, which is a muscular valve that controls the flow of bile and pancreatic juice before they enter the small intestine. Due to that control only part of the produced

bile enters the small intestine, while the remaining bile is transported back to gallbladder where it is stored (Aitchison, 2009).

Disorders of such a complex system as the biliary tree result in severe diseases, such as gallstones, cholangitis, cholecystitis, or one of the subtypes of CCA. Early detection and treatment of any abnormalities of the biliary tree can improve outcomes. Techniques used for diagnosis are based on imaging like Magnetic resonance imaging (MRI) and Computed Tomography (Bass et al. ,2014) or other procedures such as endoscopic retrograde cholangiopancreatography (ERCP). Moreover, screenings based on control of serum markers (i.e carbohydrate antigen 19-9 - CA19-9), cytological evaluation, and fluorescent *in situ* hybridization (Bass et al. , 2014) are also used for diagnosis however most of used techniques are unspecific and have low accuracy. Based on findings there are several treatment options, surgery fallowed by adjuvant therpahy (i.e capeticabine, gemcitabine with cisplatin, gemcitabine with capeticabine, 5-fluorouracil with oxaliplatin), clinical trials, chemotheraphy or palliative theraphy (Vedeld et al., 2020).

3.2 Cholangiocarcinoma (CCA)

CCA is a lethal malignancy of the hepatobiliary system that is known to be highly heterogeneous, thus making the diagnosis and the treatment challenging. It is mostly developed from malignant transformation of cholangiocytes. However, some cases of this type of cancer can also originate from the hepatocytes (the main cells of the liver) or the perbiliary glands (small glands that can be found near the bile ducts) (Fan et al., 2012; Nakagawa et al., 2017; Razumilava & Gores, 2014; Zhu & Kwong, 2020)

Due to heterogeneity, CCA classification is based on the anatomic site of origin (Fig. 1):

- intrahepatic (iCCA) arises inside of the liver parenchyma above the second-order bile ducts. It is the least common type of CCA with only approximately 10–20% of cases belonging to this subtype of CCA.
- perihilar (pCCA) is a type of extrahepatic CCA, this subtype of the cancer is formed outside of the liver in the area of left and right hepatic ducts join to form common hepatic duct. Almost 50–60% of all patients are diagnosed with pCCA, making it the most common type of CCA.

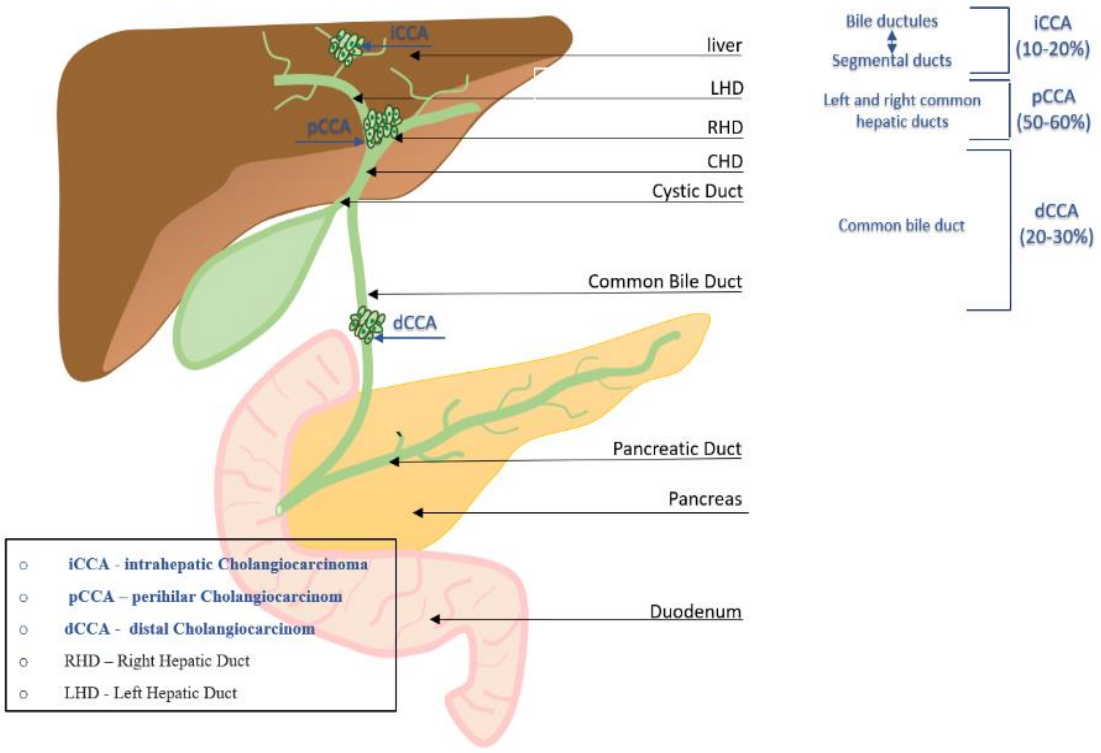

Figure 1. Anatomic classification of CCA. CCAa is classified based on anatomy into three subtypes of cancer: iCCA, pCCA and dCCA. iCCA is arising from segmental ducts located in liver, pCCA is formed in the joined left and/or right hepatic ducts or within this duct themselves. dCCA develops from common bile duct; % indicates percentage of cases diagnosed with highlighted cancer subtype among patients with CCA (Banales, Marin et al. 2020).

- distal (dCCA) is also a type of extrahepatic CCA that arises outside of the liver, in the area of ducts located close to the pancreas. 20–30% of all CCA cases are patients diagnosed with dCCA. (Banales et al., 2020; Sarcognato et al., 2021).

CCA is rated to be the second most common hepatic malignancy, with approximately 3% of gastrointestinal cancers and almost 10-15% of all primary liver tumors being identified as CCA (Bray et al., 2018; Hoyos et al., 2018). Even though there are extensive studies on this cancer entity, increasing knowledge about CCA is essential to improve both diagnosis and available therapies and to develop new clinical approaches. The survival rate of the patients is very low, with only 7–20% of CCA cases being able to survive the first 5-years after the diagnosis and even for those the risk of relapse is extremely high (Banales et al., 2020; Jansen et al., 2020).

3.2.1 Mortality and risk factors

Mortality rates of patients with CCA have increased globally. Furthermore, worldwide, men are in higher risk of dying due to CCA than women due to *i.e* differences in expression of sex dependent enzymes metabolizing drugs like in case of cytochrome gene. Females exhibit higher expression levels of CYP3A4, an enzyme was found to take a part in biotransformation of more than 50% of all clinically used drugs (Ledenko et al., 2022). It has also been statistically demonstrated that the risk is also higher for Asian countries in comparison to the Western world. That can be connected to liver fluke infections (*C. sinensis* and/or *O. viverrini*) (Watanapa & Watanapa, 2002). Variations in incidences occur due to the differences between regional risk factors and some genetic predispositions in the studied groups. For the Western world, there is no dominant risk factor that would have such a great impact in terms of CCA development.

Several risk factors commonly associated with CCA are bile stasis and chronic inflammation of the biliary epithelium. The risk of CCA development is also linked with alcohol consumption, viral infections (HBV and HCV) and smoking. There is also need of studying more carefully the possible correlation between development of CCA and obesity, nonalcoholic fatty liver disease and metabolic syndrome (Kirstein & Vogel, 2016). Future studies should also evaluate the impact of several drugs, such as aspirin and statins used for lowering levels of lipids and investigate if these drugs reduce the risk of CCA development. Careful evaluation of these findings is still necessary; however, the potential benefit could improve the health outcome of patients (Choi et al., 2016; Peng et al., 2015).

In early stages, CCA is highly asymptomatic which makes the diagnosis challenging. One of the most common symptoms of pCCA and dCCA is jaundice. On the other hand, for iCCA, jaundice occur mostly in the late stages of disease. Further indicators connected with CCA development are abdominal pain, malaise, nausea, anorexia, and weight loss. For up to 20–25% of cases of iCCA, the diagnosis is incidentally occurring during examinations for another medical condition (Alvaro et al., 2011). A variety of imaging techniques, such as ultrasonography, contrast-enhanced ultrasonography (CEUS), computed tomography (Bass et al. ,2014) or magnetic resonance imaging (MRI) is considered as leading procedure used not only for diagnosis but also as a tool for staging, follow up and control of treatment response (Bolondi et al., 2013).

Regardless of how helpful imaging techniques can be as a tool used to study CCA development, there is still necessity to confirm the diagnosis by histopathological or cytological analysis (Conrad et al., 2012; Dirks et al., 2023).

3.2.2 Potential Targetable Genes and Molecular Pathways

Previous studies on CCA were limited by the lack of available techniques that are now available for daily usage. Consequently, determining the role of individual genes involved in CCA development was extremely challenging. Genes such as *Kirsten rat sarcoma virus* (*KRAS*), *transformation-related protein 53* (*TP53*), and *cyclin-dependent kinase inhibitor 2A* (*CDKN2A*), were commonly identified in patients with CCA (Tian, Hu et al. 2020). However, application of next-generation sequencing technology has unveiled a complex genomic landscape of genes that needs to be investigated in more details to find their significance for the progression and development of CCA. New technologies improved understanding of the molecular pathways linked with CCA and provided new opportunities for future studies in this field (Jusakul et al., 2017).

Immune-based treatment is becoming standard practice due to better understanding immune profiles of patients with CCA. Innovations of therapies allow to improve the overall devastating outcome for patients diagnosed with cancer. Targeted therapies became reality, drugs targeting subset of TME cells are already in use. Currently there are approved drugs targeting *fibroblast growth factor receptor (FGFR), isocitrate dehydrogenase (IDH)* and *epidermal growth factor receptor 2 (EGFR2)* (Greten et al., 2023). Clinical trials are giving promising results for various cancer vaccines, adoptive cell therapies (CAR-T) and immune checkpoint inhibitors, like PD-L1 that is present in approximately in fifty percent of patients with CCA. Nevertheless, to ensure the safety of such treatment more studies need to be conducted to validate effectiveness of this rapidly evolving field.(Dolgin, 2023; Du et al., 2023).

Currently, thanks to NGS, the increased understanding of complex molecular pathways involved in biliary cancers allows to study new mutation signatures of patients with CCA, that includes genes like: *isocitrate dehydrogenase 1 and 2 (IDH1* and *IDH2*, respectively), *fibroblast growth factor receptor 2 (FGFR2)*, *tri-methylation of lysine 27 on histone H3 protein (H3K27me3*) (Jusakul et al., 2017). Interestingly studies focused on the influence of mutations in Wnt signaling, RAS/MAPK or PI3K/AKT/mTOR

pathway on CCA progression and development show promising outcome for future of targeted therapies.

RAS/MAPK pathway is known to be involved in development of various cancers including gastrointestinal, and genes like *KRAS*, *NRAS*, *BRAF* are special interesting for many researchers. The occurrence of mutations in KRAS domain is evidenced also among cases CCAs (Moncur et al., 2019; Xu et al., 2011)

The evidence of the role of PI3K/AKT/mTOR pathway which is involved in cell cycle regulation in numerous cancer subtypes is already widely known (Peng et al., 2022). Just PI3K itself is found to be mutated among all subtypes of CCA. The importance of these findings is proven by directly approaching the aims of personalized therapy (Bian et al., 2017; Yothaisong et al., 2013). There are already existing clinical trials with inhibitors targeting PI3K/AKT/mTOR pathway (e.g., rad001, a mTOR inhibitor) used to increase the chances for better treatment outcome in the clinics (Lau et al., 2018).

The pathway which became a common interest of many research studies is Wnt/β-catenin signaling pathway. Involved in many of crucial biological processes such as embryonic development and adult homeostasis, Wnt/β-catenin pathway has potential to become future aim of targeted therapies. The link between this pathway and its role in cancer development and progression of various cancer entities, including CCA, is already described. However, there is still a need to find a way to bring this attractive candidate to clinical studies in patients with CCA (Goeppert et al., 2014; Merino-Azpitarte et al., 2017)

Another unquestionable target for further studies is Notch pathway. The role of Notch signaling in cell differentiation, proliferation and apoptosis makes it a perfect candidate for further investigation, especially since this pathway is found to be deregulated in CCA. Few of the Notch inhibitors i.e Crenigacwstat, Cinibufagin or Brontictuzumab show potential become new attractive candidates for clinical studies or even are a part of them (Mancarella et al., 2020; Rauff et al., 2020).

Currently, the common practice for patients diagnosed with CCA is still surgical resection. However, for patients that are not qualified for an operation there is still an option of chemo- or radiotherapy (Lee et al., 2016; Ren et al., 2020). Nevertheless, decreasing mortality or at least improving survival of patients should be the new approach of future treatment. In the field of not only CCA treatment but also various subtypes of cancer, there is a focus set on targeted therapies. Precise targeting altered pathways or mutated genes without affecting healthy tissue is an exciting aim and holds the promise

to become reality in nearest future for all patients affected by this devastating disease (Montal et al., 2020).

3.3 *PiggyBac* transposon mutagenesis screen

Transposon mutagenesis screen is a powerful tool used for identifying novel genes potentially involved in cancer development. This genetic technique allows to study genome of various species, by examining the location and frequency of transposon insertions and subsequently based on that allows to predict the role of gene of interest. Furthermore, the analysis of gene function is done in quite easy, regulated and scalable manner, which makes it beneficial and attracting tool to use (Ivics et al., 2009).

Two commonly used and known transposon mutagenesis screens are *PiggyBac* (Ryland et al.) (Rad et al., 2010) and *Sleeping Beauty* (*SB*) (Voigt et al., 2016). The transposon screens allow to generate a large library that researchers can further evaluate and select the specific potentially interesting genes to study their role in numerous biological processes and pathways.

SB system was described in 1997 as a fully functional tool to study mutagenesis *in vitro* (Ivics et al., 1997). One notable limitation of this system is efficiency of transposition, *SB* screens leaves a "footprint" of a 5bp mutation. Nevertheless, it is still great tool for *in vivo* studies since there is no toxicity observed in mice in connection to activity of SB transposon or SBase. Moreover, it is reliable system for long term usage and highly specific due to its potential to integrate within designated chromosomal region (Hou et al., 2015; Keng et al., 2005).

An advantage of using *PB* is the possibility of moving large DNA fragments moreover it does not result in leaving undesirable footprints after transposition. However, the disadvantage of *PiggyBac* screen is tendency for local hopping (Rad et al., 2010; Weber et al., 2019).

PiggyBac transposon screen was conducted by Falcomatà et. al, 2021 to pinpoint genes involved in initiation of CBD cancer. This approach was possible by crossing genetically engineered mice carrying *LSL-PI3K*$^{H1047R/wt}$ under control of the promotor *Pdx1-Cre* with mice harboring mitochondrial *ATP synthase subunit alpha* (*ATP1*) transposons and *LSL-R26PB* mice. The *LSL-R26PB* is a knock in located at the Rosa26 locus with a floxed STOP cassette that prevents unspecific expression. The activation of the construct is possible only upon Cre recombinase expression, which is under the control of the Pdx1

promoter. Since *Pdx1* is expressed in several organs of gastrointestinal tract, the mutation in PI3K domain is observed in organs such as bile duct, gallbladder, pancreas, and stomach. The screen confirmed the importance of PI3K/Akt/mTor pathway for bile duct cancer development. As predicted, the majority of the analyzed mice developed a CBD cancer. Overall tissue samples harvested not only from CBD but also from pancreas were sequenced and analyzed. This analysis enabled to preselect several interesting candidates for further studies. Moreover, it unraveled the importance of discovered genes, after analysis of common insertion pattern pattern. Additionally, it was possible to predict the role of those genes in tumor development and classify them as either as tumor suppressors or proto-oncogenes based on the insertion and orientation of transposons (Falcomata et al., 2021).

3.4 RING finger family

RING finger proteins are a large family of E3 ubiquitin ligases that are characterized by the presence of a RING finger domain. Initially discovered in 1991 (Freemont, Hanson et al. 1991), this family contains more than 400 members (Capili, Edghill et al. 2004). The diverse functions make them an interesting subject to study especially since their role is still not fully known. Previous studies have shown that members of this family are involved in variety of physiological and biochemical processes and that their abnormal activity due to genetic alterations can cause or contribute to immune and neurological/disorders as well as tumor development and progression (Cai et al., 2022; van Dijk et al., 2014). In comparison to the DNA binding zinc finger domain, the activities of the RING finger domain are based on protein-protein interactions. The ubiquitin E3 ligase catalytic activity of the RING finger proteins plays a key role in mediating the transfer of ubiquitin to target proteins, which leads to their modification or degradation. Ubiquitination of Frizzled receptor, for example, directly regulates Wnt signaling pathway (Kosarev et al., 2002; Ravasi et al., 2003; Yang et al., 2021). The RING finger domain contains 40-60 amino acids arranged in a sequence of cysteine and histidine residues: C-X2-C-X9-39-C-X1-3-H-X2-3-C/H-X2-C-X4-48-C-X2-C, X stands for any aminoacid and it differs among the members of the RING finger family resulting in structural and functional diversity. The pattern of this sequence is similar to the zinc finger domainf (Fig. 2). The RING finger domain three-dimensional (3D) structure is based on “cross-braced” configuration of the cysteine and histidine that binds two of zinc ions. For

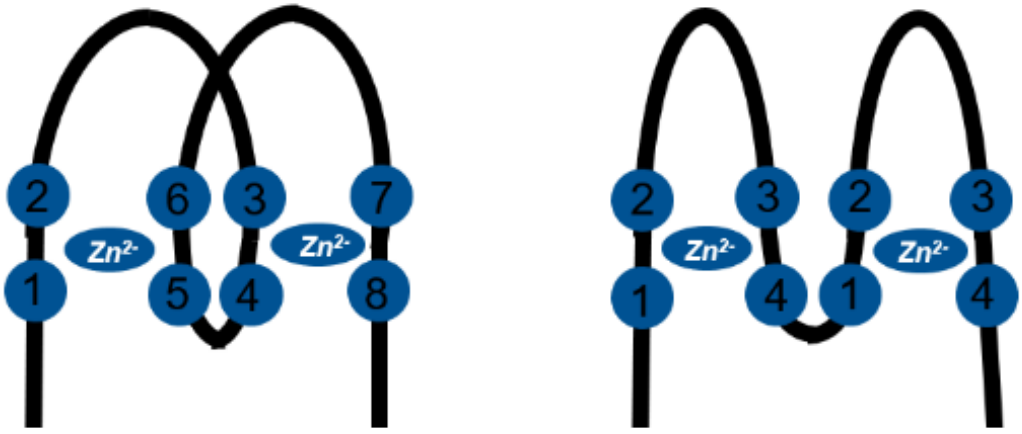

Figure 2. Schematic representation of RING and Zinc finger motif Scheme adapted from Fang, Lorick et al. 2003 RING finger is illustrated on left side, the "cross braced" fashion allow to keep 3 dimensional conformation of the proteins that belong to the RING family. Proteins Zinc fingers family (right side of the figure) do not form 3D structures; Zn^{2-} - Zinc, 1-8 numbers indicated placement of amino acids

better stabilization of the protein, the first and third pair of metal-binding residues take part in binding the first zinc ion that is commonly called site, where the second and fourth pair is binding the second zinc ion, commonly called site II. The conformation of the domain is also directly linked with the arrangement of alfa-helix loop, flexible loop that varies in the length, as well as beta-strands that are relatively short and separated from the previously mentioned loops. Overall, such an organization of amino acids is crucial to maintain the stability of the protein, correct folding, and essential interactions within the cell (Borden & Freemont, 1996; Capili et al., 2004; Kosarev et al., 2002; Sun et al., 2019).

The unique structure of RING finger domain makes it a promising target for many pharmaceutical companies to develop new drugs. The importance of novel therapeutic strategies is linked to well-known roles of these proteins in the development and progression of various cancer entities (Vedeld et al., 2020).

3.4.1 RING finger protein 43 (RNF43)

Ring finger protein 43 (*RNF43*) is one of the members of the RING finger family, which has been shown to have critical roles in various cellular processes. However, there

is still lack of understanding regarding its precise mechanism and function (Cai et al., 2022; Gao et al., 2017).

Localized on minus strand of the long arm of chromosome 17, specifically at position 22 (17q22), *RNF43* contains a regulatory region of two Wnt responsive elements within the second intron. The existence of this region indicates that the expression of *RNF43* is regulated by Wnt/β-catenin pathway (Tsukiyama et al., 2020; Yagyu et al., 2004).

The coding sequence of *RNF43* consists of 2352 base pairs (bp), which encodes a protein with 783 amino acids and a molecular mass of 85 kDa. As a transmembrane receptor, *RNF43* interacts with molecules on both sites of the cell across the membrane. The N-terminal region contains an extracellular domain with protease-associated (PA) domain, while the C-terminal region consists of a RING-type E3 domain as well as cytoplasmic serine-rich region. The characteristic RING domain takes part in transferring an ubiquitin from E2 ubiquitin conjugating enzyme to the acceptor of the protein. PA and RING finger domain together are a serine rich region strictly linked to the control of Frizzled receptor complex (Serra & Chetty, 2017; Yagyu et al., 2004).

Discovery of *RNF43* is strictly connected to the zinc finger protein 3 (*ZNFR3*). Both of the proteins are known for their role in downregulating Frizzled (Fzd) receptors located in the membrane. Regulation of these genes is based on presence of of R-spondin (RSpo) and the leucine rich repeat containing G protein-coupled receptor 4/5 (LGR4/5) complex. *RNF43* and *ZNFR3* are considered to be paralogues, however this classification is based on similar functions of both proteins within the biological processes. (Tsukiyama et al., 2021; Zebisch & Jones, 2015)

3.4.2 *RNF43* in various subtypes of a cancer

The importance of *RNF43* for tumor maintenance and development is evident in a variety of cancer entities, although its role may vary between different subtypes of tumor. While there is still a need to unravel the impact of the mutations in *RNF43* as well as the precise role of the coding protein and its interaction with signaling pathways; overall, *RNF43* appears to be an attractive target for novel drugs development.

Colorectal cancer (CRC) is a cancer type, where frequent mutations in Rnf43 were identified in tumor development and maintenance. The most common mutations are the hotspot mutations R117.fs (C6 repeat tract) in exon 3 and G659.fs (G7 repeat tract) in exon 9, which lead to synthesis of truncated RNF43 protein. Interestingly, Fang et al 2022

demonstrated a connection between the frameshift mutation G659.fs – which is one of the most common mutations of *RNF43* in CRC - and activation of PI3K/AKT signaling. This previously unknown role of *RNF43* gives a new insight into the functional consequences of inactivating *RNF43* mutations (Fang et al., 2022).

In gastric cancer (Bass et al. ,2014), mutations in *RNF43* lead to decreased activity or loss of function of the coding protein. Frequently mutated among patients with GC is connected with dysregulation in Wnt signaling and correlates with poorer outcome (Gao et al., 2017). A possible new role of *RNF43* was described by research of Neumeyer, 2021, which demonstrated a correlation between the depletion of *Rnf43* expression and increased resistance to chemotherapy due to defects in DNA damage response. They highlighted the necessity of including RNF43 in a panel used for screening patients with GC cancer since, which was primarily based on identifying RNF43 among mutated genes in their sequencing data (Neumeyer et al., 2021). Furthermore, based on analysis of deep whole-exome sequencing *RNF43 was* identified also in PDAC among genes significantly altered. Furthermore, Hosein et al 2022, investigated the impact of loss of *Rnf43* in GEMM with *Kras* as a driver oncogene and identified *Rnf43* as a tumor suppressor. Moreover, they were able to connect *Rnf43* loss of function with increased occurrence of cystic precursor lesions and change in tumor microenvironment. Their findings demonstrate that subset of patients with *Rnf43* mutation may benefit from immunotherapy (Hosein et al., 2022).

In CCA, downregulation and inactivation of *RNF43* contributes to tumor growth and poor prognosis of patients. However, the studies on the role of *RNF43* in CCA are still ongoing. Recent findings suggest tumor suppressive role not only in CCA (Pangestu et al., 2021), but also in ovarian cancer, where exome sequencing by Ryland, 2013 identified a high frequency of *RNF43* mutations spectrum in mucinous tumors of the ovary (Ryland et al., 2013).

Together, these findings indicate that *Rnf43* plays a critical role in various cancer entities, but that further research is warranted and needed to unravel its significance and the underlying mechanisms for tumor progression and development.

3.4.3 Role of *Rnf43* in canonical Wnt/β-catenin pathway

The Wnt signaling pathway is involved in several different crucial for regulation processes like cell growth, migration, and polarity as well as morphogenesis during embryonic development. Since Wnt pathway is highly conserved dysregulation in this pathway may lead to tumorigenesis (Ram Makena et al., 2019; Reya & Clevers, 2005). The interaction between Wnt protein and Frizzled-LRP5/6 receptor complex triggers intracellular events. As a consequence of Wnt binding to Frizzled-LRP5/6 receptor, the β-catenin destructive complex – consisting of the kinase glycogen synthase kinase 3b *(GSK-3b)*, scaffold protein axin, casein kinase 1 *(CK1*) and Adenomatus polypsis coli *(APC*) – is disassembled (Stamos & Weis, 2013). This leads to the accumulation of β-

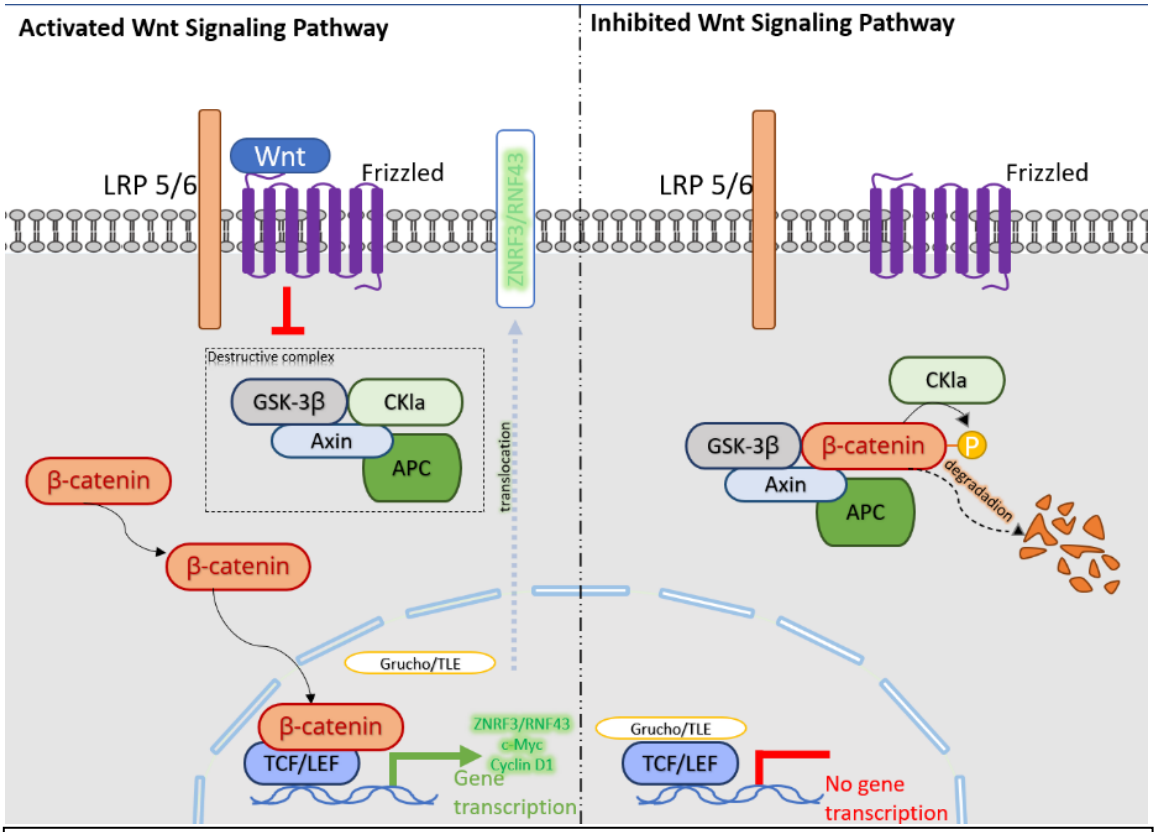

Figure 3. Schematic representation of Wnt pathway/ β-catenin Intercellular signal initiated by Wnt protein binding to FRZ receptor is sent and results in suppress activity of destructive complex that contains CK1, APC, GSK3β and Axin1. Access of β-catenin is translocated to nucleus and binds to TCF/LEF resulting in translocation of Groucho/TLE complex. Subsequently complex of β-catenin and TCF/LEF forms and activates transcription. *Rnf43* is one of the targeted genes, access of *Rnf43* is translocated to the cell membrane. *Rnf43* marks Frizzled-LRP5/6 receptor complex for ubiquitination witch results in inhibition of Wnt pathway.
In the absence of Wnt ligand destructive complex is formed and marks β-catenin for proteasomal degradation Transcription is inhibited.

catenin in the cytoplasm and its translocation to the nucleus, where Groucho/TLE complex is displaced to allow for interaction of β-catenin with members of the TCF/LEF transcription factor family, (Daniels & Weis, 2005). This cascade of events leads to expression of Wnt target genes such as cyclin D1, matrix metalloproteinase 7 (*MMP-7*), *c-myc* and vascular endothelial growth factor (*VEGF*) (Lecarpentier et al., 2019; Olsen et al., 2017). Thus, at the point when the expression of targeted genes occurs, *RNF43* as a downstream gene of Wnt signaling pathway is as well expressed. Accumulated RNF43 in the nucleus is translocated to the cell membrane, where it acts as ligase and marks Frizzled receptor for ubiquitination (Tsukiyama et al., 2020; Wang et al., 2016).

The necessity to prevent unconditional activation of Wnt signaling pathway is accomplished by negative regulation. *RNF43* together with *ZNRF3* promotes degradation of the Frizzled receptor (Tsukiyama et al., 2020; Wang et al., 2016). The lack of the Frizzled-LRP5/6 receptor complex on the surface of membrane directly blocks Wnt from binding. In the absence of signal from the binding of Wnt to the Frizzled receptor, the destructive complex is formed, which results in β-catenin being bound by this complex and thereby marked for ubiquitination and subsequent proteasomal degradation. The transcriptional activity is thereby inhibited, as β-catenin cannot translocate to the nucleus to activate transcription (Shang et al., 2017; Stamos & Weis, 2013).

3.5 Aims of the study

This thesis primarily revolves around elucidating the role of *Rnf43* in CBD cancer development and assess its potential as therapeutic target.

Rnf43 has been identified as one of the frequently mutated genes across various cancer subtypes. Following a prior *piggyBac* mutagenesis screen conducted by members of our research group (Falcomata et al., 2021), this particular gene was chosen for a comprehensive validation. The thesis encompasses an analysis of the conducted screen and it is coupled with *in vitro* studies on the effects of *Rnf43* loss in two GEMMs with different main driver oncogenes – *Pik3ca*^{H1047R} and *Kras*^{G12D}. Within these investigations, the current thesis underscores the significance of molecular pathways contributing to CBD cancer development. Two generated mouse models *Pdx1-Cre; LSL-Pik3ca*$^{H1047R/wt}$*; Rnf43* KO and *Pdx1-Cre; LSL-Kras*$^{G12D/wt}$*; Rnf43* KO are here described and used to address that question by assessing their survival, the developed tumor types, and their

respective histopathological analysis. Moreover, CBD-derived organoid culture was established to study the role of *Rnf43* KO on cell growth, the effect of this deleted gene on Wnt pathway and, by analyzing RNAseq data, evaluate the genes differently expressed in *Rnf43*-deficient organoid lines. Lastly, organoid lines were also used as an *in vitro* model to perform a large-scale drug screen to unveil potential novel therapies for CBD.

Through *in vitro* studies and conducted experiments, it was possible to present translational importance of *Rnf43* and its potential as a valuable therapeutic target. Although the full spectrum of *Rnf43* function still remains elusive, the present study sheds light on the translational importance of its loss-of-function for CBD cancer.

4. Materials

4.1 Technical Equipment

Table 1. Technical equipment

Device	Source
Analytical balance ABJ-NM/ABS-N	Kern & Sohn GmbH, Balingen, DE
Aperio Versa 8 Digital Scanner	Leica Microsystems, Heerburg
Autoclave VX-150	Systec GmbH, Linden, DE
Centrifuge 5415	Eppendorf AG, Hamburg, DE
Centrifuge 5427 R	Eppendorf AG, Hamburg, DE
Centrifuge Heraeus™ Multifuge™ X3 FR	Thermo Fisher Scientific Inc., Waltham, MA, USA
CLARIOstar® plate reader	BMG Labtech, Ortenberg
CO_2 incubator HERAcell™ VIOS 250i	Thermo Fisher Scientific, Massachusetts
Cryogenic sample storage	Worthington Industries, Inc., Columbus, OH, USA
Dewar carrying flask, type B	KGW-Isotherm, Karlsruhe
Digital orbital shaker	Heathrow Scientific, Vernon Hills, IL, USA
Electrophoresis power supply Consort EV243	AlphaMetrix Biotech GmbH, Rödermark, DE
Electrophoresis power supply Consort EV243	Amersham Biosciences Corp., Little Chalfont, GB
Electrophoresis power supply PowerPac 1000	Bio-Rad Laboratories Inc., Hercules, CA, USA
Electrophoresis power supply PowerPac™ HC	Bio-Rad Laboratories Inc., Hercules, CA, USA
FLUOstar OPTIMA	(BMG Labtech GmbH, Ortenberg, Germany
Freezer	Liebherr, Bulle, DE
Fridge	Siemens AG, Munich, DE
Gel documentation system UVP UVsolo touch	Analytik Jena GmbH, Jena, DE
Gel Electrophoresis System Biometra Compact L/XL	Analytik Jena GmbH, Jena, DE
Gel tray SUNRISE™	Life Technologies, Carlsbad
GloMax Explorer Multimode Microplate Reader	Promega, Walldorf, Germany
Heated paraffin embedding module HistoCore	Leica Microsystems GmbH, Wetzlar, DE

Arcadia H	
HERA freeze™ HFU T Series	Thermo Fisher Scientific Inc., Waltham, MA, USA
Homogenizer SilentCrusher M with tool 6F	Heidolph Instruments GmbH & Co. KG, Schwabach, DE
Incubator 206	MELAG oHG, Berlin, DE
Incubator U26	MELAG oHG, Berlin, DE
Laminar flow	Memmert, GmbH + Co.KG, Büchenbach, DE
Magnetic stirrer, Ikamag® RCT	IKA® Werke GmbH & Co. KG, Staufen, DE
Microcentrifuge LLG-uniCFUGE 2	Faust Laborbedarf AG, Schaffhausen, CH
Microscope Axio Vert.A1	Carl Zeiss AG, Oberkochen, DE
Microscope DM IL LED	Leica Microsystems GmbH, Wetzlar, DE
Microscope ICC50 W	Leica Microsystems GmbH, Wetzlar, DE
Microtome Microm HM355S	Thermo Fisher Scientific Inc., Waltham, MA, USA
Microwave MAX	Whirlpool, Benton Harbor, MI, USA
Mixer RT-3D	Fröbel Labortechnik GmbH, Lindau, DE
NanoPhotometer® N60	Implen GmbH, Munich, DE
Orbital shaker Rotamax 120	Heidolph, Instruments GmbH & Co. KG, Schwabach, DE
Paraffin tissue floating bath SB80	Microm, Walldorf, DE
pH meter pH 50+ DHS	XS Instruments, Carpi, IT
Precision balance PCB	Kern & Sohn GmbH, Balingen, DE
Qubit® 2.0 Fluorometer	Invitrogen GmbH, Karlsruhe, DE
Scanner Perfection V370 Photo	Seiko Epson Corp., Suwa, JP
Stemi SV 11 stereomicroscope	Carl Zeiss AG, Oberkochen, DE
Thermal Cycler Biometra TOne	Analytik Jena GmbH, Jena, DE
Thermomixer comfort	Eppendorf AG, Hamburg, DE
Tissue processor ASP300S	Leica Microsystems GmbH, Wetzlar, DE
Vertical laminar flow cabinet ENVAIReco® Safe Comfort	ENVAIR Ltd., Haslingden, GB
Vortex-Genie™ 2	Scientific Industries Inc., Bohemia, NY, USA
Water bath 1083	GFL Gesellschaft für Labortechnik mbH, Burgwedel, DE

4.2 Consumables

Table 2. Consumables

Consumables	Source
25 mL pipetting reservoir	Argos Technologies, Vernon Hills, IL, USA
FrameStar 384 plate Azenta Life Sciences, Wotton, UK	Thermo Fisher Scientific, Munich, Germany
Aluminum foil	Carl Roth GmbH & Co. KG, Karlsruhe, DE
Cell scrapers	Sarstedt Inc, Nümbrecht, DE
Combitips® advanced 0.2, 1 and 2.5 mL	Eppendorf AG, Hamburg, DE
Conical tubes 15 and 50 mL	Greiner Bio-One, Kremsmünster, AT
Cover slips 18 x 18 mm	Paul Marienfield GmbH & Co. KG, Lauda-Königshofen, DE
Cover slips 24 x 50 mm	Thermo Fisher Scientific Inc., Waltham, MA, USA
CryoPure tubes	Sarstedt AG & Co., Nümbrecht, DE
Dewar carrying flask, type B	KGW-Isotherm, Karlsruhe, DE
Disposable scalpels	Feather Safety Razor Co. Ltd., Osaka, JP
Dry ice	Linde plc, Dublin, IE
Falcon® 6-, 12-, 24- and 96-well clear flat bottom cell culture microplates	Corning Inc., Corning, NY, USA
Glass staining dish and 20-slide unit	VWR International Ltd., Radnor, PA, USA
Hand Tally Counter	neoLab Migge GmbH, Heidelberg, DE
Ice block COOL PACK	Coolike Regnery GmbH, Bensheim, DE
Lab glassware	Schott AG, Mainz, DE
Microscope slides Superfrost®	Thermo Fisher Scientific Inc., Waltham, MA, USA
Microtome blades S35 and C35	Feather Safety Razor Co. Ltd., Osaka, JP
Multilpy®-µStrip PCR reaction tubes	Sarstedt AG & Co., Nümbrecht, DE
Multipette® stream	Eppendorf AG, Hamburg, DE
Neubauer hemocytometer 0.100 mm Depth	Assistent, Sondheim vor der Rhön, DE
Paper role	Mobiloclean Handelsgruppe GmbH & Co. KG, Munich, DE
Parafilm™ M Laboratory Wrapping Film	Bemis Company Inc., Neenah, WI, USA
Pasteur pipettes	Hirschmann Laborgeräte GmbH & Co. KG, Eberstadt, DE

Petri dishes 10 and 15 cm	Sarstedt AG & Co., Nümbrecht, DE
Pipette tips 10, 100, 200 and 1000 µL	Sarstedt AG & Co., Nümbrecht, DE
Pipettes Reference®, Research®	Eppendorf AG, Hamburg, DE
Plastic ruler 30 cm	Möbius & Ruppert GmbH & Co. KG, Erlangen, DE
Precision wipes	Kimberly-Clark Worldwide Inc., Irving, TX, USA
Reaction tubes 0.5, 1.5 and 2 mL	Sarstedt AG & Co., Nümbrecht, DE
Rotilabo®-folded filters type 113P	Carl Roth GmbH & Co. KG, Karlsruhe, DE
Rotilabo®-stirring magnets set I	Carl Roth GmbH & Co. KG, Karlsruhe, DE
Safe-lock tubes BioPur® 1.5 and 2 mL	Eppendorf AG, Hamburg, DE
Sample vials PE, Ø External 14 mm, volume 2,5 mL (for cryopreserved tissues)	Carl Roth GmbH & Co. KG, Karlsruhe, DE
Serological pipettes 5, 10, 25 and 50 mL	Greiner Bio-One, Kremsmünster, AT
Single use needles Sterican® 20, 26 and 27 G	B. Braun Melsungen AG, Melsungen, DE
Single use syringes Omnifix® 1 mL	B. Braun Melsungen AG, Melsungen, DE
Slide storage box 25 and 100 slides	Sigma-Aldrich, St. Louis, MO, USA
Stripettor™ Ultra	Corning Inc., Corning, NY, USA
Surgical instruments	Thermo Fisher Scientific Inc., Waltham, MA, USA
Tissue culture flasks 25, 75 and 175 cm^2	Greiner Bio-One, Kremsmünster, AT
Tissue embedding cassettes Q Path® MacroStar VI and VIII	VWR International Ltd., Radnor, PA, USA
Tissue strong 100V	Lucart Professional, Villa Basilica, IT

4.3 Chemicals and Reagents

Table 3. Chemicals and reagents

Reagent	**Source**
1,4-Dithiothreitol (DTT) (order nr. 6908.1)	Carl Roth GmbH + Co. KG, Karlsruhe
100%, 96%, 80% and 70% Ethanol (EtOH) Artikelnummer 27698 ,27688, 27670 and 27669	Otto Fischar GmbH & Co. KG, Saarbrücken, DE
2-Mercaptoethanol, 98% Beilstein No.: 773648	Sigma-Aldrich Chemie GmbH, Munich
2-Propanol (isopropanol) order nr. 6752.1	Carl Roth GmbH + Co.
3,3'-Diaminobenzidine (DAB) peroxidase substrate kit	Vector Laboratories Inc., Burlingame, CA, USA

RRID:AB_2336382	
3,3,5-Triiodo-L-thyronine (T-073-1ML)	Sigma-Aldrich, Saint Luis, USA
Agarose	Sigma-Aldrich Chemie GmbH, Munich
Antigen unmasking solution, citric acid based (pH 6.0) RRID:AB_2336226	Vector Laboratories Inc., Burlingame, CA, USA
Aqua sterile water	B. Braun Melsungen AG, Melsungen, DE
Avidin/Biotin blocking kit RRID:AB_2336231	Vector Laboratories Inc., Burlingame, CA, USA
Bovine Pituitary extract (Product Number 354123)	Corning Inc., Corning, NY, USA
Cell Recovery Solution (Product Number 354253)	Corning, Corning, USA
Cholera toxin RRID:AB_258833	C8052, Sigma-Aldrich
Collagenase type 1, 2, (Catalog No. LS004194, LS004174)	Worthington Biochemical Corporation, Lakewood, NJ, USA
Dexamethasone (Product Number D4902-25MG)	D4902-25MG Sigma-Aldrich
D-Glucose	#15023-21, Gibco
Dimethylsulfoxide (DMSO) (HN47.1)	Carl Roth GmbH + Co. KG, Karlsruhe
DMSO (C6164)	AppliChem GmbH, Darmstadt, DE
dNTP mix, 10mM each (R0191)	Fermentas GmbH, St. Leon-Rot
Dulbecco's phosphate buffered saline (PBS) (D8537-500ML)	Sigma-Aldrich, St. Louis, MO, USA
Dulbecco's phosphate buffered saline (PBS) powder (D5652-10L)	Sigma-Aldrich, St. Louis, MO, USA
EGF (#315-09,)	Peprotech
Eosin 2% w/v (S007-500ML)	HiMedia Laboratories Pvt. Ltd., Mumbai, IN
Ethanol absolute 99.8% (32205-1L-M)	Sigma-Aldrich, St. Louis, MO, USA
Ethidium bromide (E1510-10ML)	Sigma-Aldrich Chemie GmbH, Munich
Ethylenediaminetetraacetic acid (EDTA) (798681-100G)	Sigma-Aldrich, St. Louis, MO, USA
Fetal bovine serum (FBS) Superior (F2442-500ML)	Sigma-Aldrich, St. Louis, MO, USA
Fetal calf serum (FCS) RRID:SCR_018769	Sigma-Aldrich, St. Louis, MO, USA
Forene® isoflurane	Abbott GmbH & Co. KG, Ludwigshafen, DE
GeneRuler™ 100 bp DNA ladder DNA ladder	Fermentas GmbH, St. Leon-Rot, DE

Gibco Advanced DMEM F12 (cat. No.12634010)	Invitrogen, Carlsbad, USA
Glycerol	Merck, Darmstadt, DE
Glycine (G5417-1KG)	Sigma-Aldrich, St. Louis, MO, USA
HEPES Pufferan® (EG-Nr. 230-907-9)	Carl Roth GmbH + Co. KG, Karlsruhe
Hydrochloric acid (HCl) 37% (320331-500ML)	Sigma-Aldrich, St. Louis, MO, USA
Hydrogen peroxide (H2O2) 30% (107209)	Merck, Darmstadt, DE
ITS + premix (354351)	Corning, Corning, USA
Magnesium chloride (order no. KK36.2)	Carl Roth GmbH & Co. KG, Karlsruhe, DE
Matrigel ®Matrix (354230)	Corning MA, USA
Methanol (order no. 8388.2)	Carl Roth GmbH & Co. KG, Karlsruhe, DE
Nicotinamide N3376-100G,	Sigma Aldrich
Nonidet P40	Roche Deutschland Holding GmbG, Grenzach-Wyhlen, DE
Nu-Serum IV (#355504)	Corning
Penicillin-Streptomycin (P0781-50ML)	Sigma-Aldrich, St. Louis, MO, USA
Proteinase K, recombinant, PCR grade	AppliChem GmbH, Darmstadt, DE
QuantiFast® SYBR® green PCR master mix (cat no. A46112)	Qiagen GmbH, Hilden
Reaction buffer S (for PCR)	Peqlab Biotechnologie GmbH, Erlangen, DE
RnaseA	Fermentas GmbH, St. Leon-Rot
RNase-free DNase set (ID: 79254)	Qiagen GmbH, Hilden
Rocki (Y27632) (order no. 688000)	Y0503, Sigma Aldrich
ROTI®Histofix 4% *(order no. P087.6)	Carl Roth GmbH & Co. KG, Karlsruhe, DE
ROTI®Histol (order no. 6640.1)	Carl Roth GmbH & Co. KG, Karlsruhe, DE
Sodium chloride (NaCl) (order no 1064040500)	Merck KGaA, Darmstadt
Sodium hydroxide solution (NaOH)	AppliChem GmbH, Darmstadt, DE
TaqMan® reverse transcription reagents (N8080234)	Applied Biosystems, Inc., Carlsbad, CA, USA
TEMED (2367.1)	Carl Roth GmbH + Co. KG, Karlsruhe
Tris Pufferan® (4855.2)	Carl Roth GmbH + Co. KG, Karlsruhe

Tris-Acetate-EDTA (TAE) buffer 50x	Klinikum rechts der Isar der TUM-Krankenhausapotheke, Munich, DE
Triton® X-100	Sigma-Aldrich, St. Louis, MO, USA
TrypLETM Express Enzyme (1x), 100 mL (12604013)	Thermo Fisher Scientific, Munich, Germany
Tween® 20 (P1379)	Sigma-Aldrich, St. Louis, MO, USA
Vectastain® elite ABC kit RRID:AB_2336825	Vector Laboratories Inc., Burlingame, CA, USA

4.4 Drugs

Table 4. Drugs used for large drug screen performer on organoid lines.

Product Name	**Target**	**Pathway**	**Formula**
Linifanib (ABT-869)	CSF-1R,PDGFR,VEGFR	Protein Tyrosine Kinase	C21H18FN5O
Veliparib (ABT-888)	PARP	DNA Damage	C13H16N4O
Axitinib	c-Kit,PDGFR,VEGFR	Protein Tyrosine Kinase	C22H18N4OS
Saracatinib (AZD0530)	Src	Angiogenesis	C27H32ClN5O5
Roxadustat (FG-4592)	HIF	Angiogenesis	C19H16N2O5
Selumetinib (AZD6244)	MEK	MAPK	C17H15BrClFN4O3
Nintedanib (BIBF 1120)	FGFR,PDGFR,VEGFR	Protein Tyrosine Kinase	C31H33N5O4
Cediranib (AZD2171)	VEGFR	Protein Tyrosine Kinase	C25H27FN4O3
Lapatinib (GW-572016) Ditosylate	EGFR,HER2	Protein Tyrosine Kinase	C43H42ClFN4O10S3
Panobinostat (LBH589)	HDAC	Epigenetics	C21H23N3O2
Sorafenib Tosylate	PDGFR,Raf,VEGFR	MAPK	C28H24ClF3N4O6S
Tozasertib (VX-680, MK-0457)	Aurora Kinase	Cell Cycle	C23H28N8OS
Y-27632 2HCl	Autophagy,ROCK	Cell Cycle	C14H23Cl2N3O
Elesclomol (STA-4783)	HSP (e.g. HSP90)	Cytoskeletal Signaling	C19H20N4O2S2
Entinostat (MS-275)	HDAC	Epigenetics	C21H20N4O3
Enzastaurin (LY317615)	PKC	TGF-beta/Smad	C32H29N5O2
Olaparib (AZD2281, Ku-0059436)	PARP	DNA Damage	C24H23FN4O3
Nutlin-3	E3 Ligase ,Mdm2	Apoptosis	C30H30Cl2N4O4
Masitinib (AB1010)	c-Kit,PDGFR	Protein Tyrosine Kinase	C28H30N6OS
Pictilisib (GDC-0941)	PI3K	PI3K/Akt/mTOR	C23H27N7O3S2
Crizotinib (PF-02341066)	ALK,c-Met	Protein Tyrosine Kinase	C21H22Cl2FN5O
Luminespib (AUY-922, NVP-AUY922)	HSP (e.g. HSP90)	Cytoskeletal Signaling	C26H31N3O5
ZSTK474	PI3K	PI3K/Akt/mTOR	C19H21F2N7O2
SB216763	GSK-3	PI3K/Akt/mTOR	C19H12Cl2N2O2
SB202190 (FHPI)	p38 MAPK	MAPK	C20H14FN3O
MK-2206 2HCl	Akt	PI3K/Akt/mTOR	C25H23Cl2N5O
Vismodegib (GDC-0449)	Hedgehog/Smoothened	Stem Cells & Wnt	C19H14Cl2N2O3S
Brivanib (BMS-540215)	FGFR,VEGFR	Protein Tyrosine Kinase	C19H19FN4O3

Iniparib (BSI-201)	PARP	DNA Damage	C7H5IN2O3
Abexinostat (PCI-24781)	HDAC	Cytoskeletal Signaling	C21H23N3O5
Linsitinib (OSI-906)	IGF-1R	Protein Tyrosine Kinase	C26H23N5O
KU-55933 (ATM Kinase Inhibitor)	ATM/ATR	DNA Damage	C21H17NO3S2
GSK1904529A	IGF-1R	Protein Tyrosine Kinase	C44H47F2N9O5S
Quisinostat (JNJ-26481585) 2HCl	HDAC	Epigenetics	C21H28Cl2N6O2
Vatalanib (PTK787) 2HCl	VEGFR	Protein Tyrosine Kinase	C20H17Cl3N4
Danusertib (PHA-739358)	Aurora Kinase,Bcr-Abl,c-RET,FGFR	Cell Cycle	C26H30N6O3
GSK690693	Akt	PI3K/Akt/mTOR	C21H27N7O3
SRT1720 HCl	Sirtuin	Epigenetics	C25H24ClN7OS
YM155 (Sepantronium Bromide)	Survivin	Apoptosis	C20H19BrN4O3
Alisertib (MLN8237)	Aurora Kinase	Cell Cycle	C27H20ClFN4O4
Barasertib (AZD1152-HQPA)	Aurora Kinase	Cell Cycle	C26H30FN7O3
Paclitaxel	Autophagy,Microtubule Associated	Cytoskeletal Signaling	C47H51NO14
PLX-4720	Raf	MAPK	C17H14ClF2N3O3S
Ganetespib (STA-9090)	HSP (e.g. HSP90)	Cytoskeletal Signaling	C20H20N4O3
Onalespib (AT13387)	HSP (e.g. HSP90)	Cytoskeletal Signaling	C24H31N3O3
ABT-751 (E7010)	Microtubule Associated	Cytoskeletal Signaling	C18H17N3O4S
JNJ-26854165 (Serdemetan)	E3 Ligase ,p53	Apoptosis	C21H20N4
Plinabulin (NPI-2358)	VDA	Angiogenesis	C19H20N4O2
Regorafenib (BAY 73-4506)	c-RET,VEGFR	Protein Tyrosine Kinase	C21H15ClF4N4O3
XAV-939	Wnt/beta-catenin	Stem Cells & Wnt	C14H11F3N2OS
Anastrozole	Aromatase	Endocrinology & Hormones	C17H19N5
CUDC-101	EGFR,HDAC,HER2	Epigenetics	C24H26N4O4
TAK-700 (Orteronel)	P450 (e.g. CYP17)	Metabolism	C18H17N3O2
Decitabine	DNA Methyltransferase	Epigenetics	C8H12N4O4
Doxorubicin (Adriamycin) HCl	Topoisomerase	DNA Damage	C27H30ClNO11
Fluorouracil (5-Fluoracil, 5-FU)	DNA/RNA Synthesis	DNA Damage	C4H3FN2O2
PFI-1 (PF-6405761)	Epigenetic Reader Domain	Epigenetics	C16H17N3O4S
OSI-930	c-Kit,CSF-1R,VEGFR	Protein Tyrosine Kinase	C22H16F3N3O2S
Etoposide	Topoisomerase	DNA Damage	C29H32O13
KU-0063794	mTOR	PI3K/Akt/mTOR	C25H31N5O4
Topotecan HCl	Topoisomerase	DNA Damage	C23H24ClN3O5
Vincristine sulfate	Autophagy,Microtubule Associated	Cytoskeletal Signaling	C46H58N4O14S
Celecoxib	COX	Neuronal Signaling	C17H14F3N3O2S
Avagacestat (BMS-708163)	Beta Amyloid,Gamma-secretase	Proteases	C20H17ClF4N4O4S
Vemurafenib (PLX4032, RG7204)	Raf	MAPK	C23H18ClF2N3O3S
BX-795	IκB/IKK,PDK	PI3K/Akt/mTOR	C23H26IN7O2S
BX-912	PDK	PI3K/Akt/mTOR	C20H23BrN8O

Ki16425	LPA Receptor	GPCR & G Protein	C23H23ClN2O5S
Glesatinib?(MGCD265)	c-Met,Tie-2,VEGFR	Protein Tyrosine Kinase	C26H20FN5O2S2
Rigosertib (ON-01910)	PLK	Cell Cycle	C21H24NNaO8S
Bafetinib (INNO-406)	Bcr-Abl	Angiogenesis	C30H31F3N8O
Ruxolitinib (INCB018424)	JAK	JAK/STAT	C17H18N6
Pelitinib (EKB-569)	EGFR	Protein Tyrosine Kinase	C24H23ClFN5O2
Droxinostat	HDAC	Cytoskeletal Signaling	C11H14ClNO3
Zileuton	Lipoxygenase	Metabolism	C11H12N2O2S
Ispinesib (SB-715992)	Kinesin	Cytoskeletal Signaling	C30H33ClN4O2
Tipifarnib	Transferase	Metabolism	C27H22Cl2N4O
Zibotentan (ZD4054)	Endothelin Receptor	GPCR & G Protein	C19H16N6O4S
SP600125	JNK	MAPK	C14H8N2O
AZD6482	PI3K	PI3K/Akt/mTOR	C22H24N4O4
Orantinib (TSU-68, SU6668)	PDGFR	Protein Tyrosine Kinase	C18H18N2O3
PIK-93	PI3K	PI3K/Akt/mTOR	C14H16ClN3O4S2
Ponatinib (AP24534)	Bcr-Abl,FGFR,PDGFR,VEGFR	Angiogenesis	C29H27F3N6O
Pracinostat (SB939)	HDAC	Cytoskeletal Signaling	C20H30N4O2
Adavosertib （MK-1775）	Wee1	Cell Cycle	C27H32N8O2
Quizartinib (AC220)	FLT3	Angiogenesis	C29H32N6O4S
AZD7762	Chk	Cell Cycle	C17H19FN4O2S
CP-673451	PDGFR	Protein Tyrosine Kinase	C24H27N5O2
Selisistat (EX 527)	Sirtuin	Epigenetics	C13H13ClN2O
Dapagliflozin	SGLT	GPCR & G Protein	C21H25ClO6
PHT-427	Akt,PDK	PI3K/Akt/mTOR	C20H31N3O2S2
BMS-777607	TAM Receptor,c-Met	Protein Tyrosine Kinase	C25H19ClF2N4O4
KU-60019	ATM/ATR	DNA Damage	C30H33N3O5S
Allopurinol Sodium	ROS	Immunology & Inflammation	C5H4N4NaO+
Tretinoin	Retinoid Receptor	Metabolism	C20H28O2
Busulfan	DNA alkylator	DNA Damage	C6H14O6S2
Azacitidine	DNA Methyltransferase	DNA Damage	C8H12N4O5
AICAR (Acadesine)	AMPK	PI3K/Akt/mTOR	C9H14N4O5
Fluvastatin Sodium	HMG-CoA Reductase	Metabolism	C24H25FNNaO4
Maraviroc	CCR	Microbiology	C29H41F2N5O
Cyclophosphamide Monohydrate	DNA alkylator	DNA Damage	C7H17Cl2N2O3P
AZD1480	JAK	JAK/STAT	C14H14ClFN8
PF-4708671	S6 Kinase	PI3K/Akt/mTOR	C19H21F3N6
Ixazomib Citrate (MLN9708)	Proteasome	Proteases	C20H23BCl2N2O9
SB743921 HCl	Kinesin	Cytoskeletal Signaling	C31H34Cl2N2O3
GSK461364	PLK	Cell Cycle	C27H28F3N5O2S
SGI-1776 free base	Pim	JAK/STAT	C20H22F3N5O
BMS-794833	c-Met,VEGFR	Protein Tyrosine Kinase	C23H15ClF2N4O3
NVP-BHG712	Bcr-Abl,Ephrin receptor,Raf,Src	Protein Tyrosine Kinase	C26H20F3N7O
Mubritinib (TAK 165)	HER2	Protein Tyrosine Kinase	C25H23F3N4O2

Irinotecan HCl Trihydrate	Topoisomerase	DNA Damage	C33H45ClN4O9
Galunisertib (LY2157299)	TGF-beta/Smad	TGF-beta/Smad	C22H19N5O
Volasertib (BI 6727)	PLK	Cell Cycle	C34H50N8O3
Degrasyn (WP1130)	Bcr-Abl,DUB	Angiogenesis	C19H18BrN3O
Silmitasertib (CX-4945)	Casein Kinase	Metabolism	C19H12ClN3O2
Colchicine	Microtubule Associated	Cell Cycle	C22H25NO6
Luteolin	PDE	Metabolism	C15H10O6
Indirubin	GSK-3	PI3K/Akt/mTOR	C16H10N2O2
Apocynin	NADPH-oxidase	Others	C9H10O3
Lonidamine	Others	Others	C15H10Cl2N2O2
Rabusertib (LY2603618)	Chk	Cell Cycle	C18H22BrN5O3
GW3965 HCl	Liver X Receptor	Others	C33H32Cl2F3NO3
Rebastinib (DCC-2036)	Bcr-Abl	Angiogenesis	C30H28FN7O3
MK-0752	Beta Amyloid,Gamma-secretase	Proteases	C21H21ClF2O4S
PF-3845	FAAH	Metabolism	C24H23F3N4O2
PF-00562271	FAK	Angiogenesis	C27H26F3N7O6S2
Trametinib (GSK1120212)	MEK	MAPK	C26H23FIN5O4
Ibrutinib (PCI-32765)	BTK	Angiogenesis	C25H24N6O2
Apitolisib (GDC-0980, RG7422)	mTOR,PI3K	PI3K/Akt/mTOR	C23H30N8O3S
A-769662	AMPK,Fatty Acid Synthase	PI3K/Akt/mTOR	C20H12N2O3S
KX2-391	Src	Angiogenesis	C26H29N3O3
Dibenzazepine (YO-01027)	Gamma-secretase	Proteases	C26H23F2N3O3
AZ 628	Raf	MAPK	C27H25N5O2
Milciclib (PHA-848125)	CDK	Cell Cycle	C25H32N8O
Dinaciclib (SCH727965)	CDK	Cell Cycle	C21H28N6O2
Dalcetrapib (JTT-705, RO4607381)	CETP	Metabolism	C23H35NO2S
CPI-613	Dehydrogenase	Metabolism	C22H28O2S2
RITA (NSC 652287)	E3 Ligase ,p53	Apoptosis	C14H12O3S2
Vistusertib (AZD2014)	mTOR	PI3K/Akt/mTOR	C25H30N6O3
Tofacitinib (CP-690550,Tasocitinib)	JAK	JAK/STAT	C16H20N6O
Sotrastaurin	PKC	TGF-beta/Smad	C25H22N6O2
AZD4547	FGFR	Angiogenesis	C26H33N5O3
Dabrafenib (GSK2118436)	Raf	MAPK	C23H20F3N5O2S2
Sapanisertib (INK 128, MLN0128)	mTOR	PI3K/Akt/mTOR	C15H15N7O
Alpelisib (BYL719)	PI3K	PI3K/Akt/mTOR	C19H22F3N5O2S
BI-D1870	S6 Kinase	PI3K/Akt/mTOR	C19H23F2N5O2
Carfilzomib (PR-171)	Proteasome	Proteases	C40H57N5O7
BML-190	Cannabinoid Receptor	GPCR & G Protein	C23H23ClN2O4
U-104	Carbonic Anhydrase	Metabolism	C13H12FN3O3S
GW441756	Trk receptor	Protein Tyrosine Kinase	C17H13N3O
BAY 11-7082	E2 conjugating,IκB/IKK	NF-κB	C10H9NO2S
GW9662	PPAR	DNA Damage	C13H9ClN2O3

Apoptosis Activator 2	Caspase	Apoptosis	C15H9Cl2NO2
Cabozantinib malate (XL184)	TAM Receptor,VEGFR	Protein Tyrosine Kinase	C32H30FN3O10
Vinorelbine Tartrate	Microtubule Associated	Cytoskeletal Signaling	C53H66N4O20
Sulfabenzamide	Anti-infection	Microbiology	C13H12N2O3S
JNK-IN-8	JNK	MAPK	C29H29N7O2
b-AP15	DUB	Ubiquitin	C22H17N3O6
BAY-61-3606	Syk	Angiogenesis	C20H20Cl2N6O3
Binimetinib (MEK162, ARRY-162, ARRY-438162)	MEK	MAPK	C17H15BrF2N4O3
LCL161	IAP	Apoptosis	C26H33FN4O3S
GDC-0152	IAP	Apoptosis	C25H34N6O3S
Birinapant	IAP	Apoptosis	C42H56F2N8O6
GSK2656157	PERK	Apoptosis	C23H21FN6O
Oprozomib (ONX 0912)	Proteasome	Proteases	C25H32N4O7S
Tezacaftor?(VX-661)	CFTR	Transmembrane Transporters	C26H27F3N2O6
Pinometostat (EPZ5676)	Histone Methyltransferase	Epigenetics	C30H42N8O3
LY2090314	GSK-3	PI3K/Akt/mTOR	C28H25FN6O3
SGC 0946	Histone Methyltransferase	Epigenetics	C28H40BrN7O4
Ceritinib (LDK378)	ALK	Protein Tyrosine Kinase	C28H36ClN5O3S
IWR-1-endo	Wnt/beta-catenin	Stem Cells & Wnt	C26H21N3O3
GSK2334470	PDK	PI3K/Akt/mTOR	C25H34N8O
UNC1215	Epigenetic Reader Domain	Epigenetics	C32H43N5O2
GSK923295	Kinesin	Cytoskeletal Signaling	C32H38ClN5O4
IPA-3	PAK	Cytoskeletal Signaling	C20H14O2S2
PF-3758309	PAK	Cytoskeletal Signaling	C25H30N8OS
LGK-974	PORCN inhibitor	Wnt/beta-catenin	C23H20N6O
Cisplatin	inhibits DNA synthesis	Apoptosis	Cl2H6N2Pt
Erastin	Ferroptosis	Metabolism	C30H31ClN4O4
IWP-L6	Wnt/beta-catenin	Stem Cells & Wnt	C25H20N4O2S2
AZ191	DYRK	Protein Tyrosine Kinase	C24H27N7O
Ribociclib (LEE011)	CDK	Cell Cycle	C23H30N8O
WIKI4	Wnt/beta-catenin	Stem Cells & Wnt	C29H23N5O3S
OF-1	Epigenetic Reader Domain	Epigenetics	C17H18BrN3O4S
Napabucasin	STAT	JAK/STAT	C14H8O4
MS023	Histone Methyltransferase	Epigenetics	C17H25N3O
Gemcitabine HCl	DNA/RNA Synthesis,Autophagy	DNA Damage	C9H12ClF2N3O4
Oxaliplatin	DNA/RNA Synthesis	DNA Damage	C8H14N2O4Pt

4.5 Buffers and Solutions

Table 5. Buffers and solutions

Buffer or Solution	Component
10x Gitschier's Buffet	670 mM Tris, pH 8.8 166 mM Ammonium sulfate 67 mM Magnesium chloride Diluted in ddH_2O

Soriano lysis buffer	0.5% Triton™ X-100 10% 10x Gitschier's buffer 1% 2-Mercaptoethanol Diluted in ddH_2O 400 µg/mL Proteinase K (add prior to use) DTT (add prior to use)
SucRot solution (for PCR)	1.5 mg/mL Cresol red 100 mM Tris (pH 9.0) 30% D(+)-saccharose
Freezing medium	70% DMEM 20% FBS 10% DMSO
PDC medium	**Compounds** — **Final Concentration** AdDMEM/F12 — - D-Glucose — 5 mg/mL ITS + premix — 0.5% 3,3,5-Triiodo-L-thyronine — 5 nM Dexamethasone — 1 µM Cholera toxin — 100 ng/mL pen/strep — 1% Nu-Serum IV — 5% EGF — 20 ng/mL Bovine Pituitary extract — 25 µg/mL Nicotinamide — 10 mM Rocki (Y27632) (order no. 688000) — 10 µM (add directly after isolation and passaging –on the top of the media already added to wells with organoids)

4.6 Kits for molecular biology.

Table 6. Kits for molecular biology.

Kit	Source
CellTiter-Glo® (cat. no. G7570) Luminescent Cell Viability Assay	Promega, Walldorf, Germany
Dual Luciferase Reporter Assay System (cat no. E1910)	Promega, Walldorf, Germany
QIAshredder (cat no. 79654)	Qiagen GmbH, Hilden
Qubit® dsDNA BR assay kit (cat no. 74104 Q32850)	Thermo Fisher Scientific Inc., Waltham, MA, USA

RNeasy mini kit (cat no. 74104)	Qiagen GmbH, Hilden

4.7 Polymerase chain reactions (PCRs) and Primers

Primers used for Polymerase Chain Reaction were synthetized in external company - Eurofins MWG GmbH (Ebersberg, DE). Lyophilized of the primers was dissolved in aqua sterile water to a concentration of 10 mM. Working stock solutions of the primers were diluted in aqua sterile water to a concentration of 10 μM.

Table 7. Primers for genotyping and recombination PCRs

PCR name	Primer name	Sequence (5' → 3')
Pdx1-Cre	Pdx-Prom-UP	GCTCATTGGGAGCGGTTTTG
	PdxKON-LP1	CACGTGGTTTACCATGGAGC
	V-Cre-LP2	ACATCTTCAGGTTCTGCGGG
LSL-Kras^{G12D}	Kras-WT-UP1	CACCAGCTTCGGCTTCCTATT
	Kras-URP-LP1	AGCTAATGGCTCTCAAAGGAATGTA
	KrasG12Dmut-UP	CCATGGCTTGAGTAAGTCTGC
LSL-Pik3ca^{H1047R}	pGL3-pA-pause4645-UP	TGAATAGTTAATTGGAGCGGCCGCAATA
	PI3K-genotyp reverse	AAATAGCCGCAGGTCACAAAGTCTCCG
RNF43^{fl}	RNF43 L	GAAGCAGACAATGAAGCGAAT
	RNF43 F	TAGTGCCACACAGAGGACA
RNF43^{fl} recombination	RNF43 F	AAAGTCGCTCTGAGTTGTTAT
	RNF43 R	GAAGCAGACAATGAAGCGAAT
	RNF43 R (recombination)	CAATAGGGCTCTCTCACACG
Mycoplasma test	Forward 1	CGCCTGAGTAGTACGTTCGC
	Forward 2	CGCCTGAGTAGTACGTACGC
	Forward 3	TGCCTGGGTAGTACATTCGC
	Forward 4	TGCCTGAGTAGTACATTCGC
	Forward 5	CGCCTGAGTAGTATGCTCGC
	Forward 6	CACCTGAGTAGTATGCTCGC
	Forward 7	CGCCTGGGTAGTACATTCGC

	Reverse 1	GCGGTGTGTACAAGACCAGA
	Reverse 2	GCGGTGTGTACAAAACCAGA
	Reverse 3	GCGGTGTGTACAAACCACGA

Table 8. Primers for quantitative real time PCR.

Gene	Primer name	Sequence (5´ → 3´)	Origin
RNF43^{fl}	RNF43 forward	CCAGTGTGTGCCATCTGTCT	Mus musculus
	RNF43 reverse	GCAAGTCCGATGCTGGTATAG	

4.8 Plasmids

Table 9. Plasmids

Plasmids	Source
pGL3-Basic (RRID:Addgene_64784)	Promega, Walldorf, Germany
pGL3-Control (RRID:Addgene_21327)	Promega, Walldorf, Germany
pFOPflash (RRID:Addgene_12457)	Promega, Walldorf, Germany
pTOPflash (RRID:Addgene_12456)	Promega, Walldorf, Germany
Renilla plasmid (RRID:Addgene_27163)	Promega, Walldorf, Germany

4.9 Software

Table 10. Software.

Software	Source
Adobe Illustrator CC; RRID:SCR_010279	Adobe Inc., San José, CA, USA
R v3.6.2; RRID: SCR_001905	The R Foundation, Indianapolis, IN, USA
GraphPad Prism 8; RRID:SCR_002798	La Jolla, CA, USA
ImageScope Ver 12.4.2.5010 (RRID:SCR_020993)	Leica Microsystems CMS GmbH Wetzlar, Germany

Leica Application Suite X 3.4.2.18368; RRID:SCR_013673	Leica Microsystems CMS GmbH Wetzlar, Germany
Microsoft Excel; RRID:SCR_016137	Microsoft Corporation, Redmont WA, USA
PyRAT animal facility software v4.2-552	PyRAT animal facility software v4.2-552
SnapGene Viewer; RRID:SCR_015052	GSL Biotech LLC, Chicago, IL, USA
StepOne Software V2.3; RRID:SCR_014281	Thermo Fisher Scientific, Munich, Germany
ZEISS ZEN v2.3, RRID:SCR_013672	Carl Zeiss AG, Oberkochen, DE

5. Methods

5.1 Mouse experiments

All animal studies were conducted meeting the requirements of the European guidelines for the care by the Institutional Animal Care and Use Committees (IACUC) as well as by the local authorities of the Technical University of Munich and the Regional Government of Bavaria (Regierung von Oberbayern).

5.1.1 Mouse strains

Mouse models with conditional *Cre/loxP* sites were used to study tissue-specific mutagenesis. Therefore, mice carrying a gene silenced by a *loxP-stop-loxP (LSL)* were interbred with mice expressing the *Cre* recombinase under the control of a tissue-specific promoter.
This allows the conditional inactivation of a gene of interest or deletion of the *LSL* cassette for an activating expression of a target gene.

Pdx1-Cre (Hingorani et al., 2003) – Transgenic mouse strain kindly provided by Prof. David Tuveson (Cold Spring Harbor Laboratory, Princeton, NJ, USA), generated by the injection of the *Pdx1-Cre* transgene into fertilized oocytes (RRID:IMSR_JAX:034623).

LSL-Kras^{G12D} (Hingorani et al., 2003; Jackson et al., 2001) – Knock-in mouse strain kindly provided by Prof. Tyler Jacks (Massachusetts Institute of Technology, Cambridge, MA, USA)containinga*G12D* point mutation. It corresponds with a frequently found mutation in human cancers. After deletion of the *LSL* cassette mediated by a *Cre* recombinase, oncogenic Kras is expressed leading to a constitutive activation of the signaling pathway (RRID:IMSR_JAX:008179).

LSL-PIK3CA^{H1047R} (Eser et al., 2013) – Knock-in mouse strain generated in the laboratory of Prof. Dieter Saur. It consists of the*PIK3CA^{H1047R}* mutation silenced by a *LSL* cassette in located in the *Rosa26* locus. *Cre*-mediated deletion of the *loxP* sites lead to the activation of the PI3K signaling pathway (RRID:IMSR_JAX:016977).

Rnf43^{tm1Cle} (Koo et al., 2012) – Knock-out mouse strain kindly provided by Prof. Hans Clevers (Hubrecht Institute, Utrecht, Netherlands). It is a conditional knock-out mouse strain, in which 2 exons encoding the RING finger domain are flanked by *loxP* sites (RRID:MGI:5439367)

5.1.2 Genotyping

During weaning, 2–3 weeks old pups in after were marked by punching holes in their ears. Tissues from that procedure was collected for identification of the genotype. DNA was isolated from the biopsies and this genomic DNA was used for further analysis of the litter genotype (described in 5.3).

5.1.3 Mouse dissection

Mice were euthanized with MMF via i.p. prior to cervical dislocation. The body of the animal was weighed, and the tip of the tail was taken for confirmation of the genotype. All instruments were disinfected with 70% ethanol prior usage for dissection and the body of the animal fixed with pins. The abdomen was gently opened, and organs were carefully separated and washed with PBS) (Sigma, D8537-500ML). Macroscopic pictures were taken from all organs, and all macroscopically observed abnormalities described in the section protocol. Samples used for in vitro studies – to optimize organoid culture – were transferred in 1x phosphate-buffered saline (PBS) on ice to primary cell culture. Cryopreserved samples of pancreas and CBD (if there was enough material for studies) were taken and stored at -80°C until DNA/RNA isolation.
Rest of the organs were carefully harvested and fixed overnight in 4% Roti®Histofix (order no. P087.6) then FFPE processed and used for histopathological analysis.

5.2 Organoid Culture

Primary murine CBD, GB and pancreatic organoids were established from endogenous mouse model harboring relevant mutation for studying Common Bile Duct tumorigenesis.

5.2.1 Generation of CBD organoid lines

Isolation of organoids was performed under conditions as sterile as possible. During dissection, tissue pieces of CBD and pancreas were transferred to reaction tubes filled with cold PBS (Sigma, D8537-500ML) and kept on ice. Then, tissues were minced on Petri dishes with a scalpel and transferred into a 50 ml reaction tube with DMEM-F12 media (cat. No. 12634010) (5ml) and collagenase II (2mg/mL, LS004174). The reaction tube was incubated for approximately 30 minutes at 37 °C in a shaker at 500rpm. To remove the excess of collagenase II (LS004174), incubated tissue was centrifuged at 350 × g for 5 min at 4°C and washed by gentle pipetting with 10 ml of PBS (Sigma, D8537-500ML). After removal of the supernatant, the pellet was resuspended with 500µL of TrypLETM Express Enzyme (1x) (12604013) and incubated for 5 minutes at RT. For the final step of centrifugation (5 min at 4°C at 350 × g) the

solution was transferred to a 1.5ml reaction tube. The supernatant was carefully removed, and the pellet resuspended in 50µL of Matrigel (354230)/well (depending on size of the pellet). To allow the Matrigel (354230) dome to polymerize, the plate with the seeded organoids was incubated for approximately 15 minutes at 37 °C. In the following step, wells with the Matrigel (354230) domes were covered with 500µL of PDC media supplemented with Rock inhibitor (5 µl per well; 1:100; Sigma, Germany, order no. 688000).

5.2.2 Maintenance and passaging of the organoid lines

Depending on the individual growth of the isolated lines, organoids were kept at 37°C and 5% CO2 for approximately 6–9 days, with supplemented media exchanged every second day. For long-term organoid culture, PDC medium was not supplied with Rock (order no. 688000) inhibitor.

After reaching confluency, organoids were passaged. Medium used for the culture was removed and Matrigel (354230) domes were topped with 250 µl of cell recovery solution and the plate was incubated for 25–30 min on ice. To further dissolve the Matrigel (354230) domes, 500 µl of PBS (Sigma, D8537-500ML) was added to each well. The solution was then mechanically disrupted by vigorous pipetting and transferred to 1,5ml reaction tubes. After centrifugation at 350 × g for 5 min, supernatant was removed, and the pellet dissolved and kept for 5 min in 250 µl of TrypLE™ Express Enzyme (1X) (12604013) in the incubator at 37°C. After incubation, organoid lines were washed in l mL of PBS (Sigma, D8537-500ML) and centrifuged for 5 min at 4°C at 350 × g. The supernatant was carefully removed, and the pellet resuspended in 50µL of Matrigel (354230)/well. As mentioned above, PDC medium with Rock (order no. 688000) inhibitor was added after polymerization.

For well-established lines RNA/DNA pellets were collected and frozen for further experiments.

5.2.3 Viability assay – CellTiter Glo

Selected lines were seeded on precoated white clear-bottom 96-well plate with mix of Matrigel (354230) and PBS (Sigma, D8537-500ML) at a ratio of 1:4. 1000 cells per well were suspended in a mixture of Matrigel (354230) and PDC media at a ratio of 1:8 and seeded for a six days treatment. The plates were kept in the incubator at 37°C. After 24 hours first plate of the assay taken and topped with 25 µl CellTiter Glo (cat. no. G7570) previously thawed. The plate was covered with aluminum foil and incubated for 20 min at RT on the shaker at 300rpm. Afterwards, luminescence measurement was performed on a FLUOstar OPTIMA microplate reader with a gain of 2500. This step was repeated for each day of the experiment.

Additionally for 6 days of viability assay measurement the images of organoid formation were taken on each day of the assay on Leica microscope.

5.2.4 TOP/FOP-Flash luciferase reporter assay

Dual reporter assay is a system that allows to simultaneously measure two luciferase reporters in the same set-up of the experiment. It is used to measure the activity of Firefly luciferase, while co-transfected Renilla (RRID:Addgene_27163) luciferase serves as an internal control for normalization. The TOP/FOP-Flash luciferase reporter assay was developed to measure the activity of canonical Wnt signaling pathway directly connected with the transcriptional activity of TCF/LEF. Two specific reporters pTOPflash (RRID:Addgene_12456) and pFOPflash (RRID:Addgene_12457) were used for that purpose. The pTOPflash (RRID:Addgene_12456)reporter construct contains binding sites of TCF/LEF (CCTTTGATC), which drives the expression of luciferase. The pFOPflash reporter, on the other hand, contains mutated binding sites for TCF/LEF, which prevents transcriptional activity and thereby serves as a control of unspecific background activity of the assay.

A 24- well plate was precoated with Matrigel (354230) and PBS (Sigma, D8537-500ML) mixture at a ratio of 1:5. Organoids were suspended in the mixture of Matrigel (354230) to PDC media in a ratio of 1:10 and 10 000 cells were seeded in each well. This step allows higher efficiency of transfection and at the same time formation of 3D lines. Prepared plate was incubated for 24 hours at 37°C in the incubator. Lines were transfected in triplicates with 100 ng pTOPflash (RRID:Addgene_12456) or pFOPflash (RRID:Addgene_12457) plasmid (per well), 10 ng Renilla (RRID:Addgene_27163) plasmid (per well). As additional control of the efficiency of transfection two additional plasmids were used pGL3-Control (RRID:Addgene_21327) and pGL3-Basic (RRID:Addgene_64784). Also, for transfection with this plasmid 100 ng per well of each was used together with 10 ng Renilla (RRID:Addgene_27163) plasmid also per well. For each well lipofectamine mix was prepared by diluting Lipofectamine 2000 1:25 in Opti-MEM (GIBCO®, cat. No. 31985062) without serum. Mix was incubated at RT for 5 min and distributed to each reaction tube with prepared mixes of plasmids. After 25 min 50 µl of the mixture was added to each well of triplicates of organoid lines seeded in 24 well plate. Transfected plate was kept in incubator at 37 °C and 5 % CO2 for 48 h. After incubation organoids were gently washed with 1x PBS (Sigma, D8537-500ML and lysed with 100 µl of 1x Passive lysis buffer added to each well. Lysed plate was kept for 30 min on a shaking platform. For measurement of the luciferase activities 20 µl of

lysate from each well was transferred to a white round-bottom 96-well plate. All reagents from the Dual Luciferase Reporter assay system kit (cat no. E1910) were prepared according to the instructions provided by manufacturer. Samples were measured using GloMax Explorer Multimode Microplate Reader. Wnt signaling activity was measured with values as the -fold increase in luciferase activity.

5.2.5 Large-scale drug test on organoids

Selected well established organoid lines derived from CBD of mice with genotype *Pdx1-Cre; LSL-Pik3ca^{H1047Rwt}; Rnf43$^{\Delta/\Delta}$* and *Pdx1-Cre; LSL-Pik3ca$^{H1047R/wt}$; Rnf43$^{wt/wt}$* were used to perform the large drug screen. 500 cells per well resuspended in Matrigel (354230) and PDC media in a ratio of 1:8, seeded in white 384 well plates and incubated overnight in the incubator at 37°C. To avoid the edge effect, the outer wells not used for the experiment were filled with PBS (Sigma, D8537-500ML).

After 24 hours, serial dilutions of the drugs mentioned in Tab12 were added to the cells. Each of the 7 different concentrations of the drugs was added in triplicate. DMSO (HN47.1) diluted in PDC media was used as an internal control and added to 8th row of seeded organoids. The plates were then incubated for 72 hours at 37°C. On the fourth day of the experiment, 5µl CellTiter-Glo® (cat. no. G7570) was added to each well. Prior to usage, CellTiter-Glo® (cat. no. G7570) was brought to the RT. After 20 minutes of incubation on the shaker at 450 rpm at RT, plates were measured for luminescence on a FLUOstar OPTIMA microplate reader.

5.2.6 GI50 and AUC calculations

All data extracted from the measured plates was normalized to the DMSO (HN47.1) control values. For analysis and plots of the results, GraphPad Prism was used.

5.2.7 Organoid lines quality controls

All isolated organoid lines were re-genotyped and tested for mycoplasma for quality control.

5.2.8 Mycoplasm contamination test

Mycoplasma contamination tests were performed by PCR, based on sample material collected from organoid lines that were cultured in media without antibiotics. After 2 weeks of culture, 2mL of media was collected and centrifuged at 350 × g, supernatant was removed leaving approximately 30.0 µL of final volume. For PCR reaction, specific primers described in Tab.7 were used. After PCR reaction, the solution was loaded on the 2% agarose gel and

analyzed. Samples that tested negative were showing no band, while in the positive samples, a band was detected at 500bp. Internal positive control was used for all experiments.

5.2.9 Human contamination analysis

Pellet collected from all organoid lines used for experiments was collected and lysed in Soriano buffer. Isolated DNA was used to perform a PCR detecting contamination with human oncogenic KRAS G12D. The results of PCR reaction were evaluated on an agarose gel.

5.3 Molecular biology

5.3.1 Isolation of genomic DNA

Tissue pieces collected during ear clipping the pups were used for genotyping the mouse strain, while pieces of mouse tail collected during dissection were used for re-genotyping. In both cases, DNA was extracted by adding 50 µL of Soriano lysis containing proteinase K and DTT (order nr. 6908.1) that were added prior to use. Prepared samples were placed in a thermocycler for 90 min at 55 ºC. For inactivation of proteinase K, samples were incubated for 15 min at 95 ºC. Afterwards, lysates were mixed by vortexing and centrifuged for 5 min at 1000 x g. Supernatant was transferred to a new reaction tube and stored at 4°C until PCR was performed. For long term storage, lysates were transferred to -20 ºC.

5.3.2 Polymerase chain reaction

For genotyping and re-genotyping of organoid lines and mouse biopsies, standard PCR was used. The components of the PCR pre-mix were prepared and stored in -20°C until usage is described in Tab.12. Components of PCR mix are shown in Tab.13 and the conditions of general PCR reaction are shown in the Tab 14. Annealing temperatures and sizes of bands for genotyping and recombination PCR are described in table 15 and 16. For each allele of interest, specific primers (Tab.7) were used for the PCR as well as an optimized PCR program with pre-tested annealing temperatures. PCR products were kept at 4 °C until further analysis by electrophoresis on agarose gels (described in 5.3.3).

Table 11. Composition of pre-mix used for PCR

Component	Volume (µL) for one reaction
dH_2O	4.375
10x buffer S	2.5
30% sucrose	2.5
SucRot	2.5
PeqTaq	0.125

Table 12. Mix used for PCR

Component	Volume (µL) for one reaction
PCR pre-mix	12.5
Forward primer (10 µM)	0.25 – 2
Reverse primer (10 µM)	0.25 – 2
DNA template	1 – 2
dH_2O	add up to 24 µL

µL, microliter; µM, micromolar; dH_2O, distilled water; PCR, polymerase chain reaction.

Table 13. PCR conditions for genotyping and recombination.

Step	Temperature (ºC)	Time	Cycles
Initial denaturation	95	300	
Denaturation	95	30-45	40x
Annealing	55 - 65	30-60	
Elongation	72	60-90	
Final elongation	72	300	
Storage	25	hold	

Table 14. Annealing temperatures and PCR products of genotyping PCRs.

Name of PCR	Annealing temperature	PCR products (bp)
Rnf43	58 °C	345(mut)/284(internal control)
Rnf43 rec	62 °C	345(mut)/284(internal control)/490bp

PIK3CA	64 °C	630(LSL-PIK3CAH1047R); 590(FSF-PIK3CAH1047R)
Rosa26	62 °C	400(LSL-PIK3CAH1047R/600(WT)
Pdx1-Cre	64 °C	670(mut)/200(internal control)
LSL-Kras	55 °C	170(mut)/270(Ryland et al.)

bp, base pairs; mut, mutant allele; WT, wild type allele.

Table 15. Annealing temperatures and PCR products of recombination PCRs

Name of PCR	Annealing temperature	PCR products (bp)
PIK3CA del	60 °C	630(mut)/550
Rnf43 del	62 °C	345(mut)/284(internal control)/490

bp, base pairs; del, deletion/deleted; mut, mutant allele.

5.3.3 Separation of DNA by agarose gel electrophoresis

To separate the nucleic acids amplified during PCR according to size, electrophoresis with 1-2% agarose gel (depending on the size of PCR product) was performed. Agarose gels were prepared by dissolving agarose in 400ml 1x TAE buffer and boiling the solution in a microwave for approximately 8 min. After cooling it down with constant stirring on magnetic stirrer, ethidium bromide (1 mg/mL, E1510-10ML) was added to allow visualization of the band under UV light. Gel was poured into prepared gel chambers with 26 well combs. GeneRuler™ 100 bp DNA ladder and PCR products were pipetted into the gel pockets and separated for 1-2h at 120 V. Visualization of the DNA bands was performed by the excitation UV light imaging system (system UVP UV solo touch).

5.3.4 Isolation of RNA

Cell pellets for RNA isolation were collected as described above for DNA isolation. Pellets used for RNA isolation were harvested from 70% confluent 3-5 wells from the organoid line. Collection tubes were frozen down directly in liquid nitrogen and stored at -80°C until further processing. RNA from collected pellets was performed by using RNeasy® Mini Kit (cat no. 74104) according to manufacturer's protocol. Prior to isolation, the fume hood used for isolation was cleaned with 70% ethanol and RNase AWAY. All pellets were kept on ice during the isolation. In order to determine the RNA concentration, Qubit® dsDNA BR Assay Kit (cat no. 74104 Q32850) on a Qubit® 2.0 fluorometer was used. After measurement, all isolated samples were stored at -80°C until further usage.

5.3.5 Quantitative Realtime PCR (RT-qPCR)

Isolated RNA was used for cDNA synthesis together with TaqMan® reverse transcription reagents (N8080234). Synthesis was performed according to the manufacturer's protocol.
To determine mRNA expression levels of *Rnf43* in organoid lines and to confirm the efficiency of the knockout, specific primers were designed, tested and provided by members of Institute for Medical Microbiology Immunology and Hygiene. All samples were tested in triplicates. Pre-diluted cDNA samples were mixed with forward and reverse primers (100nM each) and 12.5 µL SYBR (cat no. A46112) green Master mix. For the RT-qPCR, a StepOnePlus real-time PCR system was used.Analysis of the data was performed with StepOne™ software and mRNA expression levels quantified according to the $2^{-\Delta\Delta Ct}$ method described by (Livak & Schmittgen, 2001). All values were normalized to housekeeping gene GPHD.

Table 16. Program for RT-qPCR

Step	Temperature (ºC)	Time	Cycles
Pre-incubation	95	300	
Amplification	95 60 Plate read	10 30	40x
Melting curve	60	30	
Melting curves	60 + 0.5 °C/ cycle Ramp 0.5 °C/s Plate read	300	40x
Storage	12	hold	

5.3.6 Sequencing analysis

For RNA analysis of bulk tissue and organoid lines derived from the mouse models, sequencing was performed in collaboration with Prof. Roland Rad and members of his lab from Klinikum rechts der Isar, Technical University of Munich, Munich, DE.
2ug of each isolated sample was further processed with the TruSeq® Stranded mRNA Sample Preparation Kit with Agencourt AMPure XP Beads and SuperScript II as reverse transcriptase and loaded in NGS run performed with Illumina HiSeq2500.
The analysis and plots were performed by Fabio Boniolo. The alignment of the read was carried by using R version 3.6.2. (R Development Core Team, 2014), previously described by Mueller et al., 2018(Mueller et al., 2018). To find statistically significant differences between two

cohorts derived from mice *Rnf*^{fl} and *Rnf*^{wt} gene set enrichment analysis was conducted. To visualize the differences of in genes expression between *Rnf*^{fl} and *Rnf*^{wt} groups analysis using DESeq2 package was performed (based on the p-value > 0,5 or fold change LFC>2).
Reanalysis and generation of Heatmap for *piggyBac* transposon screen was performed by Anantharamanan Rajamani based on sequencing data from (Falcomata et al., 2021).

5.4 Histological analysis

5.4.1 Paraffin Sections

All organs harvested from the sacrificed mice were processed for further experiments. Depending on the applications, some of the tissues were collected for *in vitro* experiments (chapter 5.2 and 5.3) or processed and embedded in paraffin. For FFPE, tissues were harvested and directly fixed in 4% ROTI®Histofix (order no. P087.6). After 16 to 24h of incubation in the fridge at 4 °C buffer was exchanged to 1x PBS (Sigma, D8537-500ML) to prevent over-fixation of the tissues. Cleared samples were processed in tissue processor ASP300. In the final step, all organs were embedded in paraffin using heated module HistoCore Arcadia H.
All FFPE tissue were stored at RT until further use.
For organoids, all steps mentioned above were performed by members of Facility Comparative Experimental Pathology at the Institute of Pathology, TUM. The only step performed in the lab was fixation of organoids embedded in Matrigel (354230) dome for 30 minutes in clear 4% PFA and transfer to 1 x PBS (Sigma, D8537-500ML) after fixation.

5.4.2 Hematoxylin and eosin (H&E) staining of tissue sections.

For H&E stainings, tissue sections were cut with the microtome Microm HM355S and dewaxed in Roti®Histol (order no. 6640.1). Following the de-waxing, re-hydration of the tissue slides was performed through a series of washes in decreasing EtOH concentration and a final incubation in distilled water. After that, sections were stained in hematoxylin for approximately 0.5 min, depending on the thickness of the cut, and then directly vigorously washed under a stream of tap water. In the following steps, slides were stained in eosin for 10 s and once again washed in tap water. To fix the staining, all slides were de-hydrated in a series of increasing concentration of EtOH, incubated in Roti®Histol (order no. 6640.1) and mounted with Pertex. The collaboration partners from the core facility Comparative Experimental Pathology at the Institute of Pathology, Technical University of Munich performed the grading of all slides.

5.4.3 Immunohistochemistry (IHC)

All IHC stainings were done by core Facility Comparative Experimental Pathology, TUM.

5.4.4 Analysis

All H&E and IHC stainings were documented and scanned by Aperio Versa 8 Digital Scanner or digital version of staining was provided by core Facility Comparative Experimental Pathology, TUM.

6. Results

Contributions to this thesis besides the author are acknowledged in figure legends and in the methods section. Unless otherwise stated, all analyses were performed by the author.

The underlying mechanisms driving CBD tumorigenesis onset and progression remain elusive. In order to discover novel genes that are involved in ECC carcinogenesis, the research group of Prof. Dr. Dieter Saur used genome-wide *in vivo piggyBac* transposon mutagenesis screening in genetically engineered mouse models where the *Pik3ca* hotspot mutation H1047R is conditionally activated upon *Pdx1-Cre* driven recombination. Expression of the transgenic Pdx1-Cre in the extrahepatic biliary tree has been validated in the studies by Falcomatà et al, 2021 using Cre-activatable fluorescent reporters. Based on these findings, this promotor was therefore selected to target mutagenesis in CBD. The mentioned studies also showed that Pdx-1-positive cells are expressed not only in the organ of interest but also in duodenum, pancreas, gallbladder, and stomach, which makes it more challenging to differentiate direct effects of $Pik3ca^{H1047R/wt}$ mutation specifically in CBD. As this oncogene is activated in multiple organs, the ongoing tumorigenesis across different parts of gastrointestinal tract may potentially interact and affect one another. There is still a need to find more suitable GEMMs for studying progression and maintenance of CBD carcinogenesis. Notably, the significance of the PI3K-AKT-mTOR pathway is already described by studies on molecular profiling of cholangiocarcinoma (Stenzinger et al., 2023; Voss et al., 2013) using GEMMs with activated hotspot mutation in $Pik3ca^{H1047R/wt}$. CBD of mice with this genotype showed undergoing malignant transformation. In contrast, biliary tract of mice harboring $Kras^{G12D}$ mutation did not present any relevant alteration upon activation of this oncogene (Stenzinger et al., 2023; Voss et al., 2013)

6.1 *In silico* analysis of genome-wide *in vivo piggyBac* transposon mutagenesis screening reveals tumor suppressive role of *Rnf43* in both PDAC and CBD cancer

Re-analysis by Anantharamanan Rajamani of the transposon screening data by Falcomatà and colleagues allowed for identification of candidate genes involved in CBD development (Falcomata et al., 2021). To represent the frequency of transposon insertions within the top selected genes for each mouse in the cohort, the corresponding square in the heatmap was indicated using varying shades of orange (Fig. 4 A). The intensity of the color varies between each mouse and is strictly correlated with the transposon insertion per each gene. Among

interesting genes selected for further validation were *Pten*, *Fbxw7*, *Ppm1b* and *Frk*, already characterized and described in the paper of Falcomatà, 2021. Known as tumor suppressor gene involved in PI3K-Akt pathway, *Pten* is described in various human cancer as frequently mutated. Also, *Fbxw7* is classified as tumor suppressor and its clinical significance makes it an

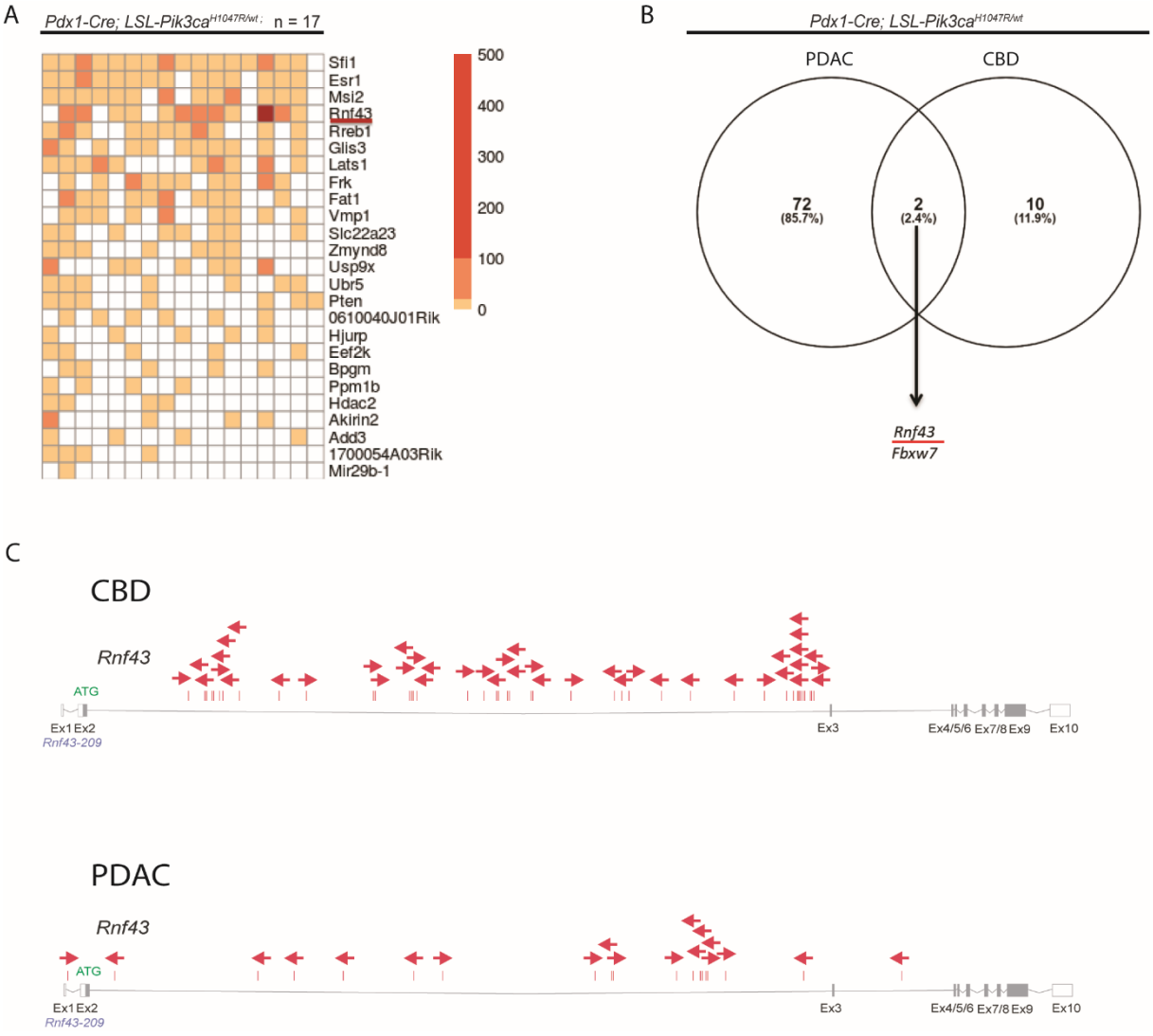

Figure 4. Comprehensive analysis of *piggyBac* transposon mutagenesis screening and identification of *Rnf43* as a potential candidate for further studies. (A) TAPDANCE analysis in 17 tumors collected from CBD of mice with CCA indicating the co-occurrence heatmap of the common insertion sites. This analysis was performed by Anantharamanan Rajamani based on sequencing data from Falcomatà et al, 2021. Total number of insertions in the respective genes is indicated by intensity ranging from white to orange and red. Each column of the heatmap corresponds to one tumor. (B) Venn diagram of compression among genes found in *piggyBac* transposon mutagenesis screening of PDAC and CBD tumors (n=38 biologically independent animals were analyzed in *Pdx1-Cre; LSL-Pik3ca*^{H1047R} mice cohort) The fraction of overlapping genes is given as percentage of total amount of genes selected *piggyBac* insertion pattern in *Rnf3* was obtained from two cancer entities: (C) common bile duct (CBD) and (D) pancreatic ductal adenocarcinoma (PDAC). Red arrow equals an insertion and represents the orientation of the CAG promoter delivered by the transposon into the gene of interest.

appealing target for therapeutical studies. Any alterations in this gene impacts directly the process of cancer development and progression due to well-known role of targeting oncoprotein *c-Myc* or *Cyclin E* for degradation. Loss of function in *Fbxw7* leads to accumulation of oncoproteins, uncontrolled cell growth and tumorigenesis. Due to certain limitation that *piggyBac* transposon is carrying, some of the genes selected as top hits are not significant. That is due to local hopping, a phenomenon of transposon integration nearby donor locus located in *Lats1*. That can be a case for some genes like *Lats1*, *Sfi1* and *Vmp1*. Like for every *in vivo* screen, also for transposon screen there is a need of validating the identified novel genes. Moreover, knowing already the limitation of this technique allowed to select promising candidates for further studies based not only on detailed screening but also on educated guess. The highlighted *Rnf43* was identified as one of the top genes in this screening, indicating its importance for CBD cancer development. Since *Pdx1* is also expressed in the pancreas, some of the mice generated for the studies on CBD cancer in the conditional *piggyBac* transposon-based somatic insertional mutagenesis system developed PDAC. Pancreatic tissue harvested from this cohort was therefore sequenced as well and the findings compared with the analysis of the mice cohort that developed CBD cancer. Intriguingly, even though both mice cohorts had exactly the same genotype, the set of genes that have been most frequently hit in the transposon screens differed between mice that developed CBD cancer to those that underwent PDAC. The only genes in common between these two cohorts were *Rnf43* and *Fbxw7* (Fig. 4 B). Interestingly, regardless of the parameters used for the analysis of this data set, *Rnf43* was always in the top genes identified to be involved in CBD development. Whereas in the PDAC cohort, *Rnf43* had two-fold less amount of transposon insertions and a low read coverage in the samples where *Rnf43* was a hit comparing to the CBD cohort. Therefore, the insertion pattern in tissues obtained from these two cohorts indicate a tumor suppressive role of *Rnf43* (Fig. 4 C and D). However, as the comparison of CIS pattern from PDAC and CBD samples demonstrates, *Rnf43* may be one of the crucial genes involved in tumor development in CBD cancer whereas for PDAC is just one of several genes involved carcinogenesis.

6.2 *In vivo* findings support tumor suppressive role of *Rnf43* in CBD cancer

In order to investigate the importance of *Rnf43* for CBD cancer, an endogenous mouse model was generated by crossing mice with deletion of *Rnf43* (Koo et al., 2012) with mice harboring $Pik3ca^{H1047R}$ hot spot mutation in *Rosa26* locus (Eser et al., 2013)under control of *Pdx1-Cre*

(Hingorani et al., 2003) transgenic promotor (Fig. 5 A and C). This transcription factor is expressed in the organ of interest – CBD – as well as in duodenum, pancreas, and stomach, which makes it a suitable to study extrahepatic biliary epithelium. At the same time, mice with a KO of *Rnf43* were crossed with mice harboring oncogenic mutation G12D in the *Kras oncogene*, in order to find out whether difference in the driver oncogene together with the additional deletion of *Rnf43* can shift the tumor spectrum from PDAC to CBD cancer. The

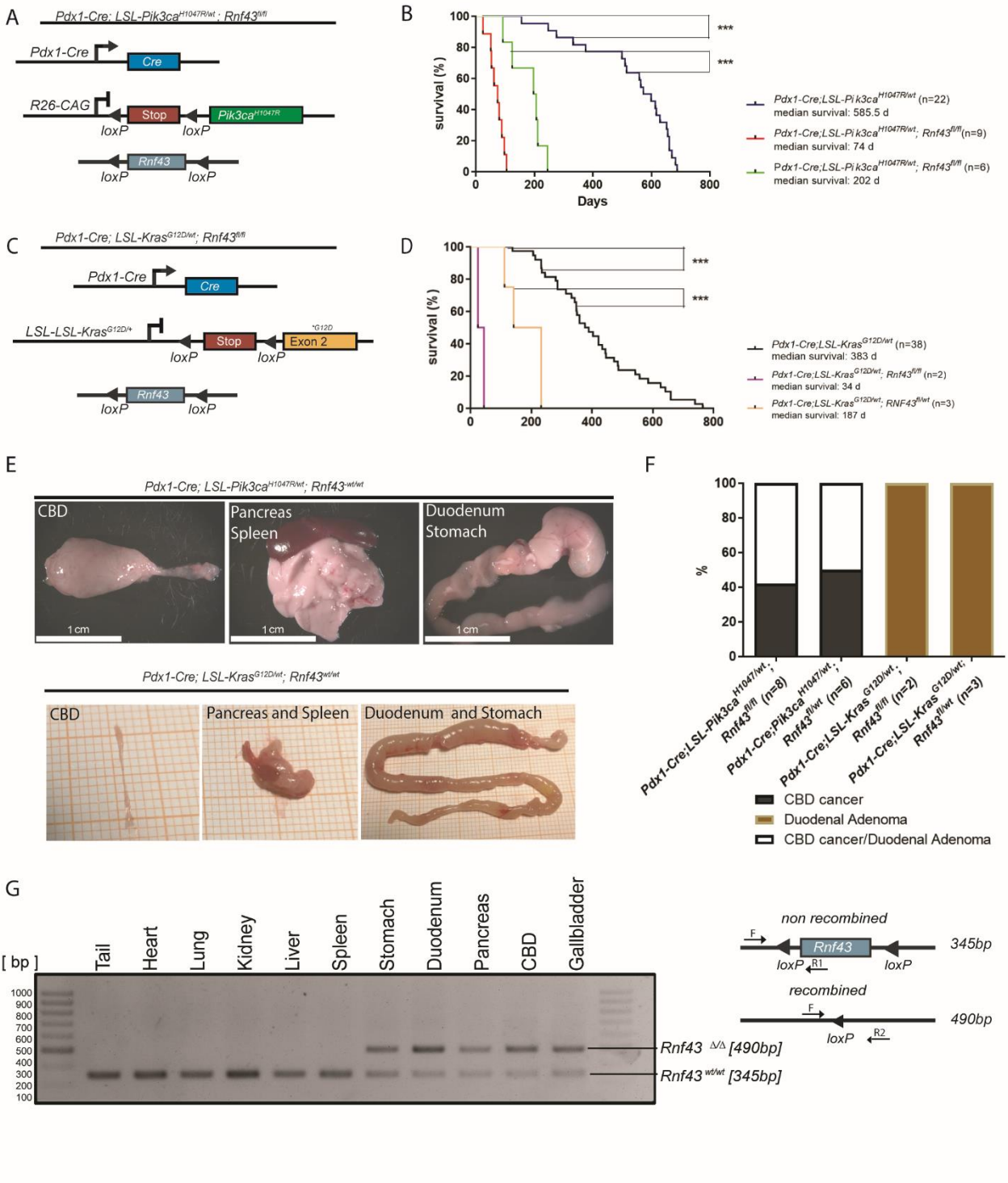

Figure 5. Deletion of *Rnf43* results in shortening of survival in two different mouse models expressing oncogenic *Pik3ca*^{H1047R} or oncogenic *Kras*^{G12D}. (A and C) Left panel: Genetic strategy and recombination scheme of conditional deletion of *Rnf43* and expressing oncogenic (A) *Pik3ca*^{H1047R} or (C) *Kras*^{G12D} under control of *Pdx1-Cre* promotor. (B and D) Right panel: Kaplan-Meier survival curves of the indicated genotypes. The median survival time is in days and the number of animals per genotype are indicated in the legend of the graph. **p < 0.01, ***p < 0.001, log-rank (Mantel-Cox) test. (E) Macroscopic images of common bile duct (CBD), pancreas with spleen and duodenum and stomach of a *Pdx1-Cre*; *LSL-Pik3ca*$^{H1047R/wt}$; *Rnf43*$^{-/-}$ animal (upper panel) and of a *Pdx1-Cre*; *LSL-Kras*$^{G12D/wt}$; *Rnf43*$^{-/-}$ animal (lower panel). Scale bars for upper panel of images, indicate 1cm. For lower panel of images : each small square represents 1 mm (F) Tumor distribution represented in percentage (%) according to histological analysis of generated and analyzed mouse models. (G) Left, polymerase chain reaction (PCR) of tissues collected from indicated organs performed in order to identify specify of *Pdx1-Cre* mediated recombination in used mouse models. The upper band indicates recombination (490bp) whereas the lower one (345bp) non recombined gene. Right, scheme of genotyping strategy to detect non recombined and recombined *Rnf43* by PCR, where F indicates the forward primer and R1 and R2 the reverse ones. Animals used for these analyses were generated and sacrificed by all members of the laboratory of Prof. Dr. med. Dieter Saur.

study of Falcomatà and colleagues already showed that mice harboring *Kras* mutation develop PDAC, whereas mice with *Pik3ca* mutation develop PDAC or CBD cancer (Falcomatà et al., 2021). In order to address this question, mice with hetero- and homozygous deletion of *Rnf43* and different driver oncogenes were analyzed. The survival times in both cohorts was shortened significantly by the deletion of *Rnf43*, regardless if one or two alleles were deleted (Fig. 5 B and D), however the effect of homozygous deletion of *Rnf43* was stronger than heterozygous. These findings thereby confirm the tumor suppressive role of *Rnf43* that was indicated in the previous transposon screen. A full KO of *Rnf43* significantly reduced the median survival of mice with *Pdx1-Cre; LSL-Pik3ca*$^{H1047R/wt}$*; Rnf43*$^{fl/fl}$ down to 74 days ($p < 0.001$; Fig. 5B) and with *Pdx1-Cre; LSL-Pik3ca*$^{H1047R/wt}$*; Rnf43*$^{wt/fl}$ down to 202 days ($p < 0.001$; Fig. 5B) compared to the control *Pdx1-Cre*; *LSL-Pik3ca*$^{H1047R/wt}$ mice (585.5 days). For mice with *Pdx1-Cre; LSL-Kras*$^{G12D/wt}$*; Rnf43*$^{fl/fl}$ and *Pdx1-Cre; LSL-Kras*$^{G12D/wt}$*; Rnf43*$^{wt/fl}$ the effect of the deletion was even stronger, with a worse outcome than the *Pik3ca* mice. Mice with homozygous deletion of *Rnf43* died 34 days after birth and the ones with heterozygous deletion after 187 days. Although, the cohort of mice with *Kras* as the driver oncogene needs to be increased as the sample size is too small and underpowered to draw statistically valid conclusions, it at least indicates a tumor suppressive role of *Rnf43* also in this GEMM. Overall, the analysis of survival of mice from both cohorts provides evidence of a tumor suppressive function of *Rnf43* in both the Kras-driven as well as the PI3K-driven context.

Macroscopic analysis of mice with deletion of *Rnf43* and different driver oncogene are shown in the Fig. 5 E. The images reveal that the *Pik3ca* activating mutation is more relevant for extrahepatic bile duct carcinogenesis than the *Kras* activating mutation. Mice with loss of *Rnf43* together with *Pik3ca* as a driver oncogene develop CBD cancer. Their bile duct was dilated and had thicker, whiter walls. Some of the mice from the survival cohort had cholelithiasis, their biliary tract was full of gallstones that were macroscopically visible even before opening bile duct. Besides evident differences in the macroscopical structure of CBD, also the pancreas appeared altered and was usually bigger and mostly fibrotic with enlarged spleen. Duodenum and stomach were also slightly altered in comparison to wild type mice. Even though changes in several organs of gastrointestinal tract were observed, the striking impact of *Rnf43* deletion on CBD was the most prominent. In contrast, analysis of the mice from the cohort harboring *Kras* mutation simultaneously with *Rnf43* deletion revealed alterations in the duodenum as the most prominent change in the phenotype of the dissected organs. Moreover, mice exhibited development of duodenal adenomas, in addition to the pancreas and spleen being visibly smaller, while the CBD did not show any macroscopic alterations. After tumor formation analysis (Fig. 5 F) of mice with KO of *Rnf43*, we observed differences between mutant *Pik3ca* and mutant *Kras* cohorts. *Kras* as a driver oncogene was observed to favor duodenal adenomas, while *Pik3ca* induced mainly CBD cancer (40% in $Rnf43^{fl/fl}$ mice and 50% in $Rnf43^{fl//wt}$ animals; Fig. 5 F), but in some cases both CBD cancer and duodenal adenomas were detected.

To reveal the efficiency of recombination of *Rnf43*, PCR was performed to identify which organs were affected by the deletion of the gene of interest (Fig. 5 G). Based on previous findings, several organs from the gastrointestinal tract as well as heart, lungs, kidney, liver and spleen were selected to perform the recombination PCR of *Rnf43*. A piece of tail of the animal was used as a negative control. The recombined band – 490bp – was present together with non-recombined band – 345bp – in the samples collected from the stomach, duodenum, pancreas, CBD and gallbladder (Fig. 5 G). These results of the PCR therefore demonstrate the partial recombination of Rnf43 in organs, which express the Pdx1-Cre promotor. The partial recombination can be expected and explained, as samples used for PCR were not from a pure population of Pdx-1 expressing cells, but also contained stromal cells that did not recombine, which is in line with previous findings (Falcomata et al., 2021). On the other hand, organs not expressing Pdx1-Cre such as heart, lung and kidney showed only the non-recombined band. However, since the PCR was conducted on bulk tumor which contain mixture of various of cell populations deletion of Rnf43 occurred exclusively in cancer cells of CBD. The partial deletion

is linked to stroma compartment that do not express Pdx1-Cre promotor. Partial loss of Rnf43 in the CBD already manifests in a change of mice phenotype, which indicates the importance of this gene in CBD cancer development. Given together our findings demonstrate tumor suppressive role in both GEMM's *Pik3ca* and *Kras*. However, for mouse model with Pik3ca as driver oncogene survival of the mice is shortened due to CBD cancer development whereas for Kras mice cohort the main reason of death is duodenal adenoma.

6.3 Histopathological analysis of organs upon *Rnf43* deletion validates *in vivo* findings.

Histopathological analysis allowed to track the effects of *Rnf43* deletion at the microscopic level. Given the range of *Pdx1-Cre* activity described above (Fig. 5 E and G), there was a need to validate the deletion of *Rnf43* in organs that express the Pdx1-Cre promotor used in this study. Histology of these organs are shown in Fig. 6 A and B, where the effects of loss of function of *Rnf43* were analyzed by H&E and IHC staining's. Findings of staining from mouse model *Pdx1-Cre; LSL-Pik3ca*$^{H1047R/wt}$*; Rnf43*$^{fl/fl}$ strongly correlated with macroscopic images of the organs. H&E of the CBD revealed invasive carcinoma with mixed composition. In this staining, it was possible to detect cells growing in abnormal patterns and in disorganized arrangement, being an indication of undergoing pathological processes. Evaluation of pancreas staining showed that this organ was also undergoing a process of remodeling. Since the composition of tissue was changed and modifications that occurred were pathological. The morphology and architecture of cells in some tissues were altered, with a high-grade dysplasia indicating a risk of progressing into cancer, yet still not in an invasive stage.

Due to limited number of animals from the cohorts *Pdx1-Cre; LSL-Kras*$^{G12D/wt}$*; Rnf43*$^{fl/fl}$ and *Pdx1-Cre; LSL-Kras*$^{G12D/wt}$*; Rnf43*$^{wt/fl}$, it was not possible to draw definitive histopathological conclusions. On the other hand, the analysis of the mice from this cohort showed alteration in duodenum. The abnormal architecture of cells and cellular pattern indicated existence of adenomas localized in the duodenum of the depicted animal tissue. The results of the staining revealed a combination of low- and high-grade polyps alongside high grade dysplasia. In order to characterize intestinal differentiation, CDX2 (RRID:AB_2722785) staining was performed. This transcription marker was selected based on its role in intestinal development, thus confirming the intestinal origin of the tissue. For that same reason, CK19 (RRID:AB_10990774) was selected as a marker of abnormal growth of ductal cells of gastrointestinal tract. Staining allowed to identify the lesions in all organs expressing for CK19.

Analysis of CBD staining's identified visually elevated levels of CK19. Furthermore, it was possible to detect ADM's and PanINs in pancreas derived from mice harboring deletion of *Rnf43* together with mutation of *Kras*. To study the differences in proliferation of the cells, a protein marker known as Ki67 (RRID:AB_2722785) was used to determine the fraction of the cells that are proliferating. Several studies have demonstrated the clear correlation of high levels of cells positive for Ki67 (RRID:AB_2722785) staining in various cancer subtypes with aggressiveness of the tumor (Zhu et al., 2020). However, due to the limited biological replicates

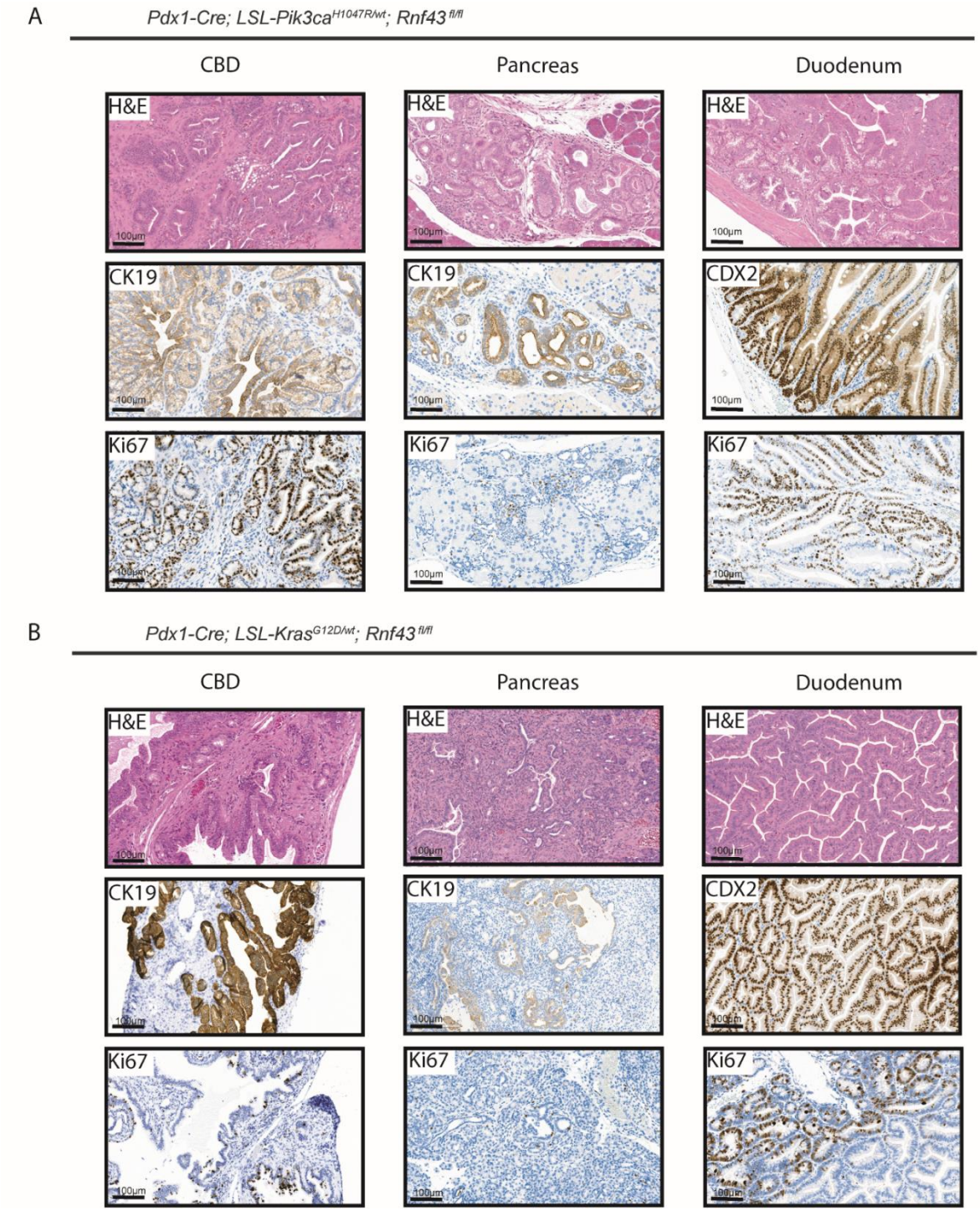

Figure 6. Deletion of *RNF43* exhibits in invasive Common Bile Duct cancer phenotype of mouse model with expression of oncogenic Pik3ca^{H1047R} opposite to mouse model with oncogenic Kras^{G12D}. Histopathological analysis of Common Bile Duct, pancreas and duodenum images from (A) *Pdx1-Cre; Pik3ca^{H1047R}; RNF43$^{fl/fl}$* vs (B) *Pdx1-Cre ; Kras^{G12D} ; RNF43$^{fl/fl}$* performed to classify complex changes occurred due to activated mutations combined with additional deletion of *RNF43*. H&E staining was used for histopathological grading and immunohistological staining for in-depth characterization of delivered tissue. CK19 (RRID:AB_10990774) ICC staining was used to identify positive epithelial cells in pancreas and common bile duct and CDX2 used for identification of tissue of intestinal origin (scale bar, 100 µm). Ki67 determinates cell population proliferation and is used as cancer related marker due to association of its high expression in cancer tissue (n=1, biologically independent animals were analyzed in the *Rnf43* KO cohort).

of tissue derived from characterized animals, it was not possible to quantify the number of Ki67-positive nuclei in the selected tissues.

Overall, these findings underscore the importance of *Rnf43* for tumor development. Given the usage of transgenic promotor *Pdx1-Cre*, the stainings confirm shift of tumorigenesis between the different tissues, where Pdx1-Cre is expressed that is dependent on the activated driver pathway. Furthermore, the interesting consequences of loss of Rnf43 in described GEMM convinced us to try to use simplified in vitro model. For better understanding basic cellular and molecular mechanism behind *Rnf43* deletion, we established organoids model derived from CBD.

6.4 Established of organoid culture derived from Common Bile Duct

To further characterize the *Rnf43* KO GEMMs, we decided to generate cell lines from CBD. Interestingly, the isolation of 2D lines proved to be quite challenging, since none of the tumor cells expanded *in vitro*. To overcome this issue, we decided to establish 3D culture for further study and characterization of the generated GEMMs. Since the 3D culture of CBD organoids was not optimized in the research group of Prof. Dr. Dieter Saur, a workflow needed to be developed (Fig. 7 A). Indeed, this approach was successful and allowed to conduct *in vitro* experiments and testing of prospective drugs in order to screen potential candidates for future targeted treatments.

Detailed description of the established workflow can be found in Chapter 5.3.1. In order to increase the chance of successful isolation of organoid lines, the tissue piece of CBD wasn't digested to single cell suspension, so that chunks of the tissue mixed with cells were embedded

in Matrigel (354230) but not fully digested pieces. After incubation with enzymes like collagenase (LS004174), the tissue was not washed, incubated with TrypLE™ Express Enzyme (1x) (12604013) solution 1x and posteriorly seeded in the 24-well format. It is worth mentioning the need of careful selection of the tissue for isolation of 3D cultures since CBD is closely connected to other organs. Since the PDC media (Chapter 4.4) used for culturing organoid lines derived from pancreas did not differ from the media used for CBD lines, the risk of contamination of the line with material from another organ was relatively high. Phenotypically CBD organoid lines did not differ between the isolated lines of *Pdx1-Cre; LSL-Pik3ca$^{H1047R/wt}$; Rnf43$^{Δ/Δ}$* and *Pdx1-Cre; LSL-Pik3ca$^{H1047R/wt}$; Rnf43$^{wt/wt}$* (Fig. 7 B). Derived from epithelial cells of CBD, 3D hollow structures maintained their phenotype consistently throughout the passaging end expansion of the lines.

In order to determine the recombination levels of Rnf43 of the organoid lines, additional PCR was designed and established. That allowed to select only organoid lines with full deletion of Rnf43 for further experiments. The aim of the PCR was to detect the recombination status of

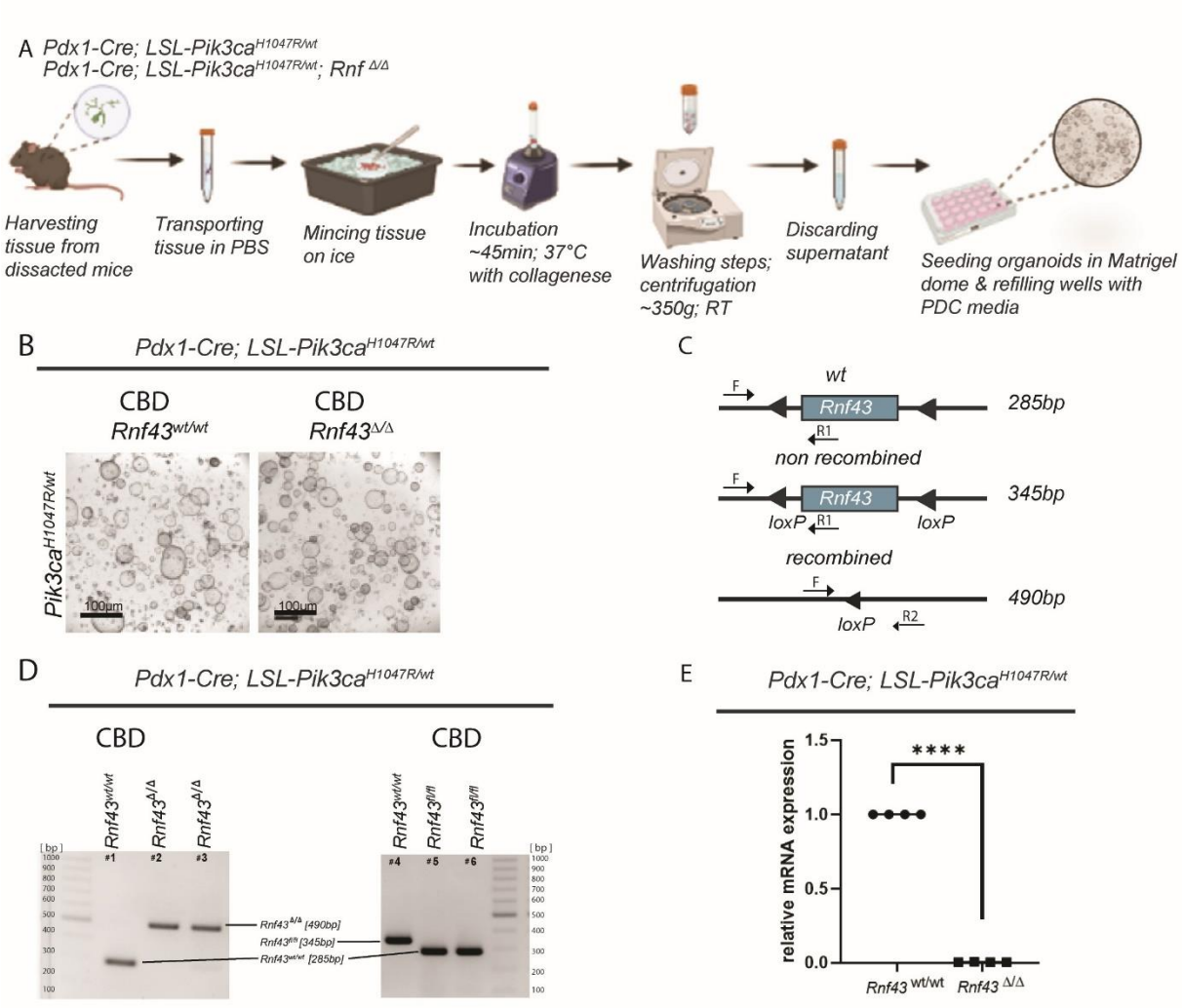

Figure 7. 3D organoids culture was necessary to be established from common bile duct. (A) scheme of isolation of organoids from common bile duct (CBD) of mice with *Pdx1-Cre; LSL-Pik3ca$^{H1047R/wt}$; Rnf43$^{Δ/Δ}$* and *Pdx1-Cre; LSL-Pik3ca$^{H1047R/wt}$; Rnf43$^{wt/wt}$* genotypes. (B) Bright field image of luminal organoids derived from CBD with deletion of *Rnf43* and from CBD of a control mice. Scale bars indicate 100 µm. (C) Scheme of the genetic strategy used in order to detect recombination status of *Rnf43.* F represents the forward primer and R1 and R2 represent the reverse ones. (D) Images of two representative polymerase chain reactions (PCR) established on organoid lines, where the upper band (490bp) represents 3D lines fully recombined for *Rnf43*, middle one band (345bp) not recombined and the lowest one wild type band (285bp). (E) mRNA levels of *Rnf43* of the established organoid lines were quantified using real-time PCR. Values were normalized to the housekeeping gene GAPDH **** $p \leq 0.0001$, unpaired t-test. The mRNA levels of *Rnf43* were measured in four independent experiments.

Rnf43 by using 3 primers designed in a way that the standard primers used for genotyping were complemented by a primer that allowed for detection of *Rnf43* deletion (Fig. 7 C).The recombination PCR (Fig. 7 D) demonstrated complete recombination of the organoids, thereby indicating that RNF43 was completely knocked out in the organoids derived from the *Pdx1-Cre; LSL-Pik3ca$^{H1047R/wt}$; Rnf43$^{Δ/Δ}$*. The conditions used to perform the PCR as well as the sequences used of oligonucleotides can be found in Chapters 4.6 and 5.4.2. Additionally, levels of *Rnf43* mRNA were checked by RT-qPCR, which confirmed the complete loss of *Rnf43* mRNA expression in the organoid lines derived from *Rnf43$^{fl/fl}$* mice (Fig. 7 E). It was essential to characterize established organoid lines to ensure that our *in vivo* studies fit to *in vitro* findings.

6.5 Characterization of organoid lines derived from CBD confirms *in vitro* findings.

Tumor derived organoid culture with deletion of *Rnf43* and activation of *Pik3ca* as well as control line harboring only hotspot mutation H1047R in *Pik3ca* domain were characterized by histopathological analysis (Fig. 8 A and B). H&E staining identified structural features of the lines and conformed lumen like organization of cells within organoids. Consequently, organoid cultures were stained with CK19 (RRID:AB_10990774), which is a marker for biliary epithelial cells (Mehrpouya et al., 2019). As shown in Figure 8 A&B, organoids stained positively for CK19 expression, thereby indicating in this context their origin from epithelial CBD cells. In order to detect proliferating cells, staining for Ki67 (RRID:AB_2722785) was conducted. To determine cell viability and monitor growth of CBD derived organoid lines, a luminescence CellTiter-Glo (G7570) assay was performed over five consecutive days (Figure 8D). In

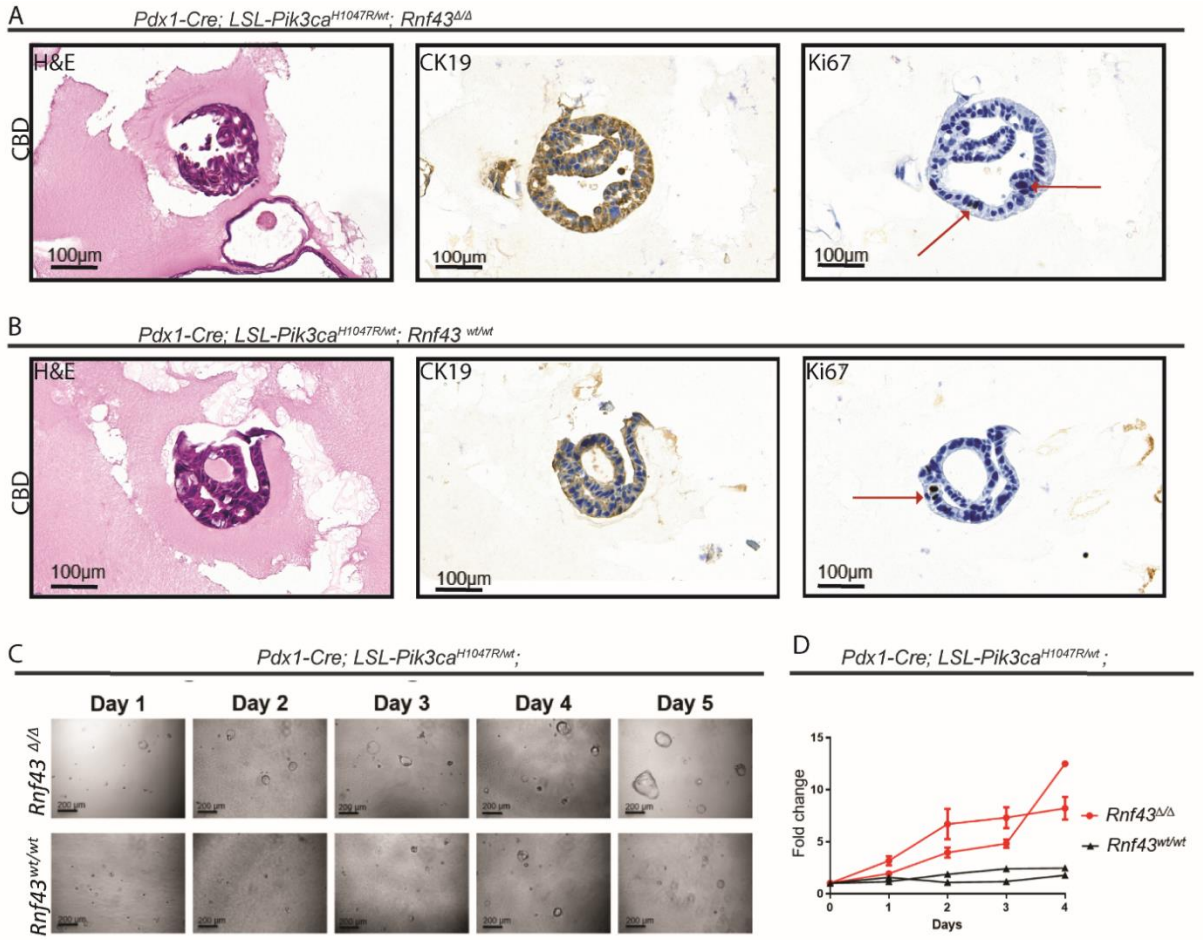

Figure 8. Hollow organoid lines culture derived from common bile duct with complete knockout of *Rnf43* showed an advantage in cell growth. (A and B) Histopathological analysis of organoid lines derived from common bile duct (CBD) of a (A) *Pdx1-Cre; LSL-Pik3ca$^{H1047R/wt}$; Rnf$^{Δ/Δ}$* mouse and a (B) *Pdx1-Cre; LSL-Pik3ca$^{H1047R/wt}$; Rnf43$^{wt/wt}$* animal. Organoids developed from CBD were stained with H&E, CK19 was used as a marker to identify epithelial cells and Ki67 (RRID:AB_2722785) was used as a proliferation indicator. (C) Bright field images from organoids with fully knockout of *Rnf43* and control organoids throughout a period of five days. Scale bars indicate 100 µm; 200 µm. (D) CellTiter-Glo (G7570) assay of organoid lines was used to determinate the differences of growth between organoid lines of different genotype. The experiment was performed in two biological replicates and conducted as three technical replicates. (± standard deviations as error bars).

addition, bright field images of the organoids were taken each day for five days (Figure 8C). Together, these data showed that deletion of *Rnf43* enhanced proliferation of organoid lines, and already two independent organoid lines shows the trend that is corresponding with our *in vivo* findings and thus confirming the tumor suppressive role of *Rnf43* . Nevertheless, more organoid lines will need to be analyzed to determine the statistical significance.

6.6 Top/Fop assay reveals Wnt overexpression upon Rnf43 deletion.

Rnf43 is described as a downstream target gene of Wnt signaling pathway (Fig. 3) and it is known for its role as negative regulator for this pathway. Given our success in establishing and characterizing our organoid model as a valuable tool for translational assays, we shifted our focus to investigate the impact of *Rnf43* deletion on Wnt pathway. To achieve this, we conducted TOP/FOP assay. We selected and cultivated organoid lines previously characterized as harboring *Pik3ca* mutation with complete loss of *Rnf43* and control lines harboring only activated hotspot mutation in *Pik3ca*.

As illustrated in Fig. 9 A, there was a need to establish a workflow to conduct this experiment, as the work with 3D culture made it challenging to conduct the experiment in its standardized way. The presence of Matrigel (354230) generated an additional barrier that limited transfection efficiency. Therefore, we needed to modify the protocol to be able to increase the efficiency of

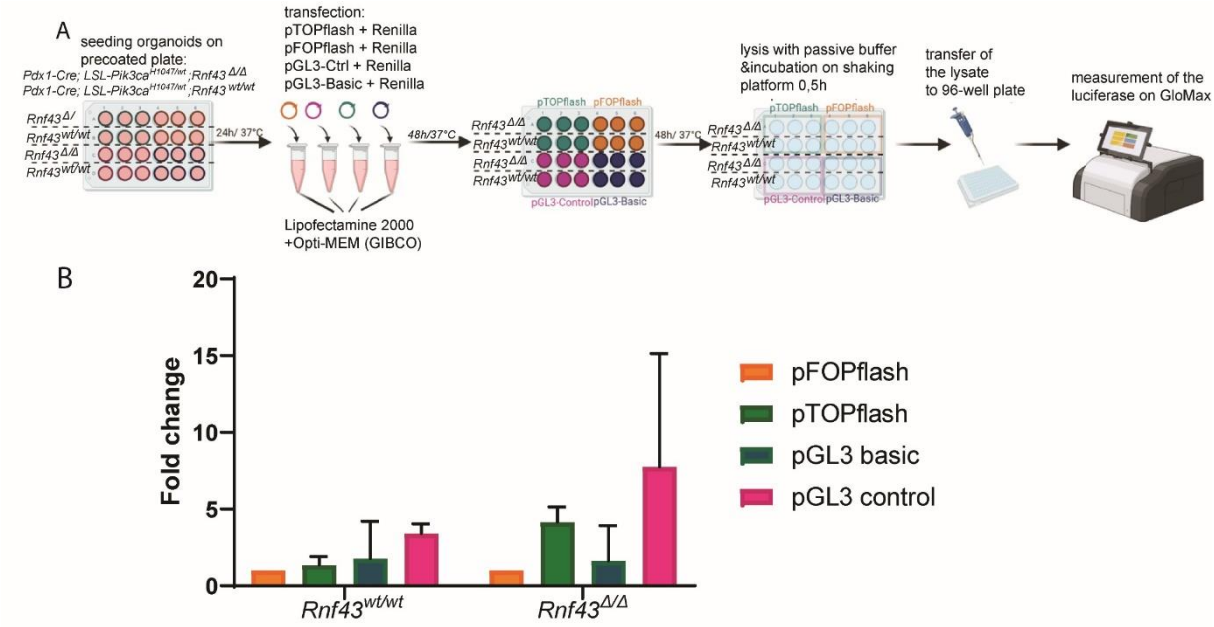

Figure 9. Deletion of *Rnf43* significantly upregulates the expression of Wnt signaling pathway (A) Scheme of establishment of TOP/FOP luciferase reporter assays in the organoid lines derived from common bile duct (CBD) of mice. (B) TOP/FOP assay identifies significant upregulation of Wnt protein between organoid lines with *Pdx1-Cre; LSL-Pik3ca*$^{H1047R/+}$*; Rnf43*$^{\Delta/\Delta}$ genotype and control organoids (*Pdx1-Cre; LSL-Pik3ca*$^{H1047R/+}$*; Rnf43*$^{wt/}$wt). The experiment was performed in three biological replicates and conducted as three technical replicates. Relative luciferase activity of the vectors is normalized to internal Renilla (RRID:Addgene_27163) control. as a negative and positive control in the study the pGL3_Basic (promoter less vector; measures the activity of promoter and enhancer, RRID:Addgene_64784) and pGL3_Control (control vector with the SV40 enhancer and promoter driving strong luciferase expression, (RRID:Addgene_21327)) vectors were used. Three independent experiments with an average (± standard deviations as error bars, ANOVA multiple comparisons test) in three technical replicate are presented.

plasmid transfection. In contrast to the protocol for the regular CBD organoid culture, the organoids were not seeded in the Matrigel (354230) dome. Instead, 24 well plates were pre-coated with a mixture of Matrigel (354230) to PBS (Sigma, D8537-500ML) at a ratio of 1: 5, and the organoids were seeded in a suspension of Matrigel (354230) to PDC media at a 1:10 ratio. That approach not only created an environment where cells were viable and kept their 3D structure, but also improved the transfection rates of the plasmids included in the TOP/FOP assay. Hereby only crucial steps for the experiments are described detailed overview of established workflow can be found in chapter in chapter 5.2.4.

As shown in Fig. 9 B, deletion of *Rnf43* resulted in higher luciferase activity, which directly correlates with expression of Wnt protein. The observed 2-fold increase in Wnt expression upon deletion of *Rnf43* underscores the importance of loss of function of *Rnf43* for Wnt signaling. These results therefore confirm the role of *Rnf43* in regulating of Wnt activity pathway and.

After confirming the important role of *Rnf43* in regulating of Wnt pathway activity, we aimed to identify further genes, whose expression is altered upon deletion of *Rnf43*. To accomplish that we performed RNA-seq and analyzed the transcriptome data obtained from the sequenced samples.

6.7 Conditional deletion of *Rnf43* reveals differences among samples of different genotypes.

The transcriptomes from established *Pik3ca* mutant CBD organoid lines with or without deletion of *Rnf43* were analyzed based on the differences in gene expression between 5 organoid lines deficient in *Rnf43* and 5 organoid line proficient in *Rnf43*. The heatmap revealed two main clusters separated by status of *Rnf43*. Although the comparison of genes that were significantly altered in the *Rnf43*-KO in contrast to the *Rnf43*-WT shows a clear separation, the set of differently expressed genes contains eight selected genes, such as *St3gal6*, *Tbx3* and *Zic5*. The amount of genes significantly altered on both cohorts is low, which makes it challenging to unravel potentially new pathways affected by the depletion of the *Rnf43*. Among the genes found upregulated in *Rnf43* KO organoid lines is *TBX3* (T-Box Transcription Factor 3), which was described as overexpressed also in pediatric hepatoblastoma linked with Wnt/beta catenin signaling (Cairo et al., 2008). Also, *St3gal6* was an interesting finding due to recent publication about role of *Rnf43* in DNA damage (Neumeyer et al., 2021). *St3gal6* was found among the

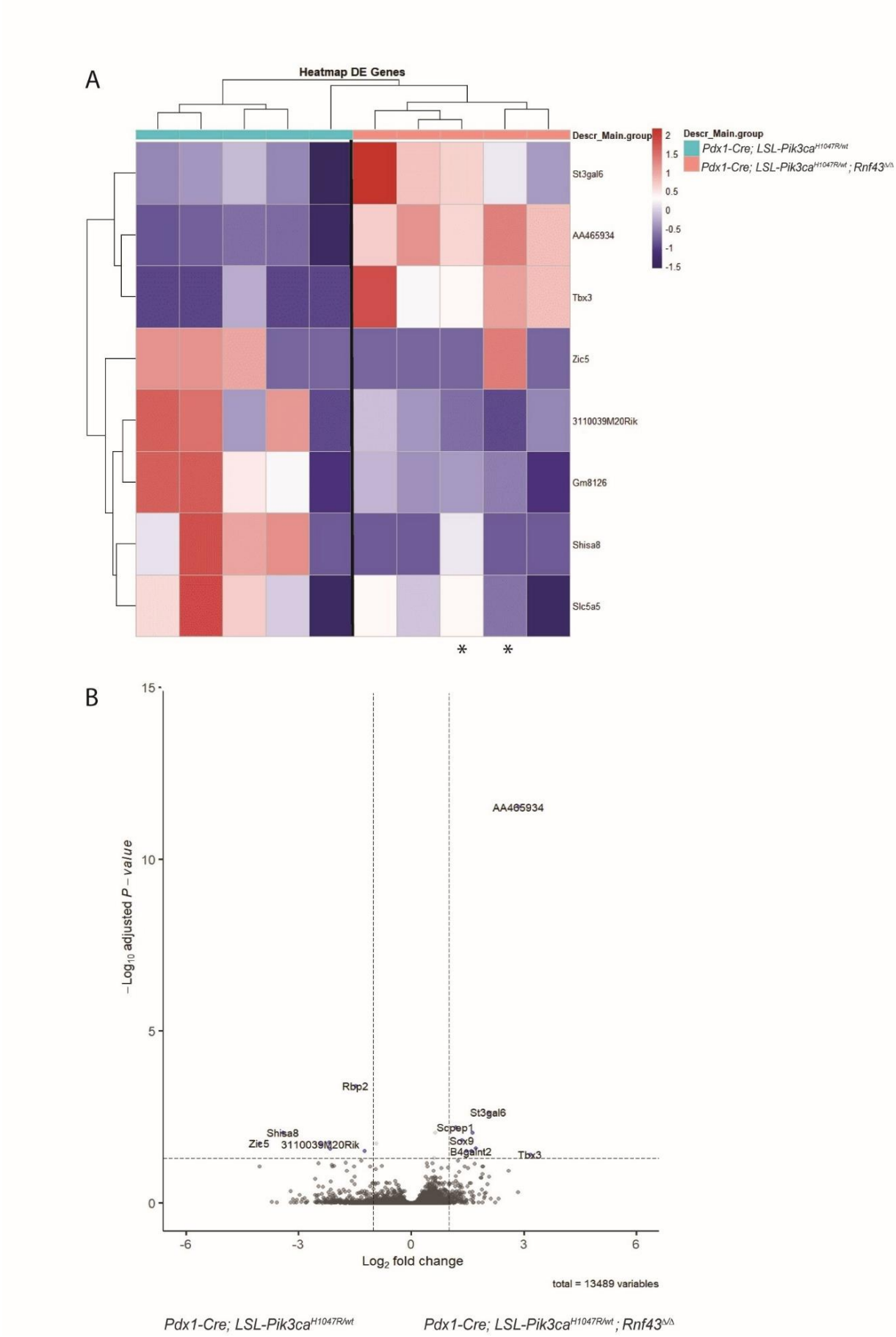
A
Heatmap DE Genes
Descr_Main.group
St3gal6
AA465934
Tbx3
Zic5
3110039M20Rik
Gm8126
Shisa8
Slc5a5
Descr_Main.group
Pdx1-Cre; LSL-Pik3ca H1047R/wt
Pdx1-Cre; LSL-Pik3ca H1047R/wt ; Rnf43 Δ/Δ
B
−Log10 adjusted P − value
Log2 fold change
AA465934
Rbp2
St3gal6
Scpep1
Sox9
B4galnt2
Tbx3
Shisa8
Zic5
3110039M20Rik
total = 13489 variables
Pdx1-Cre; LSL-Pik3ca H1047R/wt
Pdx1-Cre; LSL-Pik3ca H1047R/wt ; Rnf43 Δ/Δ

Figure 10. Analysis of RNAseq data shows differences among samples of different genotype
(A) Heatmap of differentially expressed genes across the samples derived from CBD of two different genotypes *Pdx1-Cre; LSL-Pik3ca$^{H1047R/wt}$; Rnf43$^{Δ/Δ}$* and *Pdx1-Cre; LSL-Pik3ca$^{H1047R/wt}$; Rnf43$^{wt/wt}$*. Samples were analyzed and sorted by logFC. Heatmap showing differential RNA-seq feature counts for both organoid lines with and without loss of *Rnf43.* (B) Graphical representation of differential expression analysis between *Pdx1-Cre; LSL-Pik3ca$^{H1047R/wt}$; Rnf43$^{Δ/Δ}$* and *Pdx1-Cre; LSL-Pik3ca$^{H1047R/wt}$; Rnf43$^{wt/wt}$*. The volcano plot is representing statistical significance between two cohorts of the samples by plotting by p-values against the log2-fold change of gene expression. Bioinformatic analysis of n=5 organoid lines derived from *Pdx1-Cre; LSL-Pik3ca$^{H1047R/wt}$; Rnf43$^{Δ/Δ}$* CBD vs. n=5 organoid lines derived from CBD of animals *Pdx1-Cre; LSL-Pik3ca$^{H1047R/wt}$; Rnf43$^{wt/wt}$* was performed by Fabio Boniolo. Generation and sacrifice of animals as well as establishment of organoid lines was done in the laboratory of Prof. Dr. med. Dieter Saur., Δ the recombined allele, wt the wild-type allele, * samples from the same organoid line from different passage (from left P3 and consecutively P7).

genes altered after UV irradiation which activates DNA damage, so it can be that this gene is connected in a cascade of events with *Rnf43* and takes part as well in DNA damage response. Interestingly, the most promising gene discovered in the analysis was *AA465934* (Fig. 10 B) due to being the only gene with significantly altered expression among the selected cohort. This gene was identified in processes related to heart cardiac dysfunction in studies on lncRNAs (Pant et al., 2019). In addition, *Slc5a5* (Solute Carrier Family 5 Member 5) was found to be downregulated among organoid lines derived from *Rnf43* deficient mice. Since this gene was also found to be downregulated in macrophages, it is another evidence that role of *Rnf43* remains not fully known. Intriguingly, most of the genes found during transcriptome analysis between selected two cohorts were found to be linked with immune system. That finding indicates the importance of setting focus on TME also in CBD cancer.

6.8 Large-scale drug screen identified different vulnerabilities in *Rnf43* WT and *Rnf43* KO

To further study the impact of loss of *Rnf43* and how it affects drug sensitivity, high-throughput drug screening (HTDS) was conducted. The aim was to identify the differences between the drug response in *Pdx1-Cre; LSL-Pik3ca$^{H1047R/wt}$; Rnf43$^{Δ/Δ}$* and *Pdx1-Cre; LSL-Pik3ca$^{H1047R/wt}$; Rnf43$^{wt/wt}$* organoid lines as well as to find the best candidates that could serve as an option for future targeted drug therapy. Drug candidates (Tab. 4) were selected from drugs in pre-clinical and clinical stages targeting a wide array of molecular targets to serve as a basic screen targeting various cancer-relevant pathways.

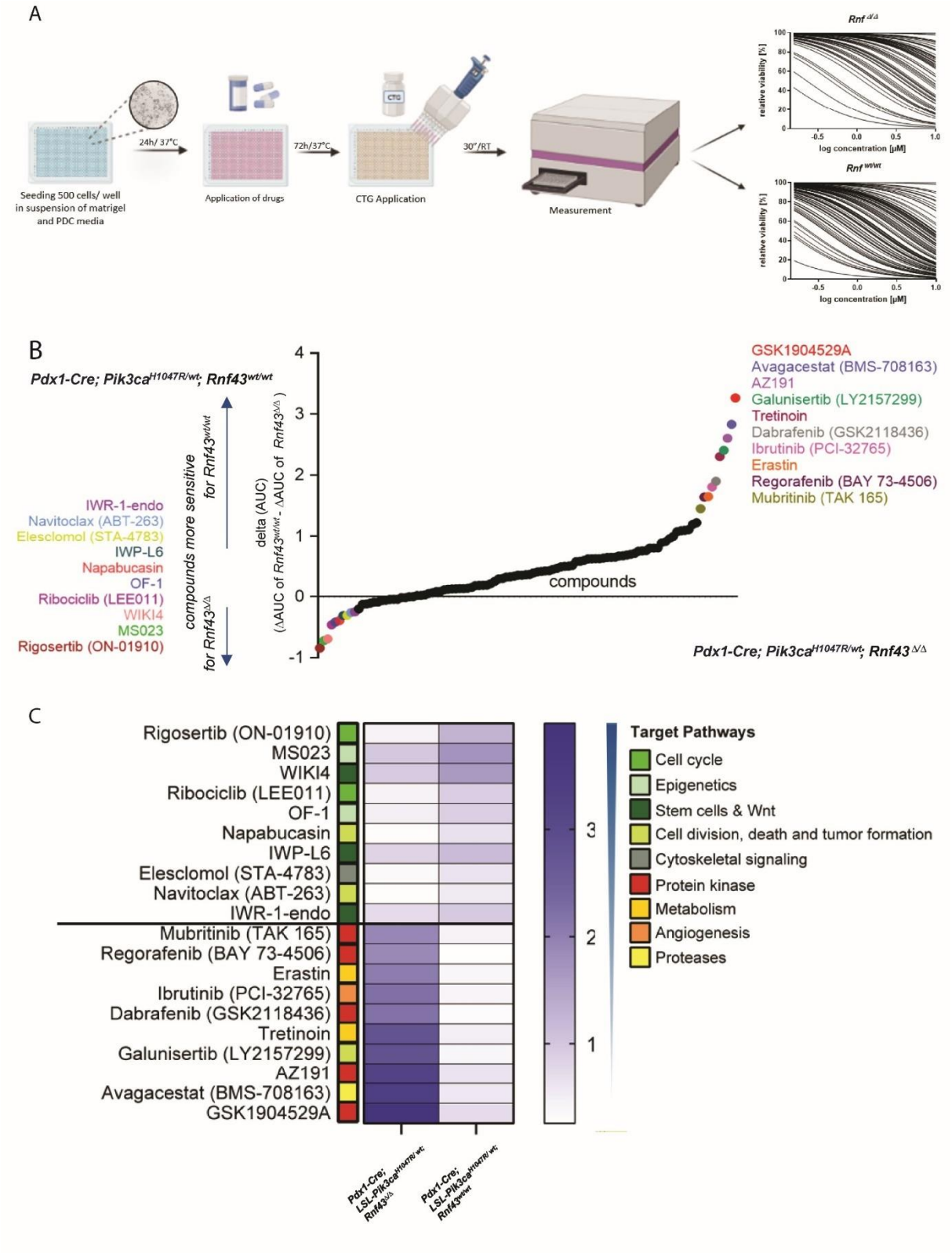
A
Seeding 500 cells/ well in suspension of matrigel and PDC media
24h/ 37°C
Application of drugs
72h/37°C
CTG Application
30''/RT
Measurement
relative viability [%]
log concentration [µM]
B
Pdx1-Cre; Pik3ca^H1047R/wt; Rnf43^wt/wt
compounds more sensitive for Rnf43^wt/wt
compounds more sensitive for Rnf43^Δ/Δ
delta (AUC)
(ΔAUC of Rnf43^wt/wt - ΔAUC of Rnf43^Δ/Δ)
compounds
IWR-1-endo
Navitoclax (ABT-263)
Elesclomol (STA-4783)
IWP-L6
Napabucasin
OF-1
Ribociclib (LEE011)
WIKI4
MS023
Rigosertib (ON-01910)
GSK1904529A
Avagacestat (BMS-708163)
AZ191
Galunisertib (LY2157299)
Tretinoin
Dabrafenib (GSK2118436)
Ibrutinib (PCI-32765)
Erastin
Regorafenib (BAY 73-4506)
Mubritinib (TAK 165)
Pdx1-Cre; Pik3ca^H1047R/wt; Rnf43^Δ/Δ
C
Rigosertib (ON-01910)
MS023
WIKI4
Ribociclib (LEE011)
OF-1
Napabucasin
IWP-L6
Elesclomol (STA-4783)
Navitoclax (ABT-263)
IWR-1-endo
Mubritinib (TAK 165)
Regorafenib (BAY 73-4506)
Erastin
Ibrutinib (PCI-32765)
Dabrafenib (GSK2118436)
Tretinoin
Galunisertib (LY2157299)
AZ191
Avagacestat (BMS-708163)
GSK1904529A
Target Pathways
Cell cycle
Epigenetics
Stem cells & Wnt
Cell division, death and tumor formation
Cytoskeletal signaling
Protein kinase
Metabolism
Angiogenesis
Proteases

Figure 11. Large-scale drug screen identified different in *Rnf43* WT and *Rnf43* fully knockout organoids Scheme of the procedure of a large-scale drug screen. (B) Drug effect is represented as the area under the curve of the dose response curves for each drug. The differential response between the *Pdx1-Cre; LSL-Pik3ca$^{H1047R/wt}$; Rnf43$^{\Delta/\Delta}$* and *Pdx1-Cre; LSL-Pik3ca$^{H1047R/wt}$; Rnf43$^{wt/wt}$* organoids is represented by the delta AUC for each compound. Compounds with a delta AUC >0 are more potent in wt organoids, while compounds with a delta AUC < 0 have a stronger effect in area under the curve determinates values of dose-response curves from each used compound. The experiment was conducted in one biological replicates. (C) Heatmap of the AUC of the top 10 drugs identified with the highest differential sensitivity in *Rnf43$^{\Delta/\Delta}$* as well as in *Rnf43$^{wt/wt}$* combined pathway. Different variations of colors indicate the pathway targeted by each drug. Shades of green correspond with drugs identified with the highest sensitivity in *Rnf43$^{\Delta/\Delta}$*, whereas the spectrum of orange was selected for the pathway most effective in *Rnf43$^{wt/wt}$* organoid lines.

In the conducted experiment, two types of organoid lines derived from murine CBD of GEMMs were screened. Due to technical reasons, the experiment was performed in 384 well plate format (Fig. 11 A). This allowed us to screen more candidates in a shorter timeframe, which is crucial in terms of implementing this methodology for further studies. The detailed description of the experiment can be found in Chapter 5.3.5. The impact of the drug on each organoid line was quantified through area under the curve calculated from dose response curves of each drug (Fig. 11 B). The drugs highlighted in color were selected as top 10 compounds for each group with the most differential drug response based on delta-AUC calculations (Fig. 11 B). For better understanding of the drug response, these top 10 drugs for each group were clustered in a heatmap. Furthermore, each drug was linked with the pathway they target. Identified inhibitors were connected to cell cycle, division death and tumor formation, epigenetic-related compounds, cytoskeleton, and protein kinase inhibitors (Fig. 11 C). The primary objective was to identify suitable compounds for inhibiting cell growth of *Rnf43* deficient organoid lines as well as to compare in the same screening the drugs with highest efficacy against organoid line with wild type *Rnf43* (proficient line). It was important to highlight the efficacy of the drug changes according to the genetic background of the organoid line. These findings prove the necessity of targeted therapies and the importance of precision medicine. The heatmap demonstrates that targeting certain pathways gives more promising results for either the line with loss of *Rnf43* or the organoid line with proficient *Rnf43*. For instance, inhibitors targeting Wnt and stem cells, cell cycle or epigenetics factors showed the most promising results, demonstrating higher efficacy against *Rnf43* deficient organoid line. On other hand, inhibitors against protein kinases, proteases metabolic processes were more efficient against the *Rnf43* proficient line. To better understand

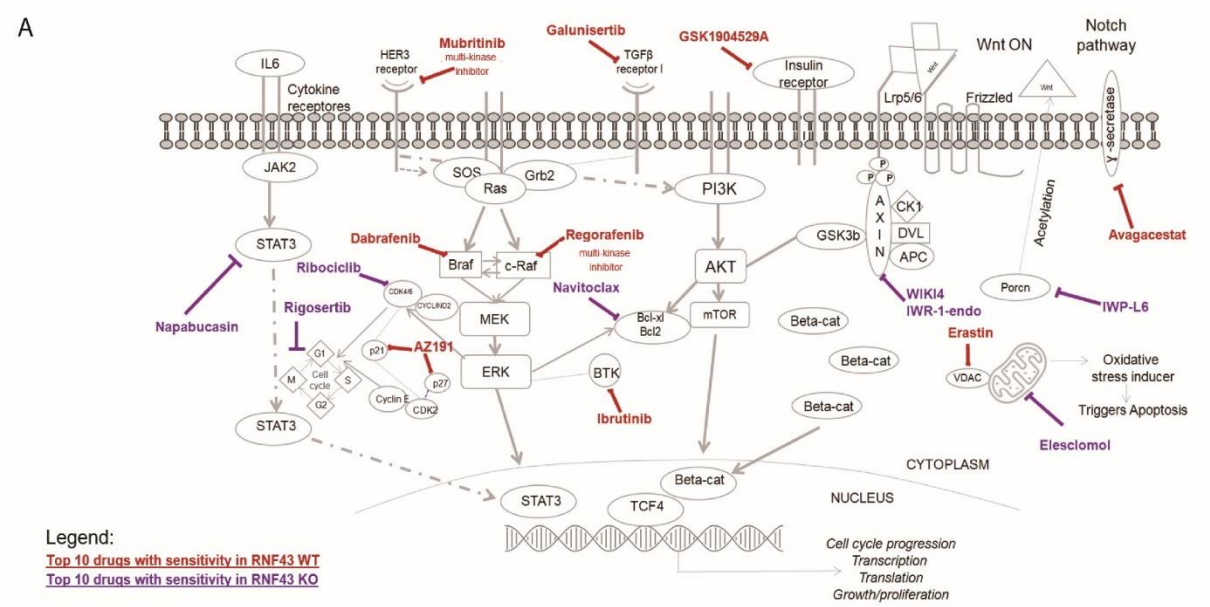

Figure 12. The top 10 drugs identified as sensitive in *Rnf43*$^{\Delta/\Delta}$ and *Rnf43*$^{wt/wt}$ lines play different roles in the important cellular signaling pathway.(A) genetic architecture of all diverse signaling pathways selected with top 10 inhibitors with sensitivity in - *Rnf43*$^{\Delta/\Delta}$ - indicated in red and *RNF43*$^{wt/wt}$ - indicated in violet – lines.

how distinct the pathways are targeted by each compound and to underscore the differences between both selected groups. a schematic representation of pathways targeted by top 10 selected drug from each cluster was depicted (Fig. 12). This data demonstrates differences between drug responses for each organoid line and provides an interesting insight into the complexity of drug therapy. The large drug screen provides valuable information about promising compounds that could be used in context of precise medicine based on genetic profile of each patient. Performed drug screen provided valuable information and its interesting findings require more validations to prove how effective these drugs are against CBD cancer.

7. Discussion and Outlook

Each year more patients are diagnosed with bile duct cancer. This rare malignant disease remains neglected and available treatment options have not improved notably over the last years. Unfortunately, there is still not much known about this subtype of cancer and the molecular mechanisms underlying the process of its development and progression. The risk of developing bile duct cancer increases with age as well as severe obesity, smoking, primary sclerosing cholangitis (PSC), hepatitis B and C virus infections, and chronic inflammatory diseases of the bile duct. Also, other conditions connected to biliary tract such as bile duct stones in the liver, choledochal cysts, diabetes mellitus, alcohol-related liver diseases can increase the risk of bile duct cancer. Since there are no standardized screening examinations to detect this cancer at an early stage and the symptoms are unspecific and easily overlooked, it is important to increase the knowledge about this subtype of the cancer to improve the outcome for diagnosed patients (Sung et al., 2021; Valle et al., 2016).

Using GEMM as a basic model to study genes contributing to initiation and progression of a disease as well as to explore therapeutic avenues are therefore crucial for identification of suitable therapeutic targets with potential clinical relevance. The recently published *piggyBac* transposon mutagenesis screen demonstrated the value of using molecular screening techniques for translation purposes to decipher genes that are relevant for CBC development (Falcomata et al., 2021). This resulted in a large dataset of novel genes potentially involved in CBD development and progression. Hereby, we focused on analysis on the role of *Rnf43*, which was one of the top hits in the conducted screen. *Rnf43* has been shown to be relevant in various cancers including gastric carcinomas, ovarian mucinous tumors, CRC and endometrial carcinomas (Giannakis et al., 2014; Neumeyer et al., 2019; Pique et al., 2020). However, its role in CBD development is not well understood. We therefore chose *Rnf43* for further validation.

Analysis of *piggyBac* transposon screen allowed to find new genes important for CBD development (Falcomata et al., 2021). One of the aims of this work was to confirm the importance and study the role of *Rnf43* in CBD cancer with various techniques both in vitro and in vivo. Starting with *in silico* analysis of CIS pattern for *Rnf43* not only in CBD – the main subject of this present study – but also in pancreas. Based on available research findings, it was expected *Rnf43* to be a tumor suppressor gene in both subtypes of cancer entities (Koo et al.,

2012; Ryland et al., 2013). The insertion of transposons was scattered throughout whole sequence of the gene, but interestingly the amount of hits that *Rnf43* had in CBD was significantly higher in comparison to pancreas, which demonstrates a tumor suppressive role of *Rnf43* and underscores the crucial role of Rnf43 for CBD cancer compared to pancreatic cancer.

New mouse model was generated to study the effect of loss of *Rnf43 in vivo*. Successfully established GEMM confirmed the relevance of *Rnf43* for initiation and progression of CBD cancer, but only for mice harboring mutations in *Pik3ca* pathway. Importance of this pathway was previously verified by various studies performed on mice and human samples (Falcomata et al., 2021; Wu et al., 2019). Deletion of *Rnf43* in GEMM harboring hotspot mutation G12D in *Kras* did not show any macroscopic changes in the bile duct. Interestingly, effects of *Rnf43* KO in this model were macroscopically detectable in duodenum. Importance of *Rnf43* on CRC development were highlighted in research of Koo and colleagues (Koo et al., 2012). In our studies, we used the *Pdx1-Cre* promotor, expression of this promotor in several different organs of the gastrointestinal tract was described in the study by Falcomata et al 2021. Hereby we also confirm the significance of the driver oncogene for cancer development. Since both GEMM's used in our studies were harboring different driver oncogenes under control of promotor expressed in different organs of gastrointestinal tract we were able to observe shift of carcinogenesis. In the mouse model *Pdx1-Cre; Pik3ca^{H1047R}; Rnf43* KO we detected CBD cancer development whereas *Pdx1-Cre; Kras^{G12D}; Rnf43* KO mice developed adenomas in duodenum. Even though a larger cohort of animals needs to be analyzed, the pattern remains clear. Although GEMM's used for our study are not perfect, they gave interesting insight of complexity behind cancer development based on investigation of different molecular pathways.

Furthermore, we collected material for histopathological analysis. We could confirm that *Pdx1-Cre; Pik3ca^{H1047R}; Rnf43* KO mouse model developed carcinoma in CBD. We could also observe abnormalities in the cell pattern of duodenum, which indicates development of adenomas. Although, compared with *Pik3ca* macroscopic we couldn't observe any changes in CBD of *Pdx1-Cre; Kras^{G12D}; Rnf43* KO mice it was possible to find some abnormalities also there. Some parts of the CBD derived tissues were showing neoplastic changes in the epithelium. This interesting finding may indicate the need for co-occurrence of additional mutation for CBD cancer initiation, since Kras G12D is identified as one of the most frequently mutated gene among patients diagnosed with CBD cancer (Guo, Zhou et al. 2022).

In the duodenum, the observed abnormalities of architecture in villous and crypt epithelium resembled duodenal adenomas. As already mentioned above, *in vivo* studies had confirmed the tumor suppressive role of *Rnf43.* To understand better the impact of loss of *Rnf43,* we aimed to establish 2D cell lines derived from our GEMM, which was however not successful, as the cell did not adhere to the plastic of the cell culture flasks. We therefore decided to switch to 3D culture. Establishment of organoid culture derived from CBD was successful after small adjustments of the protocol that was previously established for isolation of pancreatic organoid lines. We observed that fully digested tissue to single cell suspension – as described in the protocol for isolation of pancreatic organoids - does not have the proliferative ability to form 3D structures. We observed increased effectiveness of isolation after embedding also chunks of tissue together with single cells. To further improve the isolation process, we also decided to not strain the suspension after digestion but wash it and culture it in Matrigel (354230).

Moreover, we aimed to conduct basic characterization of derived from CBD organoids. Comparison of macroscopic images of lines with and without loss of *Rnf43* demonstrated 3D lumen structures remained phenotypically consistent throughout long term culture. Also, H&E staining confirmed these findings. We used CK19 (RRID:AB_10990774) as a marker for the presence of epithelial cells derived from CBD. Unfortunately, we are lacking a specific marker for CBD, as CK19 (RRID:AB_10990774) can be used as marker for organoids derived from pancreas since they share a common ductal lineage. This indicates the importance of finding better markers that would allow to differentiate cells derived from these tissues.

The observed growth advantage of lines with *Rnf43* KO over the control line, supports our *in vivo* and in vitro findings Furthermore it fits with results of analysis of transposon screen conducted on GEMM. Based on our studies we were able to identify Rnf43 as tumor suppressor in CBD cancer.

Established organoid lines from *Pdx1-Cre; Pik3Ca$^{H1047R/wt}$; Rnf43* KO line together with *Pdx1-Cre; Pik3Ca$^{H1047R/wt}$* were used to study the connection of *Rnf43* expression and endogenous Wnt signaling activity. Widely applied TOP/FOP Luciferase reporter assay was used to measure activity of Wnt pathway. Organoid lines used for our studies allowed to not only confirm the link between *Rnf43* deletion and Wnt signaling activity, but also demonstrated the significance of *Rnf43* loss for the overactivation of Wnt/β-catenin pathway. These findings confirmed the connection of our studied gene, *Rnf43*, and it is function in regulating of Wnt activity (Jiang et al., 2013; Loregger et al., 2015). Impact of excessively activated Wnt pathway

promotes tumor growth. Dysregulation in this pathway leads to uncontrolled cell division, which is commonly associated with cancer. In studies conducted by Moreno-Londoño et al research observed ability of CRC's spheroids to exit cell cycle arrest and re-grow after treatment with 5FU. The mechanisms behind this phenomenon remain unknown, although their findings indicate significant role of canonical Wnt signaling in chemoresistance development(Gou et al., 2019; Moreno-Londono et al., 2023).

In order to understand the impact of *Rnf43* loss on gene expression pattern, organoids derived from CBD were RNA-sequenced together with the appropriate controls. Organoid culture serves as a great tool to study genetics of cancer development. Among the upregulated genes in the *Rnf43* knockouts was i.e. *TBX3* and St*3gal6* but their role in CBA cancer needs to be further evaluated. Recent studies about therole of *Rnf43* revealed novel function of this gene in DNA damage response. Loss of *Rnf43* was correlated with higher resistance to radio- and chemotherapy (Neumeyer et al., 2021). In addition, depletion of *Rnf43* was found to trigger apoptosis upon etoposide-induced DNA damage (Wikiniyadhanee et al., 2020). The need of exploring the function of *Rnf43* is still existing. To address the limitations of RNAseq, new tools are already widely used in order to study diversity among the cancer cells and gene pattern expression within them. Single cell RNA could offer meaningful insights to identify differentially expressed genes of CBD cancer and could answer the question about the mechanism driving loss of *Rnf43* at the singe-cell level. Additionally conducting a single cell RNA-seq analysis of the bulk tumor could also help with understanding the impact of tumor environment on the gene expression. Studies on TME offers new insight on correlation between different cell populations and their impact on tumor growth or resistance (Chan et al., 2019). The impact of loss *Rnf43* on TME remodeling of mice with PDAC was shown by Hosein and his colleagues. Upon loss of *Rnf43* mice from studied cohort develop more cystic lesions detailed analysis of conducted scRNa seq revealed depletion in macrophages and increase of T and B lymphocytes. Immune microenvironment was altered due to deletion of Rnf43, these findings highlight the potential of research focused on TME (Hosein et al., 2022).Since the function of Rnf43 is not fully understood, conducting scRNA on bulk tumor could provide insights into potential correlations between deficiency of this gene, alterations genes pattern expression, as well as the interplay of different cell populations present in TME in our bulk samples.

In the final experiment of our work, we conducted a drug screen on organoid lines derived from *Pdx1-Cre; LSL-Pik3ca$^{H1047R/wt}$* and *Pdx1-Cre; LSL-Pik3ca$^{H1047R/wt}$; Rnf43$^{fl/fl}$* mice. Since there

were no clear hints in the sequencing data on which genes or pathway we should target, we decided to perform large scale screen with more than 100 compounds. Variety of selected drugs allowed to reveal potentially interesting targets, like cell cycle (Ribociclib) or expected Wnt pathway (WIKI4, IWP-L6), for validation and shed some light on translation aspects of the present study. As already pointed out here and shown by different research studies, *Rnf43* holds potential as promising focus for development of specific targeted therapies. Even though finding new therapeutic approaches for targeting selected mutations may sound like a right course to achieve personalized, accurate and promising therapies for patients, the real work has just begun (Pauli et al., 2017). There are many aspects to be considered with this type of approach: first of all, some of the drugs have dose-limitations since they showed toxicity potential; second, directly targeting compound of the pathway may also affect the normal Wnt activity, which could lead to developmental disorders and disruption in homeostasis; third, there is also a problem of cross functionality since all of the cellular processes are linked. The need to validate such screens is a necessity. Various studies are already aiming Wnt pathway as a target, resulting in development of promising drugs, such as PORCN inhibitor (WNT974) (Rodon et al., 2021) and Pyrvinium (Rodgers et al., 2022). Examples of these drugs have been tested in different phases of clinical studies. Selecting most promising candidates for combinatory therapies among the components used for large drug screen could shed a new light on drugs efficacy. The concept of using such a treatment is already widely studied for years since it is shown that this type of therapy improves the outcome of patients due to synergistic activities of the drugs (Quinn et al., 2017). Even drugs which are already in usage for years in different combinations and ratios can yield better results. Targeting cells with a component against specific mutations decreases side effects due to lower dosage and the toxicity potential of combined compounds (Albain et al., 2008; Yuan et al., 2017). Nevertheless, it is essential to investigate the side effects of the treatment to balance the benefits and take into account the risks that usage of newly discovered drug brings (Sun et al., 2022). For better understanding the mechanism behind drug response, it would be interesting to use orthotopic implantation model. To the best of our knowledge, so far there is none described for CBD, however Erlangga and colleagues developed a model of injecting gallbladder cancer-derived organoids mixed with Matrigel (354230) directly to lumen of the organ of origin (Erlangga et al., 2019). In the future, it would be interesting to establish the same procedure in Prof. Dr. Dieter Saur's research group using CBD cancer-derived organoids. Moreover, generation of biobank from human derived organoids from patients diagnosed with CBD cancer would be game changing for assessing drug efficacy in implanted mouse model. This type of studies gives an overview on *in vivo*

relevance of applied drug. Benefits of conducting experiment resembling more natural tumor microenvironment (TME) increases reliability of drug efficacy for clinical applications. In context of physiological complexity studies on TME enhances effectiveness and accuracy of outcome. Even though researchers are focusing more and more on interactions between tumor cells and other tissue surrounding components, this topic/subject is widely unknown (Murgai et al., 2017; Xiao & Yu, 2021). Impact of loss of *RNF43* on TME may give valuable insights on direction for targeted therapies specifically on patient derived organoids (PDO) screened for mutations in *RNF43*. Combining multiple diverse techniques for more comprehensive approach of understanding mechanism underlying CBD cancer development is nowadays possible. Each day the scientific world is providing more groundbreaking discoveries gathered from the research. Now more than broad spectrum of accessible techniques used for studying cancer development and progression, discovery of novel approaches for prevention, early detection, and treatment brings us one step closer to overcome cancer.

In the final remarks of described results, conducted research on role of *Rnf43* shed some lights on molecular aspects of CBD cancer development. Hereby analyzed data underscore tumor suppressive role of *Rnf43*. The analysis of CIS pattern among data derived from sequencing pancreatic and CBD samples confirmed this finding. Moreover, it showed significantly higher impact of loss of this gene on CBD cancer development as compared to pancreas. *In vitro* studies highlighted the importance of driver oncogene on shift of tumorigenesis. Once again, pathway mutations in *Pi3k* were confirmed to be more important for CBD cancer development, and combined with loss of *Rnf43* it enhanced the process. In contrast, activation of *Kras* pathway combined with KO of *Rnf43* did not have any impact on CBD while demonstrating alterations in duodenum. Established CBD-derived organoid lines allowed in *in vitro* studies to prove correlation between loss of *Rnf43* and Wnt overexpression.

In summary, there is a necessity to conduct more experiments with the aim of validating the findings of *Rnf43* loss on CBD development. The need to increase the cohort of analyzed animals from both cohorts would not only increase the reliability of survival data but also allowed to collect more samples for further analysis. It is essential to use them for sequencing analysis as well as for basic research like quantitative staining. Furthermore, it would be interesting to validate the results of the HTDS and check the alteration in gene expression pattern based on applied drug. Additionally, analyzing the impact of *Rnf43* deletion on downstream genes of Wnt pathway could give a hit on possibility of existence of rescue mechanism. Establishing primers for RT-qPCR for genes involved in the pathway could give

first impression of how mRNA levels of these genes are affected by *Rnf43* loss. Moreover, it would be interesting to see on the protein level the potential shift in expression. Selection and optimization of antibodies that would work is a difficult task since the commercially available antibodies in most of the cases are not efficient and development of new ones takes time. Access to different techniques could help with identifying such mechanisms and unveil therapeutic strategies in order to reverse an effect on *Rnf43* loss. Interesting option is as well research on TME and impact on single cell on aggressiveness of cancer. Since it is overlooked but also an important part of studies on CBD cancer development and progression.

Regardless all the efforts, *Rnf43* still remains a challenging target for further studies. Loss of function contributes to tumorigenesis of several cancer entities (Neumeyer et al., 2021; Neumeyer et al., 2019). Unfortunately, there is still not much known about the molecular mechanisms underlying this process that stays elusive. Dysregulation of Wnt/β-catenin pathway is strongly linked with cancer development. It is important to carefully study inactivating mutations concerning this pathway since it can deregulate the delicately balanced homeostasis in the entire mammalian organism (Wang et al., 2016; Zhang & Wang, 2020). Furthermore, it would be also interesting topic to study other functions of *Rnf43*, since recent discoveries indicated the relevance of impact in loss of this gene in other pathways (Tsukiyama et al., 2020).

The amount of possibilities is countless, being limited only by creativity in application of multidisciplinary techniques in the studies. The urgency to increase the survival rates among the patients diagnosed with this rare disease is real and combined effort of specialists from different fields is crucial to provide optimal care to patients diagnosed with CBD cancer.

8. Disclosures

The work described in this doctoral thesis is composed by mouse lines, experiments, and data analysis shared with other members from Prof. Dr. med. Dieter Saur's research group. *Pdx1-Cre; LSL-Pik3ca$^{H1047R/wt}$; Rnf43$^{fl/fl}$* and *Pdx1-Cre; LSL-Pik3ca$^{H1047R/wt}$; Rnf43$^{wt/wt}$* mouse lines were bred, weekly monitored, and sacrificed. Samples from *Pdx1-Cre; LSL-Pik3ca$^{H1047R/wt}$* mouse line were taken from the cohort bred by Tatiana Martins. Bulk tumor RNA-seq data analyses, namely correlation matrixes, and volcano plot representation between PPI3KRNFand PPI3K samples, were performed by Fabio Boniolo. Further analysis of transposon screen data used in paper Falcomatà et al, 2021 was performed by Anantharamanan Rajamani.

Regarding the other work described throughout the thesis, i.e., breedings, mice dissection, and establishment of primary murine organoid lines derived from CBD of GEMM together with analysis was performed by Joanna Madej. Parts of the figures used in this thesis were created with BioRender.com (e.g. 7A, 9A and 11A).

9. Acknowledgements

Hereby, I would like to thank everyone who contributed to the success of this PhD thesis.

First, I thank Prof. Dr. med. Dieter Saur for giving me the opportunity to work on this interesting project, for his advice, valuable comments, and support on the projects and revision of the thesis.

I owe my gratitude to Prof. Dr. rer. nat. Klaus-Peter Janssen and Prof. Dr. med. Maximilian Reichert for their kindness being members of my thesis committee and for all the help that I received while working on this project.

I would also like to thank Bettina Kratzer and Raphaela Blum, from the TUM Graduate Center for their help and constant support with any questions concerning my graduation.

Furthermore, I owe my gratitude to…

… Dr. med. vet. Katja Steiger and Nils Wirges for the histopathological evaluation of the Cdh1 pancreatic tumor tissues.

… Dr. Christian Schneeweiß for careful revision of the thesis and for all the help and kindness received not only during the time of writing but continuously throughout all the years

… Christian Veltkamp PhD for the patience while teaching, discussions and the time and support received at any circumstances.

…Sebastian Karg for his selfless help and patience while answering all the questions while sharing his knowledge

…Dr. Katja Peschke for constant help and support

… Tânia Custódio Santos PhD not only for being my mouse partner and for and sharing her knowledge and expertise, but also for supporting me through all way, for being kind, compassion and thoughtful. And for becoming my friend, even though it wasn't expected, and for staying by my side no matter what.

… all animal caretakers from the Zentrum für Präklinische Forschung, for caring for the mice.

Finally, I especially thank my family and my friends who always supported and believed in me. Without them, my dissertation would not have been possible.

Especially, I would like to thank Jana, Katka, Meng Lei, Zonera and Kasia T. for becoming my friend and for constant support.

Finally, I would also like to thank all the amazing people that crossed their paths with mine and made this experience so much better.

Na koniec chciałabym podziękować

...mojej siostrze Oli, która rozumie mnie jak nikt inny, za to że jest niezastąpiona częścią mojego życia.

...oraz mojej najlepszej przyjaciółce Marlenie, która zawsze znajdzie czas dla mnie i pomimo dzielącego nas dystansu zawsze jest obok mnie, wspierająca, kochana, utwierdzająca mnie w przekonaniu, że istnieją relacje, które są silniejsze niż więzy krwi.

10. References

Aitchison, F. (2009). *A Guide to Radiological Procedures*. Saunders Elsevier. https://books.google.de/books?id=_tkoApDyntwC

Albain, K. S., Nag, S. M., Calderillo-Ruiz, G., Jordaan, J. P., Llombart, A. C., Pluzanska, A., Rolski, J., Melemed, A. S., Reyes-Vidal, J. M., Sekhon, J. S., Simms, L., & O'Shaughnessy, J. (2008). Gemcitabine plus Paclitaxel versus Paclitaxel monotherapy in patients with metastatic breast cancer and prior anthracycline treatment. *J Clin Oncol*, *26*(24), 3950-3957. https://doi.org/10.1200/JCO.2007.11.9362

Alvaro, D., Bragazzi, M. C., Benedetti, A., Fabris, L., Fava, G., Invernizzi, P., Marzioni, M., Nuzzo, G., Strazzabosco, M., Stroffolini, T., & committee, A. C. (2011). Cholangiocarcinoma in Italy: A national survey on clinical characteristics, diagnostic modalities and treatment. Results from the "Cholangiocarcinoma" committee of the Italian Association for the Study of Liver disease. *Dig Liver Dis*, *43*(1), 60-65. https://doi.org/10.1016/j.dld.2010.05.002

Banales, J. M., Marin, J. J. G., Lamarca, A., Rodrigues, P. M., Khan, S. A., Roberts, L. R., Cardinale, V., Carpino, G., Andersen, J. B., Braconi, C., Calvisi, D. F., Perugorria, M. J., Fabris, L., Boulter, L., Macias, R. I. R., Gaudio, E., Alvaro, D., Gradilone, S. A., Strazzabosco, M., . . . Gores, G. J. (2020). Cholangiocarcinoma 2020: the next horizon in mechanisms and management. *Nat Rev Gastroenterol Hepatol*, *17*(9), 557-588. https://doi.org/10.1038/s41575-020-0310-z

Bass, A. J., Thorsson, V., Shmulevich, I., Reynolds, S. M., Miller, M., Bernard, B., Hinoue, T., Laird, P. W., Curtis, C., Shen, H., Weisenberger, D. J., Schultz, N., Shen, R., Weinhold, N., Kelsen, D. P., Bowlby, R., Chu, A., Kasaian, K., Mungall, A. J., . . . Center, U. N. C. L. C. C. (2014). Comprehensive molecular characterization of gastric adenocarcinoma. *Nature*, *513*(7517), 202-209. https://doi.org/10.1038/nature13480

Bian, J. L., Wang, M. M., Tong, E. J., Sun, J., Li, M., Miao, Z. B., Li, Y. L., Zhu, B. H., & Xu, J. J. (2017). Benefit of everolimus in treatment of an intrahepatic cholangiocarcinoma patient with a PIK3CA mutation. *World J Gastroenterol*, *23*(23), 4311-4316. https://doi.org/10.3748/wjg.v23.i23.4311

Bolondi, L., Cillo, U., Colombo, M., Craxi, A., Farinati, F., Giannini, E. G., Golfieri, R., Levrero, M., Pinna, A. D., Piscaglia, F., Raimondo, G., Trevisani, F., Bruno, R., Caraceni, P., Ciancio, A., Coco, B., Fraquelli, M., Rendina, M., Squadrito, G., & Toniutto, P. (2013). Position paper of the Italian Association for the Study of the Liver (AISF): the multidisciplinary clinical approach to hepatocellular carcinoma. *Dig Liver Dis*, *45*(9), 712-723. https://doi.org/10.1016/j.dld.2013.01.012

Borden, K. L., & Freemont, P. S. (1996). The RING finger domain: a recent example of a sequence-structure family. *Curr Opin Struct Biol*, *6*(3), 395-401. https://doi.org/10.1016/s0959-440x(96)80060-1

Boyer, J. L. (2013). Bile formation and secretion. *Compr Physiol*, *3*(3), 1035-1078. https://doi.org/10.1002/cphy.c120027

Bray, F., Ferlay, J., Soerjomataram, I., Siegel, R. L., Torre, L. A., & Jemal, A. (2018). Global cancer statistics 2018: GLOBOCAN estimates of incidence and mortality worldwide for 36 cancers in 185 countries. *CA Cancer J Clin*, *68*(6), 394-424. https://doi.org/10.3322/caac.21492

Cai, C., Tang, Y.-D., Zhai, J., & Zheng, C. (2022). The RING finger protein family in health and disease. *Signal Transduction and Targeted Therapy*, *7*(1), 300. https://doi.org/10.1038/s41392-022-01152-2

Cairo, S., Armengol, C., De Reynies, A., Wei, Y., Thomas, E., Renard, C. A., Goga, A., Balakrishnan, A., Semeraro, M., Gresh, L., Pontoglio, M., Strick-Marchand, H., Levillayer, F., Nouet, Y., Rickman, D., Gauthier, F., Branchereau, S., Brugieres, L., Laithier, V., . . . Buendia, M. A. (2008). Hepatic stem-like phenotype and interplay of Wnt/beta-catenin and Myc signaling in aggressive childhood liver cancer. *Cancer Cell*, *14*(6), 471-484. https://doi.org/10.1016/j.ccr.2008.11.002

Capili, A. D., Edghill, E. L., Wu, K., & Borden, K. L. (2004). Structure of the C-terminal RING finger from a RING-IBR-RING/TRIAD motif reveals a novel zinc-binding domain distinct from a RING. *J Mol Biol*, *340*(5), 1117-1129. https://doi.org/10.1016/j.jmb.2004.05.035

Castaing, D. (2008). Surgical anatomy of the biliary tract. *HPB (Oxford)*, *10*(2), 72-76. https://doi.org/10.1080/13651820801992518

Chan, T. S., Shaked, Y., & Tsai, K. K. (2019). Targeting the Interplay Between Cancer Fibroblasts, Mesenchymal Stem Cells, and Cancer Stem Cells in Desmoplastic Cancers. *Front Oncol*, *9*, 688. https://doi.org/10.3389/fonc.2019.00688

Choi, J., Ghoz, H. M., Peeraphatdit, T., Baichoo, E., Addissie, B. D., Harmsen, W. S., Therneau, T. M., Olson, J. E., Chaiteerakij, R., & Roberts, L. R. (2016). Aspirin use and the risk of cholangiocarcinoma. *Hepatology*, *64*(3), 785-796. https://doi.org/10.1002/hep.28529

Conrad, R., ShobhaCastelino, P., Cobb, C., & Raza, A. (2012). Role of cytopathology in the diagnosis and management of gastrointestinal tract cancers. *J Gastrointest Oncol*, *3*(3), 285-298. https://doi.org/10.3978/j.issn.2078-6891.2012.023

Daniels, D. L., & Weis, W. I. (2005). Beta-catenin directly displaces Groucho/TLE repressors from Tcf/Lef in Wnt-mediated transcription activation. *Nat Struct Mol Biol*, *12*(4), 364-371. https://doi.org/10.1038/nsmb912

Dirks, M., Ewerbeck, N. K., Ballhause, T. M., Weiss, S., Luebke, A., Schlickewei, C., Frosch, K. H., & Priemel, M. (2023). The diagnostic accuracy of 332 incisional biopsies in patients with malignant tumors in the musculoskeletal system. *World J Surg Oncol*, *21*(1), 4. https://doi.org/10.1186/s12957-022-02883-w

Dolgin, E. (2023). Personalized cancer vaccines pass first major clinical test. *Nat Rev Drug Discov*, *22*(8), 607-609. https://doi.org/10.1038/d41573-023-00118-5

Du, J., Lv, X., Zhang, Z., Huang, Z., & Zhang, E. (2023). Revisiting targeted therapy and immunotherapy for advanced cholangiocarcinoma. *Front Immunol*, *14*, 1142690. https://doi.org/10.3389/fimmu.2023.1142690

Erlangga, Z., Wolff, K., Poth, T., Peltzer, A., Nahnsen, S., Spielberg, S., Timrott, K., Woller, N., Kuhnel, F., Manns, M. P., Saborowski, A., Vogel, A., & Saborowski, M. (2019). Potent Antitumor Activity of Liposomal Irinotecan in an Organoid- and CRISPR-Cas9-Based Murine Model of Gallbladder Cancer. *Cancers (Basel)*, *11*(12). https://doi.org/10.3390/cancers11121904

Eser, S., Reiff, N., Messer, M., Seidler, B., Gottschalk, K., Dobler, M., Hieber, M., Arbeiter, A., Klein, S., Kong, B., Michalski, C. W., Schlitter, A. M., Esposito, I., Kind, A. J., Rad, L., Schnieke, A. E., Baccarini, M., Alessi, D. R., Rad, R., . . . Saur, D. (2013). Selective requirement of PI3K/PDK1 signaling for Kras oncogene-driven pancreatic cell plasticity and cancer. *Cancer Cell*, *23*(3), 406-420. https://doi.org/10.1016/j.ccr.2013.01.023

Esteller, A. (2008). Physiology of bile secretion. *World J Gastroenterol*, *14*(37), 5641-5649. https://doi.org/10.3748/wjg.14.5641

Falcomata, C., Barthel, S., Ulrich, A., Diersch, S., Veltkamp, C., Rad, L., Boniolo, F., Solar, M., Steiger, K., Seidler, B., Zukowska, M., Madej, J., Wang, M., Ollinger, R., Maresch, R., Barenboim, M., Eser, S., Tschurtschenthaler, M., Mehrabi, A., . . . Saur, D. (2021). Genetic Screens Identify a Context-Specific PI3K/p27Kip1 Node Driving Extrahepatic Biliary Cancer. *Cancer Discov*, *11*(12), 3158-3177. https://doi.org/10.1158/2159-8290.CD-21-0209

Fan, B., Malato, Y., Calvisi, D. F., Naqvi, S., Razumilava, N., Ribback, S., Gores, G. J., Dombrowski, F., Evert, M., Chen, X., & Willenbring, H. (2012). Cholangiocarcinomas can originate from hepatocytes in mice. *J Clin Invest*, *122*(8), 2911-2915. https://doi.org/10.1172/JCI63212

Fang, L., Ford-Roshon, D., Russo, M., O'Brien, C., Xiong, X., Gurjao, C., Grandclaudon, M., Raghavan, S., Corsello, S. M., Carr, S. A., Udeshi, N. D., Berstler, J., Sicinska, E., Ng, K., & Giannakis, M. (2022). RNF43 G659fs is an oncogenic colorectal cancer mutation and sensitizes tumor cells to PI3K/mTOR inhibition. *Nat Commun*, *13*(1), 3181. https://doi.org/10.1038/s41467-022-30794-7

Gao, Y., Cai, A., Xi, H., Li, J., Xu, W., Zhang, Y., Zhang, K., Cui, J., Wu, X., Wei, B., & Chen, L. (2017). Ring finger protein 43 associates with gastric cancer progression and attenuates the stemness of gastric cancer stem-like cells via the Wnt-beta/catenin signaling pathway. *Stem Cell Res Ther*, *8*(1), 98. https://doi.org/10.1186/s13287-017-0548-8

Giannakis, M., Hodis, E., Jasmine Mu, X., Yamauchi, M., Rosenbluh, J., Cibulskis, K., Saksena, G., Lawrence, M. S., Qian, Z. R., Nishihara, R., Van Allen, E. M., Hahn, W. C., Gabriel, S. B., Lander, E. S., Getz, G., Ogino, S., Fuchs, C. S., & Garraway, L. A. (2014). RNF43 is frequently mutated in colorectal and endometrial cancers. *Nat Genet*, *46*(12), 1264-1266. https://doi.org/10.1038/ng.3127

Goeppert, B., Konermann, C., Schmidt, C. R., Bogatyrova, O., Geiselhart, L., Ernst, C., Gu, L., Becker, N., Zucknick, M., Mehrabi, A., Hafezi, M., Klauschen, F., Stenzinger, A., Warth, A., Breuhahn, K., Renner, M., Weichert, W., Schirmacher, P., Plass, C., & Weichenhan, D. (2014). Global alterations of DNA methylation in cholangiocarcinoma target the Wnt signaling pathway. *Hepatology*, *59*(2), 544-554. https://doi.org/10.1002/hep.26721

Gou, Q., Dong, C., Jin, J., Liu, Q., Lu, W., Shi, J., & Hou, Y. (2019). PPARalpha agonist alleviates tumor growth and chemo-resistance associated with the inhibition of glucose metabolic pathway. *Eur J Pharmacol*, *863*, 172664. https://doi.org/10.1016/j.ejphar.2019.172664

Greten, T. F., Schwabe, R., Bardeesy, N., Ma, L., Goyal, L., Kelley, R. K., & Wang, X. W. (2023). Immunology and immunotherapy of cholangiocarcinoma. *Nat Rev Gastroenterol Hepatol*, *20*(6), 349-365. https://doi.org/10.1038/s41575-022-00741-4

Hingorani, S. R., Petricoin, E. F., Maitra, A., Rajapakse, V., King, C., Jacobetz, M. A., Ross, S., Conrads, T. P., Veenstra, T. D., Hitt, B. A., Kawaguchi, Y., Johann, D., Liotta, L. A., Crawford, H. C., Putt, M. E., Jacks, T., Wright, C. V., Hruban, R. H., Lowy, A. M., & Tuveson, D. A. (2003). Preinvasive and invasive ductal pancreatic cancer and its early detection in the mouse. *Cancer Cell*, *4*(6), 437-450. https://doi.org/10.1016/s1535-6108(03)00309-x

Hosein, A. N., Dangol, G., Okumura, T., Roszik, J., Rajapakshe, K., Siemann, M., Zaid, M., Ghosh, B., Monberg, M., Guerrero, P. A., Singhi, A., Haymaker, C. L., Clevers, H., Abou-Elkacem, L., Woermann, S. M., & Maitra, A. (2022). Loss of Rnf43 Accelerates Kras-Mediated Neoplasia and Remodels the Tumor Immune Microenvironment in Pancreatic Adenocarcinoma. *Gastroenterology*, *162*(4), 1303-1318 e1318. https://doi.org/10.1053/j.gastro.2021.12.273

Hou, X., Du, Y., Deng, Y., Wu, J., & Cao, G. (2015). Sleeping Beauty transposon system for genetic etiological research and gene therapy of cancers. *Cancer Biol Ther*, *16*(1), 8-16. https://doi.org/10.4161/15384047.2014.986944

Hoyos, S., Navas, M. C., Restrepo, J. C., & Botero, R. C. (2018). Current controversies in cholangiocarcinoma. *Biochim Biophys Acta Mol Basis Dis*, *1864*(4 Pt B), 1461-1467. https://doi.org/10.1016/j.bbadis.2017.07.027

Ivics, Z., Hackett, P. B., Plasterk, R. H., & Izsvak, Z. (1997). Molecular reconstruction of Sleeping Beauty, a Tc1-like transposon from fish, and its transposition in human cells. *Cell*, *91*(4), 501-510. https://doi.org/10.1016/s0092-8674(00)80436-5

Ivics, Z., Li, M. A., Mates, L., Boeke, J. D., Nagy, A., Bradley, A., & Izsvak, Z. (2009). Transposon-mediated genome manipulation in vertebrates. *Nat Methods*, *6*(6), 415-422. https://doi.org/10.1038/nmeth.1332

Jackson, E. L., Willis, N., Mercer, K., Bronson, R. T., Crowley, D., Montoya, R., Jacks, T., & Tuveson, D. A. (2001). Analysis of lung tumor initiation and progression using conditional expression of oncogenic K-ras. *Genes Dev*, *15*(24), 3243-3248. https://doi.org/10.1101/gad.943001

Jansen, H., Pape, U. F., & Utku, N. (2020). A review of systemic therapy in biliary tract carcinoma. *J Gastrointest Oncol*, *11*(4), 770-789. https://doi.org/10.21037/jgo-20-203

Jiang, X., Hao, H. X., Growney, J. D., Woolfenden, S., Bottiglio, C., Ng, N., Lu, B., Hsieh, M. H., Bagdasarian, L., Meyer, R., Smith, T. R., Avello, M., Charlat, O., Xie, Y., Porter, J. A., Pan, S., Liu, J., McLaughlin, M. E., & Cong, F. (2013). Inactivating mutations of RNF43 confer Wnt

dependency in pancreatic ductal adenocarcinoma. *Proc Natl Acad Sci U S A*, *110*(31), 12649-12654. https://doi.org/10.1073/pnas.1307218110

Jusakul, A., Cutcutache, I., Yong, C. H., Lim, J. Q., Huang, M. N., Padmanabhan, N., Nellore, V., Kongpetch, S., Ng, A. W. T., Ng, L. M., Choo, S. P., Myint, S. S., Thanan, R., Nagarajan, S., Lim, W. K., Ng, C. C. Y., Boot, A., Liu, M., Ong, C. K., . . . Tan, P. (2017). Whole-Genome and Epigenomic Landscapes of Etiologically Distinct Subtypes of Cholangiocarcinoma. *Cancer Discov*, *7*(10), 1116-1135. https://doi.org/10.1158/2159-8290.Cd-17-0368

Keng, V. W., Yae, K., Hayakawa, T., Mizuno, S., Uno, Y., Yusa, K., Kokubu, C., Kinoshita, T., Akagi, K., Jenkins, N. A., Copeland, N. G., Horie, K., & Takeda, J. (2005). Region-specific saturation germline mutagenesis in mice using the Sleeping Beauty transposon system. *Nat Methods*, *2*(10), 763-769. https://doi.org/10.1038/nmeth795

Kirstein, M. M., & Vogel, A. (2016). Epidemiology and Risk Factors of Cholangiocarcinoma. *Visc Med*, *32*(6), 395-400. https://doi.org/10.1159/000453013

Koo, B. K., Spit, M., Jordens, I., Low, T. Y., Stange, D. E., van de Wetering, M., van Es, J. H., Mohammed, S., Heck, A. J., Maurice, M. M., & Clevers, H. (2012). Tumour suppressor RNF43 is a stem-cell E3 ligase that induces endocytosis of Wnt receptors. *Nature*, *488*(7413), 665-669. https://doi.org/10.1038/nature11308

Kosarev, P., Mayer, K. F., & Hardtke, C. S. (2002). Evaluation and classification of RING-finger domains encoded by the Arabidopsis genome. *Genome Biol*, *3*(4), RESEARCH0016. https://doi.org/10.1186/gb-2002-3-4-research0016

Lau, D. K., Tay, R. Y., Yeung, Y. H., Chionh, F., Mooi, J., Murone, C., Skrinos, E., Price, T. J., Mariadason, J. M., & Tebbutt, N. C. (2018). Phase II study of everolimus (RAD001) monotherapy as first-line treatment in advanced biliary tract cancer with biomarker exploration: the RADiChol Study. *Br J Cancer*, *118*(7), 966-971. https://doi.org/10.1038/s41416-018-0021-1

Lecarpentier, Y., Schussler, O., Hebert, J. L., & Vallee, A. (2019). Multiple Targets of the Canonical WNT/beta-Catenin Signaling in Cancers. *Front Oncol*, *9*, 1248. https://doi.org/10.3389/fonc.2019.01248

Ledenko, M., Antwi, S. O., Arima, S., Driscoll, J., Furuse, J., Klumpen, H. J., Larsen, F. O., Lau, D. K., Maderer, A., Markussen, A., Moehler, M., Nooijen, L. E., Shaib, W. L., Tebbutt, N. C., Andre, T., Ueno, M., Woodford, R., Yoo, C., Zalupski, M. M., & Patel, T. (2022). Sex-related disparities in outcomes of cholangiocarcinoma patients in treatment trials. *Front Oncol*, *12*, 963753. https://doi.org/10.3389/fonc.2022.963753

Lee, W., Park, J. H., Kim, J. Y., Kwag, S. J., Park, T., Jeong, S. H., Ju, Y. T., Jung, E. J., Lee, Y. J., Hong, S. C., Choi, S. K., & Jeong, C. Y. (2016). Comparison of perioperative and oncologic outcomes between open and laparoscopic liver resection for intrahepatic cholangiocarcinoma. *Surg Endosc*, *30*(11), 4835-4840. https://doi.org/10.1007/s00464-016-4817-x

Livak, K. J., & Schmittgen, T. D. (2001). Analysis of relative gene expression data using real-time quantitative PCR and the 2(-Delta Delta C(T)) Method. *Methods*, *25*(4), 402-408. https://doi.org/10.1006/meth.2001.1262

Loregger, A., Grandl, M., Mejias-Luque, R., Allgauer, M., Degenhart, K., Haselmann, V., Oikonomou, C., Hatzis, P., Janssen, K. P., Nitsche, U., Gradl, D., van den Broek, O., Destree, O., Ulm, K., Neumaier, M., Kalali, B., Jung, A., Varela, I., Schmid, R. M., . . . Gerhard, M. (2015). The E3 ligase RNF43 inhibits Wnt signaling downstream of mutated beta-catenin by sequestering TCF4 to the nuclear membrane. *Sci Signal*, *8*(393), ra90. https://doi.org/10.1126/scisignal.aac6757

Mancarella, S., Serino, G., Dituri, F., Cigliano, A., Ribback, S., Wang, J., Chen, X., Calvisi, D. F., & Giannelli, G. (2020). Crenigacestat, a selective NOTCH1 inhibitor, reduces intrahepatic cholangiocarcinoma progression by blocking VEGFA/DLL4/MMP13 axis. *Cell Death Differ*, *27*(8), 2330-2343. https://doi.org/10.1038/s41418-020-0505-4

Mehrpouya, M., Pourhashem, Z., Yardehnavi, N., & Oladnabi, M. (2019). Evaluation of cytokeratin 19 as a prognostic tumoral and metastatic marker with focus on improved detection methods. *J Cell Physiol*, *234*(12), 21425-21435. https://doi.org/10.1002/jcp.28768

Merino-Azpitarte, M., Lozano, E., Perugorria, M. J., Esparza-Baquer, A., Erice, O., Santos-Laso, A., O'Rourke, C. J., Andersen, J. B., Jimenez-Aguero, R., Lacasta, A., D'Amato, M., Briz, O., Jalan-Sakrikar, N., Huebert, R. C., Thelen, K. M., Gradilone, S. A., Aransay, A. M., Lavin, J. L., Fernandez-Barrena, M. G., . . . Banales, J. M. (2017). SOX17 regulates cholangiocyte differentiation and acts as a tumor suppressor in cholangiocarcinoma. *J Hepatol*, *67*(1), 72-83. https://doi.org/10.1016/j.jhep.2017.02.017

Moncur, J. T., Bartley, A. N., Bridge, J. A., Kamel-Reid, S., Lazar, A. J., Lindeman, N. I., Long, T. A., Merker, J. D., Rai, A. J., Rimm, D. L., Rothberg, P. G., Vasalos, P., & Kim, A. S. (2019). Performance Comparison of Different Analytic Methods in Proficiency Testing for Mutations in the BRAF, EGFR, and KRAS Genes: A Study of the College of American Pathologists Molecular Oncology Committee. *Arch Pathol Lab Med*, *143*(10), 1203-1211. https://doi.org/10.5858/arpa.2018-0396-CP

Montal, R., Sia, D., Montironi, C., Leow, W. Q., Esteban-Fabro, R., Pinyol, R., Torres-Martin, M., Bassaganyas, L., Moeini, A., Peix, J., Cabellos, L., Maeda, M., Villacorta-Martin, C., Tabrizian, P., Rodriguez-Carunchio, L., Castellano, G., Sempoux, C., Minguez, B., Pawlik, T. M., . . . Llovet, J. M. (2020). Molecular classification and therapeutic targets in extrahepatic cholangiocarcinoma. *J Hepatol*, *73*(2), 315-327. https://doi.org/10.1016/j.jhep.2020.03.008

Moreno-Londono, A. P., Castaneda-Patlan, M. C., Sarabia-Sanchez, M. A., Macias-Silva, M., & Robles-Flores, M. (2023). Canonical Wnt Pathway Is Involved in Chemoresistance and Cell Cycle Arrest Induction in Colon Cancer Cell Line Spheroids. *Int J Mol Sci*, *24*(6). https://doi.org/10.3390/ijms24065252

Mortele, K. J., Rocha, T. C., Streeter, J. L., & Taylor, A. J. (2006). Multimodality imaging of pancreatic and biliary congenital anomalies. *Radiographics*, *26*(3), 715-731. https://doi.org/10.1148/rg.263055164

Mueller, S., Engleitner, T., Maresch, R., Zukowska, M., Lange, S., Kaltenbacher, T., Konukiewitz, B., Ollinger, R., Zwiebel, M., Strong, A., Yen, H. Y., Banerjee, R., Louzada, S., Fu, B., Seidler, B., Gotzfried, J., Schuck, K., Hassan, Z., Arbeiter, A., . . . Rad, R. (2018). Evolutionary routes and KRAS dosage define pancreatic cancer phenotypes. *Nature*, *554*(7690), 62-68. https://doi.org/10.1038/nature25459

Murgai, M., Ju, W., Eason, M., Kline, J., Beury, D. W., Kaczanowska, S., Miettinen, M. M., Kruhlak, M., Lei, H., Shern, J. F., Cherepanova, O. A., Owens, G. K., & Kaplan, R. N. (2017). KLF4-dependent perivascular cell plasticity mediates pre-metastatic niche formation and metastasis. *Nat Med*, *23*(10), 1176-1190. https://doi.org/10.1038/nm.4400

Nakagawa, H., Suzuki, N., Hirata, Y., Hikiba, Y., Hayakawa, Y., Kinoshita, H., Ihara, S., Uchino, K., Nishikawa, Y., Ijichi, H., Otsuka, M., Arita, J., Sakamoto, Y., Hasegawa, K., Kokudo, N., Tateishi, K., & Koike, K. (2017). Biliary epithelial injury-induced regenerative response by IL-33 promotes cholangiocarcinogenesis from peribiliary glands. *Proc Natl Acad Sci U S A*, *114*(19), E3806-E3815. https://doi.org/10.1073/pnas.1619416114

Neumeyer, V., Brutau-Abia, A., Allgauer, M., Pfarr, N., Weichert, W., Falkeis-Veits, C., Kremmer, E., Vieth, M., Gerhard, M., & Mejias-Luque, R. (2021). Loss of RNF43 Function Contributes to Gastric Carcinogenesis by Impairing DNA Damage Response. *Cell Mol Gastroenterol Hepatol*, *11*(4), 1071-1094. https://doi.org/10.1016/j.jcmgh.2020.11.005

Neumeyer, V., Grandl, M., Dietl, A., Brutau-Abia, A., Allgauer, M., Kalali, B., Zhang, Y., Pan, K. F., Steiger, K., Vieth, M., Anton, M., Mejias-Luque, R., & Gerhard, M. (2019). Loss of endogenous RNF43 function enhances proliferation and tumour growth of intestinal and gastric cells. *Carcinogenesis*, *40*(4), 551-559. https://doi.org/10.1093/carcin/bgy152

Olsen, J. J., Pohl, S. O., Deshmukh, A., Visweswaran, M., Ward, N. C., Arfuso, F., Agostino, M., & Dharmarajan, A. (2017). The Role of Wnt Signalling in Angiogenesis. *Clin Biochem Rev*, *38*(3), 131-142. https://www.ncbi.nlm.nih.gov/pubmed/29332977

Pangestu, N. S., Chueakwon, P., Talabnin, K., Khiaowichit, J., & Talabnin, C. (2021). RNF43 overexpression attenuates the Wnt/beta-catenin signalling pathway to suppress tumour

progression in cholangiocarcinoma. *Oncol Lett*, *22*(6), 846. https://doi.org/10.3892/ol.2021.13107

Pant, T., Dhanasekaran, A., Bai, X., Zhao, M., Thorp, E. B., Forbess, J. M., Bosnjak, Z. J., & Ge, Z. D. (2019). Genome-wide differential expression profiling of lncRNAs and mRNAs associated with early diabetic cardiomyopathy. *Sci Rep*, *9*(1), 15345. https://doi.org/10.1038/s41598-019-51872-9

Pauli, C., Hopkins, B. D., Prandi, D., Shaw, R., Fedrizzi, T., Sboner, A., Sailer, V., Augello, M., Puca, L., Rosati, R., McNary, T. J., Churakova, Y., Cheung, C., Triscott, J., Pisapia, D., Rao, R., Mosquera, J. M., Robinson, B., Faltas, B. M., . . . Rubin, M. A. (2017). Personalized In Vitro and In Vivo Cancer Models to Guide Precision Medicine. *Cancer Discov*, *7*(5), 462-477. https://doi.org/10.1158/2159-8290.CD-16-1154

Peng, Y., Wang, Y., Zhou, C., Mei, W., & Zeng, C. (2022). PI3K/Akt/mTOR Pathway and Its Role in Cancer Therapeutics: Are We Making Headway? *Front Oncol*, *12*, 819128. https://doi.org/10.3389/fonc.2022.819128

Peng, Y. C., Lin, C. L., Hsu, W. Y., Chang, C. S., Yeh, H. Z., Tung, C. F., Wu, Y. L., Sung, F. C., & Kao, C. H. (2015). Statins are associated with a reduced risk of cholangiocarcinoma: a population-based case-control study. *Br J Clin Pharmacol*, *80*(4), 755-761. https://doi.org/10.1111/bcp.12641

Pique, D. G., Greally, J. M., & Mar, J. C. (2020). Identification of a novel subgroup of endometrial cancer patients with loss of thyroid hormone receptor beta expression and improved survival. *BMC Cancer*, *20*(1), 857. https://doi.org/10.1186/s12885-020-07325-y

Quinn, R. A., Nothias, L. F., Vining, O., Meehan, M., Esquenazi, E., & Dorrestein, P. C. (2017). Molecular Networking As a Drug Discovery, Drug Metabolism, and Precision Medicine Strategy. *Trends Pharmacol Sci*, *38*(2), 143-154. https://doi.org/10.1016/j.tips.2016.10.011

Qureshi, K., Jesudoss, R., & Al-Osaimi, A. M. (2014). The treatment of cholangiocarcinoma: a hepatologist's perspective. *Curr Gastroenterol Rep*, *16*(10), 412. https://doi.org/10.1007/s11894-014-0412-2

Rad, R., Rad, L., Wang, W., Cadinanos, J., Vassiliou, G., Rice, S., Campos, L. S., Yusa, K., Banerjee, R., Li, M. A., de la Rosa, J., Strong, A., Lu, D., Ellis, P., Conte, N., Yang, F. T., Liu, P., & Bradley, A. (2010). PiggyBac transposon mutagenesis: a tool for cancer gene discovery in mice. *Science*, *330*(6007), 1104-1107. https://doi.org/10.1126/science.1193004

Ram Makena, M., Gatla, H., Verlekar, D., Sukhavasi, S., M, K. P., & K, C. P. (2019). Wnt/beta-Catenin Signaling: The Culprit in Pancreatic Carcinogenesis and Therapeutic Resistance. *Int J Mol Sci*, *20*(17). https://doi.org/10.3390/ijms20174242

Rauff, B., Malik, A., Bhatti, Y. A., Chudhary, S. A., Qadri, I., & Rafiq, S. (2020). Notch signalling pathway in development of cholangiocarcinoma. *World J Gastrointest Oncol*, *12*(9), 957-974. https://doi.org/10.4251/wjgo.v12.i9.957

Ravasi, T., Huber, T., Zavolan, M., Forrest, A., Gaasterland, T., Grimmond, S., Hume, D. A., Group, R. G., & Members, G. S. L. (2003). Systematic characterization of the zinc-finger-containing proteins in the mouse transcriptome. *Genome Res*, *13*(6B), 1430-1442. https://doi.org/10.1101/gr.949803

Razumilava, N., & Gores, G. J. (2014). Cholangiocarcinoma. *Lancet*, *383*(9935), 2168-2179. https://doi.org/10.1016/S0140-6736(13)61903-0

Ren, B., Guo, Q., Yang, Y., Liu, L., Wei, S., Chen, W., & Tian, Y. (2020). A meta-analysis of the efficacy of postoperative adjuvant radiotherapy versus no radiotherapy for extrahepatic cholangiocarcinoma and gallbladder carcinoma. *Radiat Oncol*, *15*(1), 15. https://doi.org/10.1186/s13014-020-1459-x

Reya, T., & Clevers, H. (2005). Wnt signalling in stem cells and cancer. *Nature*, *434*(7035), 843-850. https://doi.org/10.1038/nature03319

Rizvi, S., & Gores, G. J. (2013). Pathogenesis, diagnosis, and management of cholangiocarcinoma. *Gastroenterology*, *145*(6), 1215-1229. https://doi.org/10.1053/j.gastro.2013.10.013

Rizvi, S., & Gores, G. J. (2017). Emerging molecular therapeutic targets for cholangiocarcinoma. *J Hepatol*, *67*(3), 632-644. https://doi.org/10.1016/j.jhep.2017.03.026

Rodgers, S. J., Ooms, L. M., & Mitchell, C. A. (2022). The FDA-Approved Drug Pyrvinium Selectively Targets ER(+) Breast Cancer Cells with High INPP4B Expression. *Cancers (Basel)*, *15*(1). https://doi.org/10.3390/cancers15010135

Rodon, J., Argiles, G., Connolly, R. M., Vaishampayan, U., de Jonge, M., Garralda, E., Giannakis, M., Smith, D. C., Dobson, J. R., McLaughlin, M. E., Seroutou, A., Ji, Y., Morawiak, J., Moody, S. E., & Janku, F. (2021). Phase 1 study of single-agent WNT974, a first-in-class Porcupine inhibitor, in patients with advanced solid tumours. *Br J Cancer*, *125*(1), 28-37. https://doi.org/10.1038/s41416-021-01389-8

Ryland, G. L., Hunter, S. M., Doyle, M. A., Rowley, S. M., Christie, M., Allan, P. E., Bowtell, D. D., Australian Ovarian Cancer Study, G., Gorringe, K. L., & Campbell, I. G. (2013). RNF43 is a tumour suppressor gene mutated in mucinous tumours of the ovary. *J Pathol*, *229*(3), 469-476. https://doi.org/10.1002/path.4134

Sarcognato, S., Sacchi, D., Fassan, M., Fabris, L., Cadamuro, M., Zanus, G., Cataldo, I., Capelli, P., Baciorri, F., Cacciatore, M., & Guido, M. (2021). Cholangiocarcinoma. *Pathologica*, *113*(3), 158-169. https://doi.org/10.32074/1591-951X-252

Serra, S., & Chetty, R. (2017). Rnf43. *Journal of Clinical Pathology*, *71*, jclinpath-2017. https://doi.org/10.1136/jclinpath-2017-204763

Shang, S., Hua, F., & Hu, Z. W. (2017). The regulation of beta-catenin activity and function in cancer: therapeutic opportunities. *Oncotarget*, *8*(20), 33972-33989. https://doi.org/10.18632/oncotarget.15687

Stamos, J. L., & Weis, W. I. (2013). The beta-catenin destruction complex. *Cold Spring Harb Perspect Biol*, *5*(1), a007898. https://doi.org/10.1101/cshperspect.a007898

Stenzinger, A., Vogel, A., Lehmann, U., Lamarca, A., Hofman, P., Terracciano, L., & Normanno, N. (2023). Molecular profiling in cholangiocarcinoma: A practical guide to next-generation sequencing. *Cancer Treat Rev*, *122*, 102649. https://doi.org/10.1016/j.ctrv.2023.102649

Sun, D., Gao, W., Hu, H., & Zhou, S. (2022). Why 90% of clinical drug development fails and how to improve it? *Acta Pharm Sin B*, *12*(7), 3049-3062. https://doi.org/10.1016/j.apsb.2022.02.002

Sun, J., Sun, Y., Ahmed, R. I., Ren, A., & Xie, A. M. (2019). Research Progress on Plant RING-Finger Proteins. *Genes (Basel)*, *10*(12). https://doi.org/10.3390/genes10120973

Sung, H., Ferlay, J., Siegel, R. L., Laversanne, M., Soerjomataram, I., Jemal, A., & Bray, F. (2021). Global Cancer Statistics 2020: GLOBOCAN Estimates of Incidence and Mortality Worldwide for 36 Cancers in 185 Countries. *CA Cancer J Clin*, *71*(3), 209-249. https://doi.org/10.3322/caac.21660

Tsukiyama, T., Koo, B.-K., & Hatakeyama, S. (2021). Post-translational Wnt receptor regulation: Is the fog slowly clearing? *BioEssays*, *43*(4), 2000297. https://doi.org/https://doi.org/10.1002/bies.202000297

Tsukiyama, T., Zou, J., Kim, J., Ogamino, S., Shino, Y., Masuda, T., Merenda, A., Matsumoto, M., Fujioka, Y., Hirose, T., Terai, S., Takahashi, H., Ishitani, T., Nakayama, K. I., Ohba, Y., Koo, B. K., & Hatakeyama, S. (2020). A phospho-switch controls RNF43-mediated degradation of Wnt receptors to suppress tumorigenesis. *Nat Commun*, *11*(1), 4586. https://doi.org/10.1038/s41467-020-18257-3

Valle, J. W., Borbath, I., Khan, S. A., Huguet, F., Gruenberger, T., Arnold, D., & Committee, E. G. (2016). Biliary cancer: ESMO Clinical Practice Guidelines for diagnosis, treatment and follow-up. *Ann Oncol*, *27*(suppl 5), v28-v37. https://doi.org/10.1093/annonc/mdw324

van Dijk, J. R., Yamazaki, Y., & Palmer, R. H. (2014). Tumour-associated mutations of PA-TM-RING ubiquitin ligases RNF167/RNF13 identify the PA domain as a determinant for endosomal localization. *Biochem J*, *459*(1), 27-36. https://doi.org/10.1042/BJ20131067

Vedeld, H. M., Folseraas, T., & Lind, G. E. (2020). Detecting cholangiocarcinoma in patients with primary sclerosing cholangitis - The promise of DNA methylation and molecular biomarkers. *JHEP Rep*, *2*(5), 100143. https://doi.org/10.1016/j.jhepr.2020.100143

Voigt, F., Wiedemann, L., Zuliani, C., Querques, I., Sebe, A., Mates, L., Izsvak, Z., Ivics, Z., & Barabas, O. (2016). Sleeping Beauty transposase structure allows rational design of hyperactive variants for genetic engineering. *Nat Commun*, *7*, 11126. https://doi.org/10.1038/ncomms11126

Voss, J. S., Holtegaard, L. M., Kerr, S. E., Fritcher, E. G., Roberts, L. R., Gores, G. J., Zhang, J., Highsmith, W. E., Halling, K. C., & Kipp, B. R. (2013). Molecular profiling of cholangiocarcinoma shows potential for targeted therapy treatment decisions. *Hum Pathol*, *44*(7), 1216-1222. https://doi.org/10.1016/j.humpath.2012.11.006

Wang, D., Tan, J., Xu, Y., Han, M., Tu, Y., Zhu, Z., Dou, C., Xin, J., Tan, X., Zeng, J. P., Zhao, G., & Liu, Z. (2016). The ubiquitin ligase RNF43 downregulation increases membrane expression of frizzled receptor in pancreatic ductal adenocarcinoma. *Tumour Biol*, *37*(1), 627-631. https://doi.org/10.1007/s13277-015-3499-7

Watanapa, P., & Watanapa, W. B. (2002). Liver fluke-associated cholangiocarcinoma. *Br J Surg*, *89*(8), 962-970. https://doi.org/10.1046/j.1365-2168.2002.02143.x

Weber, J., de la Rosa, J., Grove, C. S., Schick, M., Rad, L., Baranov, O., Strong, A., Pfaus, A., Friedrich, M. J., Engleitner, T., Lersch, R., Ollinger, R., Grau, M., Menendez, I. G., Martella, M., Kohlhofer, U., Banerjee, R., Turchaninova, M. A., Scherger, A., . . . Rad, R. (2019). PiggyBac transposon tools for recessive screening identify B-cell lymphoma drivers in mice. *Nat Commun*, *10*(1), 1415. https://doi.org/10.1038/s41467-019-09180-3

Wikiniyadhanee, R., Lerksuthirat, T., Stitchantrakul, W., Chitphuk, S., Sura, T., & Dejsuphong, D. (2020). TRIM29 is required for efficient recruitment of 53BP1 in response to DNA double-strand breaks in vertebrate cells. *FEBS Open Bio*, *10*(10), 2055-2071. https://doi.org/10.1002/2211-5463.12954

Wu, C. E., Chen, M. H., & Yeh, C. N. (2019). mTOR Inhibitors in Advanced Biliary Tract Cancers. *Int J Mol Sci*, *20*(3). https://doi.org/10.3390/ijms20030500

Xiao, Y., & Yu, D. (2021). Tumor microenvironment as a therapeutic target in cancer. *Pharmacol Ther*, *221*, 107753. https://doi.org/10.1016/j.pharmthera.2020.107753

Xu, R. F., Sun, J. P., Zhang, S. R., Zhu, G. S., Li, L. B., Liao, Y. L., Xie, J. M., & Liao, W. J. (2011). KRAS and PIK3CA but not BRAF genes are frequently mutated in Chinese cholangiocarcinoma patients. *Biomed Pharmacother*, *65*(1), 22-26. https://doi.org/10.1016/j.biopha.2010.06.009

Yagyu, R., Furukawa, Y., Lin, Y. M., Shimokawa, T., Yamamura, T., & Nakamura, Y. (2004). A novel oncoprotein RNF43 functions in an autocrine manner in colorectal cancer. *Int J Oncol*, *25*(5), 1343-1348. https://www.ncbi.nlm.nih.gov/pubmed/15492824

Yang, Q., Zhao, J., Chen, D., & Wang, Y. (2021). E3 ubiquitin ligases: styles, structures and functions. *Mol Biomed*, *2*(1), 23. https://doi.org/10.1186/s43556-021-00043-2

Yothaisong, S., Dokduang, H., Techasen, A., Namwat, N., Yongvanit, P., Bhudhisawasdi, V., Puapairoj, A., Riggins, G. J., & Loilome, W. (2013). Increased activation of PI3K/AKT signaling pathway is associated with cholangiocarcinoma metastasis and PI3K/mTOR inhibition presents a possible therapeutic strategy. *Tumour Biol*, *34*(6), 3637-3648. https://doi.org/10.1007/s13277-013-0945-2

Yuan, Z., Chen, S., Sun, Q., Wang, N., Li, D., Miao, S., Gao, C., Chen, Y., Tan, C., & Jiang, Y. (2017). Olaparib hydroxamic acid derivatives as dual PARP and HDAC inhibitors for cancer therapy. *Bioorg Med Chem*, *25*(15), 4100-4109. https://doi.org/10.1016/j.bmc.2017.05.058

Zebisch, M., & Jones, E. Y. (2015). Crystal structure of R-spondin 2 in complex with the ectodomains of its receptors LGR5 and ZNRF3. *J Struct Biol*, *191*(2), 149-155. https://doi.org/10.1016/j.jsb.2015.05.008

Zhang, Y., & Wang, X. (2020). Targeting the Wnt/beta-catenin signaling pathway in cancer. *J Hematol Oncol*, *13*(1), 165. https://doi.org/10.1186/s13045-020-00990-3

Zhu, X., Chen, L., Huang, B., Wang, Y., Ji, L., Wu, J., Di, G., Liu, G., Yu, K., Shao, Z., & Wang, Z. (2020). The prognostic and predictive potential of Ki-67 in triple-negative breast cancer. *Sci Rep*, *10*(1), 225. https://doi.org/10.1038/s41598-019-57094-3

Zhu, Y., & Kwong, L. N. (2020). Insights Into the Origin of Intrahepatic Cholangiocarcinoma From Mouse Models. *Hepatology*, *72*(1), 305-314. https://doi.org/10.1002/hep.31200